Hedgehog signaling in cutaneous squamous cell carcinoma

Dissertation

for the award of the degree
"Doctor rerum naturalium (Dr. rer. nat.)"
of the Georg-August University Göttingen

within the doctoral program Molecular Medicine
of the Georg-August University School of Science (GAUSS)

submitted by

Joanna Pyczek
from Krakow

Göttingen 2017

Members of the Thesis Committee

Supervisor:

Prof. Dr. Heidi Hahn

Dept. of Human Genetics; University Medical Center Göttingen

Second member of the thesis committee:

Prof. Dr. Michael Schön

Dept. of Dermatology, Venereology and Allergology; University Medical Center Göttingen

Third member of the thesis committee:

Prof. Dr. Holger Bastians

Dept. of Molecular Oncology; University Medical Center Göttingen

Date of Disputation: 30.05.2017

Affidavit

Here I declare that my doctoral thesis entitled "Hedgehog signaling in cutaneous squamous cell carcinoma" has been written independently with no other sources and aids than quoted.

Joanna Pyczek

Göttingen, April 2017

Contents

List of Figures

List of Tables

1. Summary

Cutaneous squamous cell carcinoma (cSCC) is the second most common non-melanoma skin tumor in humans with increasing incidence. cSCC is a result of malignant transformation of epidermal cells with ultraviolet (UV) radiation being the major cause of the disease. Currently, gold standard therapy involves surgical excision, which in most of the cases is sufficient to remove a primary tumor. However, a subset of patients develops recurrent or metastatic disease, for which there are no treatment options. Therefore, understanding of molecular mechanisms governing cSCC development and progression are pending to propose new targeted therapy.

cSCC is often characterized by overexpression of epidermal growth factor receptor (EGFR), which nowadays is a main target in clinical trials. Besides, cSCCs often display activation of RAS/MEK/ERK, PI3K/AKT and mTOR signaling pathways. Clinical data show that mTOR inhibition markedly reduces the risk of cSCC development in organ transplant recipients (OTRs). Recently, also the Hedgehog (HH) signaling pathway, which is often deregulated in various cancers, has been shown to be involved in cSCC. Thus, mutations in Patched1 (PTCH), the receptor for HH ligands, were described in 15% of the cases and several studies show expression of HH pathway components in cSCC including *glioma-associated oncogene homolog 1* (*GLI1*), the major readout for HH pathway activity. However, the importance of these pathways and their putative crosstalk in cSCC remain elusive.

In this thesis, the role and putative interaction of HH and EGF signaling as well as its downstream effector pathways i.e. MEK/ERK, PI3K/AKT and mTOR were investigated in human cSCC. By *in situ* hybridization and immunohistochemical analysis we showed that both *GLI1* and EGF are strongly expressed in human cSCC tissue sections. However, while nearly the entire tumor was positive for EGF, *GLI1* was highly expressed only in the center of the tumor while outer parts and invading cells were *GLI1* negative or only moderately positive. As opposed, phosphorylated ribosomal protein S6 (pS6), the main readout for mTOR activity was strongly expressed in outer parts of the tumor and cells invading the dermis while its expression in the tumor center was weak. Moreover, *GLI1* positive areas were surrounded by pERK positive stromal cells. Indeed, in cell culture model we showed that co-culture of cSCC cells with fibroblasts resulted in *GLI1* inhibition in the tumor cells supporting the role of microenvironment in paracrine regulation of gene expression in cSCC.

Together with the lack of Sonic Hedgehog (SHH), the major ligand that activates HH signaling throughout the tumor tissue, the data indicate that *GLI1* is regulated rather in a SHH-independent and thus noncanonical way in cSCC.

Indeed, our *in vitro* data show that canonical HH signaling does not play a role in cSCC. However, the data provide evidence that *GLI1* can be regulated via MEK/ERK, PI3K/AKT and mTOR pathways in cSCC cell lines. Thus, pharmacological inhibition of PI3K, AKT or mTOR with specific inhibitors resulted in a significant decrease in *GLI1* expression level in SCL-I, MET-1 and MET-4 cells suggesting a positive regulation of *GLI1* by these pathways. However, transfection with constitutively active or dominant negative Akt1 variants did not affect *GLI1* expression in SCL-I and MET-4 cells thereby questioning the role of AKT in cSCC. On the other hand, MEK1/2 inhibition with UO126 resulted in upregulation of *GLI1* expression in SCL-I cells and did not alter *GLI1* transcript levels in MET-1 and MET-4 cells. This indicates that MEK/ERK can negatively regulate *GLI1* expression in some cSCCs. Interestingly, when we applied EGF ligand to the cells, we noted a strong inhibition of *GLI1* transcription in all three cell lines. Moreover, combination of EGF with UO126, led to an upregulation of *GLI1* expression level when compared to EGF treatment alone. Together the data suggest that EGF inhibits *GLI1* expression via activation of MEK/ERK signaling in cSCC cell lines.

In addition, we analyzed an impact of MEK/ERK, PI3K/AKT, mTOR and HH pathway inhibition on cell viability, proliferation and apoptosis. In general, the data showed that PI3K/AKT inhibitors and the HH pathway inhibitor HhA remarkably reduced cell viability and proliferation, while mTOR and MEK inhibitors as well as the HH pathway inhibitor vismodegib showed only moderate decrease in the percentage of viable or proliferating cells. However, the magnitude of change for each inhibitor was cell line-dependent. Moreover, cytotoxic effects of the inhibitors could not be excluded. Concerning apoptosis, UO126 increased the number of early apoptotic SCL-1 cells. Together with increased *GLI1* expression upon treatment with UO126 in this very cell line, it can be speculated that *GLI1* can promote apoptosis.

In the last part of this thesis we investigated the role of *GLI1* in proliferation of cSCC cells. We showed that neither knockdown nor overexpression of *GLI1* affected BrdU incorporation into DNA of replicating cells.

2

Summary

In summary, our data indicate that EGF negatively regulates *GLI1* expression via activation of MEK/ERK signaling in cSCC cells. Moreover, we propose that *GLI1* is dispensable for cSCC proliferation.

2. Introduction

2.1. Cutaneous squamous cell carcinoma (cSCC)

Cutaneous squamous cell carcinoma (cSCC) is, following basal cell carcinoma (BCC), the second most common non-melanoma skin tumor in humans with increasing incidence. The highest incidence rate of cSCC is recorded in Australia with 387 new cases per 100000 person-years (py) (Staples *et al.*, 2006) and in North America with the numbers ranging from 60 to 290 cases per 100000 py (Harris *et al.*, 2001; Jung *et al.*, 2010). In Europe the highest number of new cases is noted in the U.K. (15-33/100000 py) (Lomas *et al.*, 2012), Netherlands (22-35/100000 py) (Hollestein *et al.*, 2014) and Norway (15-20/100000 py) (Robsahm *et al.*, 2015). Surgical excision is usually sufficient to remove a primary tumor. However, a 10-years retrospective study of a large cohort of cSCC revealed local recurrence in 4.6%, nodal metastasis in 3.7% and disease-associated death in 2.1% of patients (Schmults *et al.*, 2013). Moreover, epidemiological data show that men are more frequently affected than women and the risk of cSCC development markedly rises with increasing age. Additionally, cSCC most commonly develops in fair-skinned people with pale hair and blue eyes who are prone to sunburn (reviewed in (Green and Olsen, 2017)). This is linked to the fact that the main cause of cSCC is cumulative ultraviolet (UV) exposure, mainly UVB, which usually results in multistage carcinogenesis.

The process of cSCC formation starts with actinic keratosis (AK), which is a precursor lesion for cSCC and which occurs as scaly, reddish plaques. It may give rise to locally advanced cSCC manifested as ulcerating papules and may further develop into invasive or metastatic tumors (reviewed in (Alam and Ratner, 2001)). Microarray data show a similar genetic profile between AK and cSCC with however additional genetic abnormalities in the latter one. This is an indication that AK is a pre-cancerous lesion of cSCC (Padilla *et al.*, 2010; Ra *et al.*, 2011). cSCC may also develop *de novo* in immunosuppressed organ transplant recipients (OTRs) or in chronically inflamed skin areas. In fact, the risk of cSCC development in OTRs is 65-250 higher than in the general population (Euvrard *et al.*, 2003). Besides, patients suffering from acquired immune deficiency syndrome (AIDS) or chronic lymphocytic leukemia as well as patients with rheumatoid arthritis who receive immunomodulatory medicines display higher rates of cSCC occurrence (Amari *et al.*, 2011; Levi *et al.*, 1996; Zhao *et al.*, 2016). Glucocorticoids that are used for treatment of inflammatory diseases have been also shown to

increase the risk of cSCC (Jensen *et al.*, 2009; Karagas *et al.*, 2001). Altogether, these and many more reports establish a strong link between immunosuppression and cSCC development. Additional minor risk factors that are implicated in development of cSCC include ionization radiation, tobacco smoking, infection with papilloma virus and exposure to chemical agents. Moreover, some hereditary disorders such as xeroderma pigmentosum or oculocutaneous albinism may also predispose to cSCC development (Nikolaou *et al.*, 2012).

As mentioned above, standard treatment involves surgical excision, which is usually effective in most of cSCC cases. Alternative treatment options involve topical application of 5-fluoruracil (5-FU), imiquimod or diclofenac (McGillis and Fein, 2004), electrodessication, curettage, cryotherapy and fractionated radiation (reviewed in (Alam and Ratner, 2001)). Nevertheless, in some cases these treatment options are not applicable due to tumor location or recurrence/metastasis. Therefore, there is a need for better understanding of molecular mechanisms responsible for cSCC tumor formation to develop new treatment strategies.

Despite the knowledge about several cSCC-predisposing factors, not much is known about molecular mechanisms driving malignant transformation of normal keratinocytes to cSCC. *PATCHED1* (*PTCH)* mutations have been described in a subset of cSCC but the relevance of canonical HH/GLI signaling pathway in the pathogenesis of cSCC still remains unknown (see below for detailed description). Several studies unraveled certain pathways that are specifically upregulated in cSCC when compared to normal skin. Mutations in the well-known tumor suppressor p53 are common in cSCC and are found in approximately 58 % of cases (Brash *et al.*, 1991). These mutations carry hallmarks of UV-induced mutagenesis i.e. C-T or CC-TT transitions. The relevance of p53 mutations as a driving force for the neoplastic transformation is further supported by *in vivo* studies in mice, in which somatic inactivation of *Trp53* leads to the spontaneous development of cSCC in the murine epidermis, which can be accelerated by simultaneous inactivation of *retinoblastoma* (*Rb)* (Martinez-Cruz *et al.*, 2008). Thus, UV-induced p53 mutations are considered to be a driving force in a majority of cSCC. Additionally, microarray data show upregulation of Wnt/ß-catenin-, calcium- and integrin- signaling pathways in cSCC when compared to normal skin (Ra et al., 2011). The Wnt/ß-catenin signaling pathway regulates cellular proliferation via induction of *c-myc* and *cyclin D1* expression and is also active in many other cancers (Doglioni *et al.*, 2003; El-Bahrawy *et al.*, 2003). Also, calcium may play a role in cSCC pathogenesis. Calcium is a second messenger, which is involved in many crucial processes within the cell

i.e. cell-cycle regulation, proliferation and apoptosis. Indeed, rearrangement of calcium pumps has been linked to carcinogenesis (Capiod *et al.*, 2007) and calcium is especially important for keratinocytes differentiation (Bikle *et al.*, 2004). Furthermore, integrins, which are usually associated with invasive and metastatic potential of different malignancies, were shown to play an important role in inhibition of apoptosis and differentiation processes in the epidermis. Integrin overexpression has also been shown to be associated with SCC formation (reviewed in (Janes and Watt, 2006)).

Finally, many studies point to the relevance of EGFR and its downstream effectors i.e. pAKT, pERK and mTOR in pathology of cSCC (see below for detailed description). Currently, EGFR is the most promising target for therapy of cSCC. Nowadays many EGFR inhibitors are being tested in clinical trials for different tumor entities but their efficacy in the treatment of cSCC is still under evaluation (see below 2.3.4.). Another important target in cSCC therapy is the mTOR signaling cascade. Indeed, several reports demonstrated that immunosuppressive drugs, which belong to the group of mTOR inhibitors i.e. rapamycin (sirolimus) display strong anti-cSCC activity in OTRs, who are prone to cSCC development. Thus, patients receiving sirolimus develop significantly fewer new cSCC and even show regression of already existing lesions (Salgo *et al.*, 2010; Tessmer *et al.*, 2006).

2.2.   The Hedgehog signaling pathway

Many components of the Hh signaling cascade were initially described by the two Nobel laureates Nüsslein-Volhard and Wieschaus in 1980. In their systematic search for *Drosophila melanogaster* mutants they identified several genes that when mutated, altered the segmental pattern of the larva. One of the mutant larvae failed to develop the naked posterior part of each segment and showed duplication of the anterior denticle band. Since these mutants were almost entirely covered with denticles leading to a 'hedgehog-like' appearance, the responsible gene was named *Hedgehog* (*Hh*). Besides the *Hh* gene, other genes were identified, which later turned out to be key components of the Hh signaling pathway. These genes include the Hh receptor *Patched* (*Ptch*), the downstream kinase *fused* (*fu*) and transcription factor *cubitus interuptus* (*ci*) (Nusslein-Volhard and Wieschaus, 1980). Later it was discovered that the Hh pathway is conserved between species and also plays a very important role in mammals, being crucial for embryonic development, tissue patterning, cellular proliferation and cell fate decision. Physiologically, the HH pathway is active during embryogenesis and becomes

substantially silenced in an adult organism. However, it remains functional in a subset of cells and is very important for stem cells maintenance, cell differentiation, tissue repair and homeostasis (reviewed in (Petrova and Joyner, 2014)).

2.2.1. Canonical Hedgehog signaling

The most important components of the canonical HH signaling axis are the ligand HH, the 12-pass transmembrane receptor PATCHED1 (PTCH), its interacting partner SMOOTHENED (SMO), which is a 7-pass transmembrane protein and the family of glioma-associated oncogene (GLI) transcription factors. In mammals, three different forms of HH ligands exist, which play distinct roles in the organism. Sonic hedgehog (SHH) is the most potent and widely expressed HH ligand and regulates the development of the central nervous system and the limbs (reviewed in (Ingham *et al.*, 2011)). Indian hedgehog (IHH) is expressed in the gut and cartilage and mainly regulates cartilage and bone development (U. I. Chung *et al.*, 2001). The expression of Desert hedgehog (DHH) is restricted to Sertoli cells in the testis, where it is important for the development of germ cells (Clark *et al.*, 2000) and to Schwann cells, where it is responsible for proper peripheral nerve development (Parmantier *et al.*, 1999). The ligands are synthesized within the cell in an inactive form and undergo cleavage as well as post-translational modification to become active soluble ligands (reviewed in (Briscoe and Therond, 2013)). All three HH ligands can bind to their receptor PTCH. In the absence of the ligands, PTCH inhibits the activity of SMO. The inhibitory mechanism is still poorly understood but there is evidence that PTCH mediates the transmembrane transport of sterol-like small molecules that are able to inhibit SMO, which is known to have a sterol binding domain (Nedelcu *et al.*, 2013). When SMO is inactive, the GLI transcription factors GLI2 and GLI3 that are present in the cytoplasm become phosphorylated by proteinase kinase A (PKA), glycogen synthase kinase 3-ß (GSK3ß) and casein kinase 1 (CK1) (reviewed in (Aberger and Ruiz, 2014)). This phosphorylation occurs at six conserved serine (Ser) residues at the carboxyterminal (C-terminal) ends of the proteins and leads to the recruitment of E3 ubiquitin ligase. This results in the proteolytic cleavage of GLIs into their respective repressor forms (Niewiadomski *et al.*, 2014). More specifically, GLI3 processing by E3 ubiquitin ligase leads to the formation of a truncated repressor form of GLI3. On the other hand, GLI1 is fully degraded while GLI2 is regulated in both ways i.e. generation of the repressor form and degradation of the whole protein (Di Marcotullio *et al.*, 2007). This results in the repression of target gene transcription. Additionally, Suppressor of Fused (SuFu) sequesters GLI

transcription factors in the cytoplasm, thereby preventing their translocation into the nucleus (reviewed in (Briscoe and Therond, 2013)). Thus, in addition to PTCH, SuFu is another negative regulator of the pathway. Moreover, SuFu was also shown to stabilize full-length, unprocessed GLIs and to protect them from ubiquitin-mediated degradation, thereby increasing the overall level of potential GLI activator and repressor forms (S. J. Chen *et al.*, 2009).

When the HH ligands bind to PTCH, the pathway becomes active, because binding of HH inhibits the function of PTCH and thus restores SMO activity. Activation of SMO is based on trafficking into primary cilium as well as on conformational changes (Wilson *et al.*, 2009). This results in stabilization of GLI activator forms. Formation of GLI activator forms is a multistep process, which first requires dephosphorylation of C-terminal Ser residues. This is then followed by phosphorylation of GLI amino acids residues located at amino terminus (N-terminus) by different kinases i.e. PKA, AKT, ERK or S6K1. This indicates that the N-terminus of GLI proteins is an integration site for different signaling pathways (reviewed in (Aberger and Ruiz, 2014)). Upon GLI phosphorylation, activated GLI forms dissociate from the SuFu complex, translocate into the nucleus and drive the transcription of target genes. Target genes include components of the pathway itself such like *GLI1*, the most reliable readout for HH pathway activity and that amplifies the HH signal on transcriptional level. Indeed, the mRNA level of *GLI1* as the most important marker for HH signaling activity has been studied in many cancer entities. Other targets are *PTCH* and *hedgehog interacting protein* (*HHIP*), which can be expressed upon activation of HH signaling in specific tissues and which then establish a negative feedback for the pathway's activity. HHIP is a vertebrate-specific membrane glycoprotein that is known to bind all three HH ligands with similar affinity as PTCH and to attenuate HH signaling (Chuang and McMahon, 1999). The schematic representation of ON- and OFF- pathway state is depicted in Figure 1.
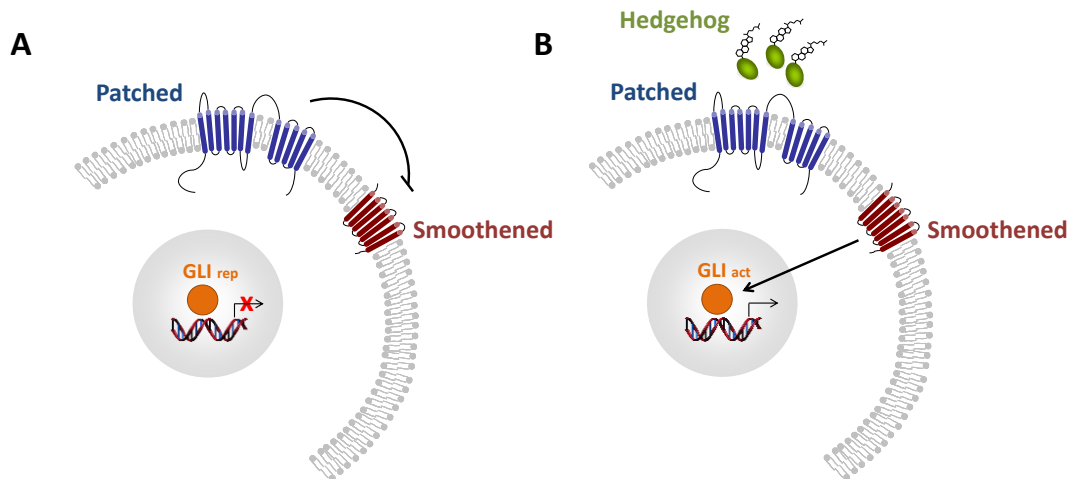
Figure 1: Schematic and simplified representation of the canonical HH signaling pathway. Four major components of the pathway are indicated; the ligand Hedgehog (HH), the 12-transmembrane receptor Patched (PTCH), the 7-transmembrane signal transduction protein Smoothened (SMO) and the GLI transcription factors in an activator and repressor form (GLI act and GLI rep, respectively). **A.** In the absence of the HH ligand, PTCH inhibits SMO. This results in the cleavage of GLIs into their repressor forms. GLI rep translocates into the nucleus and inhibits the transcription of target genes. **B.** Upon HH ligand binding to its receptor PTCH, the inhibition on SMO is suspended. This results in stabilization of the GLI activator forms, their translocation to the nucleus and the transcription of target genes.

2.2.2. Canonical Hedgehog signaling in cancer

Due to the role of HH signaling pathway in proliferation, apoptosis and stem cell maintenance (described above), deregulation of this pathway has a great potential to drive tumorigenesis. The primary link between HH pathway activation and tumor development was established by two independent groups showing that loss of heterozygosity (LOH) of the *PTCH* locus is a hallmark of basal cell nevus syndrome, which is a hereditary disorder that predisposes patients to development of BCC and medulloblastoma (MB) (Hahn *et al.*, 1996; Johnson *et al.*, 1996). To this day, numerous studies have shown that pathological activation of canonical HH signaling is the driving force for many tumor entities including gliomas (Takezaki *et al.*, 2011), BCC, MB (Hahn et al., 1996; Johnson et al., 1996) or prostate cancer (reviewed in (Xie, 2005)). Two different mechanisms for overactivation of the canonical HH/PTCH/SMO/GLI axis can be distinguished. Whereas the ligand-dependent mode of action is based on the excess of HH ligand that continuously binds to PTCH (see Fig. 2 A) the ligand-independent mode is driven by inactivating mutations in HH pathway suppressors (PTCH or SuFu), by activating mutation in SMO or GLI amplification (see Fig. 2 B; reviewed in (Amakye *et al.*, 2013)).

Ligand-dependent HH signaling overactivation has been described in several different tumor entities. For example, ligand-dependent activation is necessary to maintain glioma progenitor cells within a subset of gliomas (Ehtesham *et al.*, 2007). Another study shows that transgenic mice overexpressing SHH in skin develop BCC, which implies that ligand overexpression is sufficient to drive tumorigenesis in an autocrine manner (Oro *et al.*, 1997). However, ligand-dependent HH pathway activation might also require tumor-stroma cells interaction due to paracrine signaling (Yauch *et al.*, 2008). Indeed, activation of HH signaling in stromal cells promotes growth of human prostate cancer in the mouse xenograft model (Shaw *et al.*, 2009).

Ligand-independent activation of canonical HH signaling occurs frequently due to mutations in *PTCH*. *PTCH* inactivating mutations have been well described in BCC and MB. Indeed, the vast majority of BCC arises due to mutations in this gene (reviewed in (Epstein, 2008)) and only a small subset of BCC shows activating *SMO* or inactivating *SuFu* mutations, which also can be modelled in mice (Lam *et al.*, 1999; Xie *et al.*, 1998). Furthermore, *PTCH* mutations have been identified in 9% of MB (Taylor *et al.*, 2002), in 7% of esophageal SCC (Maesawa *et al.*, 1998) and in 4% of colorectal tumors (J. H. Chung and Bunz, 2013). MB also can harbor inactivating mutations in the *SuFu* tumor suppressor (Taylor et al., 2002). Loss-of-function mutations in *SuFu* have also been detected in prostate cancer, although HH pathway activation in this tumor entity is mainly ligand-dependent (Sheng *et al.*, 2004). Activating mutations in *SMO* causing abnormal HH pathway signaling have been described in primitive neuroectodermal tumors (Reifenberger *et al.*, 1998), in 10% of gastric cancers (Z. C. Wang *et al.*, 2013) and, as already said in BCC. In contrast, mutations in *GLI* have not been described so far. However, *GLI1* amplification accompanied by increased *GLI1* mRNA level was described in malignant glioma tumors and a cell line derived from one of these lesions (Kinzler *et al.*, 1987; Wong *et al.*, 1987). Furthermore, molecular and cytogenetic analysis reveals amplification of *GLI1* in a subset of alveolar rhabdomyosarcoma (RMS) (Gordon *et al.*, 2000). Additionally, a so-called Shh-subgroup of MB, which is thought to be driven by pathological HH pathway activation (Taylor *et al.*, 2012) carries amplified copy numbers of *GLI2,* which correlates with poor prognosis (Northcott *et al.*, 2011; Northcott *et al.*, 2009).
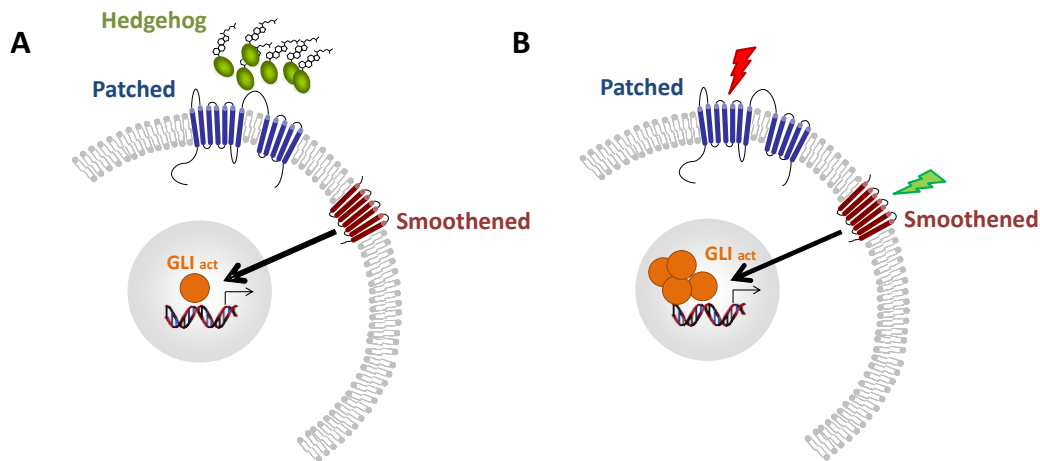
Figure 2: Most frequent alterations in the canonical HH signaling pathway in cancer. Two mechanisms of HH pathway overactivation are presented. **A.** Upregulation of the pathway's activity in a ligand-dependent manner. HH ligands are highly produced by either the tumor itself or by the tumor stroma and bind to the PTCH receptor leading to activation of SMO and translocation of GLI to the nucleus. **B.** Activation of the pathway in a ligand-independent manner. Inactivating mutations in PTCH (indicated in red) or activating mutations in SMO (indicated in green) or GLI amplification can lead to enhanced activity of GLI transcription factors and thus constitutive pathway activation.

Due to overactivation of HH signaling in a broad spectrum of different tumors, HH pathway inhibitors have gained great interest in the past. The first HH pathway inhibitor identified was cyclopamine. Cyclopamine is a naturally occurring alkaloid that was isolated from the corn lily *Veratrum californicum* and was shown to cause developmental defects in lambs via binding to and inhibiting the function of SMO (Binns *et al.*, 1968; J. K. Chen *et al.*, 2002a). However, due to its poor oral solubility, low potency and relevant toxicity, it is not suitable for therapy in humans (Lipinski *et al.*, 2008). Therefore, other more potent small-molecule inhibitors targeting SMO have been developed and synthesized and are currently being investigated in many clinical trials of a variety of cancers including pancreatic cancer, breast cancer, esophageal cancer, inoperable metastatic gastric cancer as well as hematologic malignancies (reviewed in (Amakye et al., 2013)). Up to date two of them reached US Food and Drug Administration (FDA) approval for treatment of locally advanced and metastatic BCC. These drugs are vismodegib from Curis/Roche (also named GDC-0449, approved in 2012) and sonidegib from Novartis (also named LDE225, approved in 2015). However, SMO inhibitors are only efficient in tumors overexpressing HH ligands or in those bearing *PTCH* mutations, whereas malignancies driven by *SMO* activating mutations or *GLI* amplification are insensitive to this type of therapy. Besides, the activation of GLI transcription factors

might occur due to GLI regulation by other signaling pathways that are independent of SMO. This mechanism is known as noncanonical HH signaling and is described in detail in chapter 2.2.4. (see below). In this scenario, SMO inhibitors fail to inhibit tumor growth and thus development of alternative therapies is urgently needed.

2.2.3. Canonical Hedgehog signaling in cSCC

Mutations in members of the HH signaling pathway have also been described in cSCC. Thus, 15% of cSCC cases show mutations in *PTCH* (Ping *et al.*, 2001). Moreover, screening of a large cohort of cSCC revealed LOH at the *PTCH* locus on chromosome 9q22 in approximately 50% of cases (Danaee *et al.*, 2006). In addition, besides SHH and PTCH1, cSCC expresses GLI1, the major target of active HH signaling. As shown by immunohistochemistry SHH was expressed in 67%, PTCH1 in 90% and GLI1 in 42% of analyzed human cSCC samples (Schneider *et al.*, 2011). This indicates that HH signaling may be active in cSCC. However, these results are different from ours and are discussed in more detail in section 7.1.1.

Nevertheless, the role of HH signaling pathway in cSCC is still poorly understood. While SMO inhibitors e.g. vismodegib (Dubey *et al.*, 2013) or sonidegib (Burness, 2015) have been approved for the treatment of BCC that harbor *PTCH* mutations, several of these cases developed actinic keratosis (Aasi *et al.*, 2013). Later, several similar studies were published, reporting even patients who developed cSCC under the treatment of BCC with vismodegib (Orouji *et al.*, 2014; Poulalhon *et al.*, 2015; Saintes *et al.*, 2015). So far, SMO inhibitors have not been tested in cSCC. It is possible that some of cSCC e.g. those bearing PTCH mutations would benefit from the therapy with SMO inhibitors. However, it seems that a subset of cSCC can also develop after this type of treatment. Altogether, these data clearly show that there is a need for profound understanding of the role of HH signaling pathway in cSCC.

2.2.4. Noncanonical Hedgehog signaling

Noncanonical HH signaling can be defined by two distinct modes of action. One assumes the function of either PTCH or SMO independently of GLI transcription factors while the second one involves regulation of GLIs by other signaling pathways. Indeed, it was shown that PTCH can have a direct effect on cellular biology without involvement of other components of the canonical HH signaling axis. Several independent studies in vertebrates have shown that Ptch

has a pro-apoptotic function that is independent of Smo or Gli and rather relies on a caspase-mediated cleavage of the C-terminal cytoplasmic domain of Ptch (Thibert *et al.*, 2003). Moreover, Ptch can act as a direct interaction partner of phosphorylated cyclin B1 and block cell cycle progression by promoting cytoplasmic localization of cyclin B1 (Barnes *et al.*, 2001). Other studies showed that the Shh/Ptch/Smo axis is involved in the cytoskeletal rearrangements that are mediated via ras homolog family member A (RhoA) and Ras-related C3 botulinum toxin substrate 1 (Rac1) but not by Gli (Polizio *et al.*, 2011). However, the exact mechanism by which Smo activates these 2 small GTPases still needs to be elucidated.

Regulation of GLI transcriptional activity in a SMO-independent manner has recently reached strong interest mostly due to many unsuccessful clinical trials using inhibitors that specifically target SMO (see below; (Berlin *et al.*, 2013; Kaye *et al.*, 2012; Kim *et al.*, 2014)). There are many studies showing involvement of other signaling pathways in the regulation of GLIs. These pathways involve transforming growth factor β (TGFβ) signaling, protein kinase C (PKC) signaling, mitogen-activated protein kinase kinase/extracellular signal-regulated kinases (MEK/ERK), phosphatidylinositol-4,5-bisphosphate 3-kinase/protein kinase B (PI3K/AKT) or the mechanistic target of rapamycin (mTOR).

2.2.5. Noncanonical Hedgehog signaling in cancer and cSCC

Noncanonical HH signaling has been described in many tumor entities. There is growing evidence that TGFβ may regulate expression of GLIs independently of SMO. Thus, Smad-mediated TGFβ signaling stimulated the rapid expression of *GLI2* followed by delayed upregulation of *GLI1* in human HaCaT keratinocytes, neonatal dermal fibroblasts and in a breast carcinoma cell line (Dennler *et al.*, 2007). Moreover, cyclopamine treatment did not inhibit TGFβ-mediated upregulation of *GLI1* suggesting a SMO-independent mode of action. The authors also showed that overexpression of TGF-β1 in the epidermis of transgenic mice resulted in elevated levels of *Gli1* and *Gli2* in comparison to control mice (Dennler *et al.*, 2007). TGFβ-associated *GLI1* and *GLI3* overexpression was also noted in SMO-depleted pancreatic ductual adenocarcinoma cells supporting the SMO-independent mechanism (Nolan-Stevaux *et al.*, 2009). Furthermore, analysis of the human *GLI2* promoter region revealed binding sites for SMAD transcription factors and lymphoid enhancer factor/T cell factor (LEF/TCF). These data suggest a direct regulation of *GLI2* by SMAD proteins as well as involvment of Wnt signaling in *GLI2* transcriptional regulation (Dennler *et al.*, 2009). The

cooperation between Wnt/β-catenin/LEF and HH signaling pathway was indeed shown to play a role in cancer formation. In *in vitro* models of stomach, colon and lung cancer, exogenous overexpresison of β-catenin increased the transcriptional activity of GLI transcription factors, which however seemed to be TCF/LEF-independent (Maeda *et al.*, 2006). Further experiments in embryonic kindey 293T cells suggested that Wnt/β-catenin increases *GLI1* expression and its transcriptional activity via induction of coding region determinant-binding protein (CRD-BP). CRD-BP is an mRNA binding protein, which stabilizes *GLI1* mRNA leading to increased GLI1 protein level and increased *GLI1* transcription as a result of positive feedback loop (Noubissi *et al.*, 2009).

Other studies focused on the crosstalk between HH/GLI signaling and IGF-2. Igf-2 expression is enhanced in RMS, MB as well as normal tissue of *Ptch* deficient mice and indispensable for RMS and MB formation driven by Ptch loss of function (Hahn *et al.*, 2000). In cerebellar granule cell precursors that are believed to be the origin of desmoplastic MB, Shh and Igf-2 were shown to synergistically induce expression of HH pathway target genes i.e. *Gli1* and *cyclin D1* (Hartmann *et al.*, 2005).

GLI protein activity and *GLI* transcriptional level can also be regulated by kinases that act independently of SMO i.e. PKC-σ, DYRK1 or DYRK2. For example in NIH3T3 cells it has been shown that activation of PKC-σ by phorbol esters i.e. 12-O-tetradecanoylphorbol 13-acetate (TPA) leads to ligand-independent activation of Gli transcriptional activity as well as elevated *Gli1* and *Ptch1* transcription level. Nevertheless, a certain level of PKC-σ activity seems to be also necessary for Shh-driven Gli activity (Riobo *et al.*, 2006). In addition, further studies have demonstrated that PKC-σ positively regulates GLI transcriptional activity downstream of SuFu (Lauth *et al.*, 2007). GLI function can also be regulated by DYRK1 and DYRK2. DYRK1A has been shown to promote translocation of GLI1 to the nucleus and thus to enhance its transcriptional activity (Mao *et al.*, 2002). On the other hand, DYRK2 has been shown to phosphorylate GLI2 and thereby to promote its proteasomal degradation (Varjosalo *et al.*, 2008). Also the EWS-FLI1 fusion oncogene observed in Ewing sarcoma can increase *GLI1* transcription by direct binding to its promotor (Beauchamp *et al.*, 2009; Beauchamp *et al.*, 2011). Several independent studies also present a negative crosstalk between GLI1 and the tumor suppressor p53 (Abe *et al.*, 2008; Stecca and Ruiz i Altaba, 2009; Yoon *et al.*, 2015). The exact mechanism by which p53 represses GLI1 function is not known but p53 can prevent nuclear localization and thus transcriptional activity of GLI1. GLI1 can in turn

negatively regulate p53, which suggests the existence of a negative feedback loop between these two proteins (Stecca and Ruiz i Altaba, 2009). Also Notch signaling has been identified as another negative regulator of Gli transcription factors in murine skin. Specifically, depletion of Notch1 results in elevated expression of *Gli2* and development of BCC-like tumors in the murine epidermis. Moreover this mechanism seems to be mediated by derepression of ß-catenin signaling (Nicolas *et al.*, 2003). On the other hand, in mice, Smo-driven MB shows the expected increase in *Gli1* expression but concomitantly elevated level of Notch target genes i.e. *Hes5*. This suggests that Hh pathway activation is sufficient to activate Notch signaling and that activity of both pathways is required for MB development in mice. Also in human MB, HH pathway components and Notch signaling target genes were concomitantly elevated when compared to normal cerebellum (Hallahan *et al.*, 2004).

The activity of GLI proteins can also be mediated via growth factor receptor signaling such as the epidermal growth factor EGF and its receptor EGFR (please see also section 2.3.). These so-called receptor tyrosine kinase (RTK) can activate e.g. RAS/RAF/MEK. The interaction of the latter pathway with GLIs was extensively studied in pancreatic cancers and showed a positive influence on GLI transcriptional activity (Eberl *et al.*, 2012; Ji *et al.*, 2007). The detailed mechanism still remains to be discovered but computational predictions suggest that mitogen-activated protein kinase (MAPK or ERK) can directly phosphorylate and thus activate GLI transcription factors (Whisenant *et al.*, 2010). Additionally, in keratinocytes it has been shown that EGFR-mediated activation of MEK/ERK cooperates with GLI transcription factors to induce neoplastic transformation (Kasper *et al.*, 2006a; Schnidar *et al.*, 2009). However, in MB, fibroblast growth factor (FGF)-mediated ERK activation inhibits HH pathway target genes expression including *GLI1* (M. P. Fogarty *et al.*, 2007b). This suggests that growth factors can impact on GLI in either a cell type- or growth factor-specific manner.

Another important pathway that acts downstream of RTKs and is involved in GLI regulation is the PI3K/AKT axis. For example in melanoma this pathway promotes nuclear localization and thus transcriptional activity of GLI transcription factors (Stecca *et al.*, 2007). Moreover, PI3K/AKT synergizes with SHH signaling to support tumor growth of MB cells, most likely via activation of the mTOR pathway (Filbin *et al.*, 2013). Indeed, the latter pathway can phosphorylate GLI1 in esophageal adenocarcinoma via activation of ribosomal protein S6 kinase beta-1 (S6K1) (Y. Wang *et al.*, 2012), which results in dissociation of phosphorylated

GLI1 from SuFu and its translocation into the nucleus. Moreover, this study showed that GLI1 activation is important for viability, proliferation and invasion of the tumor cells.

The relevance of noncanonical HH signaling in cSCC is not known. Although activation of many oncogenic pathways i.e. EGF/EGFR, PI3K/AKT, MEK/ERK and mTOR was shown in cSCC (see section 2.1. and 2.3.4.) their role in the regulation of GLI has not been studied so far.

As described above, the involvement of noncanonical HH signaling in cancer has been established in various tumors and in many cases explains the inefficiency of SMO inhibitors as a treatment strategy. Therefore, to overcome the influence of downstream signaling pathways on GLI activity, inhibitors against GLIs as terminal effectors of HH pathway are currently in development. Two forms of GLI1 antagonists (GANT) have been discovered in GLI luciferase reporter assay in HEK293 cells, which are GANT-58 and GANT-61. GANT-61 is more specific than GANT-58 and is able to inhibit GLI1 and GLI2 DNA-binding capability. It was shown to be effective in the cell lines derived from various cancers i.e. RMS, osteosarcoma, neuroblastoma and ovarian cancer. However, up to date there are no clinical trials using GANT inhibitors. Another GLI inhibitor is arsenic trioxide (ATO). It has been described to effectively block GLI1 and GLI2 transcriptional activity *in vitro* and *in vivo*. But it was also shown to induce apoptosis via interaction with glutathione-related enzymes or via degradation of peroxides. The exact mechanism of action is not yet known, however it was proposed that ATO promotes apoptosis via activation of Jun N-terminal kinase (Sun *et al.*, 2016). Despite the multitude of action, ATO has met approval of the FDA for the treatment of acute promyelocytic leukemia and is currently being evaluated in clinical trials for the treatment of various cancers i.e. non-small cell lung cancer (NSCLC), malignant gliomas, hepatocellular carcinoma and many hematological malignancies (reviewed in (Rimkus *et al.*, 2016)).

2.3. Epidermal growth factor/Epidermal growth factor receptor signaling

The epidermal growth factor receptor (EGFR, ErbB1, HER1) is a transmembrane receptor displaying tyrosine kinase activity. As a RTK it regulates activity of downstream signal transduction pathways that are crucial for proliferation and survival of normal and cancerous cells. It belongs to the family of HER (ErbB) receptors comprised of HER1 (EGFR), HER2, HER3 and HER4, which may form homo- or heterodimers. Ligands for HER receptor also

constitute a family of small molecules that includes epidermal growth factor (EGF), transforming growth factor-α (TGF-α) and amphiregulin, which specifically bind to EGFR. Other molecules such as epiregulin, betacellulin and heparin-binding EGF associate with EGFR and HER4, whereas some neuregulins bind selectively to HER3 and/or HER4 (reviewed in (Brand *et al.*, 2011)).

EGF was initially isolated from the murine submaxillary gland and was reported to accelerate eyelid separation and incisors eruption in mice (Cohen, 1962). This study was followed by identification and isolation of human EGF from urine, which was shown to stimulate growth of human foreskin fibroblasts *in vitro* and corneal epithelial cells in organ culture. *In vivo* it had similar effects as murine EGF and induced premature eyelids opening (Cohen and Carpenter, 1975). Up to date there have been a lot of studies focusing on EGF/EGFR interaction and signaling as well as its biological relevance. Nowadays, the EGF ligand is a prototype for all ligands that can bind EGFR (HER1). These ligands all share structural similarity in the extracellular domain called EGF-like motif, which is composed of six conserved cysteine residues within 35-40 amino acids sequence (reviewed in (Zeng and Harris, 2014)). The cysteine residues pair and form disulfide bonds that are necessary for their biological activity and binding to EGFR (Savage *et al.*, 1973). The disulfide bonds provide a three-looped structure to EGF with linear N- and C-terminus. The amino acid composition of the N-terminal part is crucial for the ligand specificity. For example, a substitution of four N-terminal amino acids of heregulin (ligand belonging to a group of neuregulins) with a N-terminal sequence specific for EGF was sufficient to allow affinity binding of the chimeric heregulin to the HER1 receptor (Barbacci *et al.*, 1995). Another example is the decreased EGF binding affinity and specificity upon replacement of as few as 2 amino acids within its N-terminal linear region (Stortelers *et al.*, 2002). Altogether, despite structural similarities between EGF-like ligands within the looped structure, the N-terminal amino acid composition plays a crucial role in tight regulation of ligand specificity. Additionally, binding of EGF to EGFR is regulated by post-translational modifications of the receptor's extracellular domain. For example, site-specific methylation by protein arginine methyltransferase 1 (PRMT1) of the extracellular domain of EGFR enhances EGF binding affinity, thereby inducing receptor dimerization and signal transduction (Liao *et al.*, 2015). Depending on the ligand type and the composition of the dimer, HER receptors activate different signaling molecules that mediate various functions within the cell. Dimerization upon ligand binding is required for the

tyrosine kinase activity of the receptor, which leads to autophosphorylation of the C-terminal domain of the receptor. The respective phosphorylated tyrosine (Tyr) residues constitute a docking site for different signaling molecules that contain Src Homology 2 (SH2) domain. This further activates downstream signaling molecules or signaling cascades such as the RAS/RAF/MEK/ERK, PI3K/AKT or phospholipase CΥ/protein kinase C (PLCΥ/PKC) that are all involved in cellular proliferation, apoptosis, differentiation, migration or invasion. Moreover, several studies have shown that EGFR can localize into the nucleus of many cell types and thus function as transcription factor itself. However, it remains to be unraveled whether it can directly bind to DNA (Lin *et al.*, 2001).

2.3.1. Activation of RAS/RAF/MEK/ERK signaling pathway

The mechanism of signal transduction by EGFR is similar for the whole group of RTKs including fibroblast growth factor receptor (FGFR), vascular endothelial growth factor receptor (VEGFR) and platelet derived growth factor receptor (PDGFR). One of the main pathways activated by EGFR signaling is the RAS/RAF/MEK/ERK cascade. Upon activation of autophosphorylation, phosphorylated Tyr residues on the C-terminal of the receptor are recognized and bound by growth factor receptor-bound protein 2 (Grb2) containing a Src homology 3 domain (SH3), which recruits the son of sevenless (SOS) guanine nucleotide exchange factor. This further promotes guanosine triphosphate (GTP)-dependent activation of Rat sarcoma (RAS). RAS belongs to the family of small GTPases, which transmit signals within the cells. GTP-RAS stimulates RAF/MEK/ERK kinase cascade by recruitment of the rapidly accelerated fibrosarcoma (RAF) kinase to the plasma membrane and its subsequent activation. RAF then phosphorylates and activates MEK kinases. MEKs constitute an evolutionary conserved group of kinases. In mammals, it occurs in 3 isoforms i.e. MEK1 (45 kDa), inactive MEK1b (43 kDa) and MEK2 (46 kDa). MEK1 and MEK2 are composed of a N-terminal regulatory domain, a catalytic kinase domain and a C-terminal domain. Typically, their activation is triggered by phosphorylation of two Ser residues (Ser 218 and Ser 222) by MAPKKK i.e. A-Raf, B-Raf, Raf-1 or MOS kinases. In fact, the regulation of MEK activity is a much more complex process, which involves phosphorylation of other Ser and threonine (Thr) residues by a spectrum of other kinases. Inactivation of MEK1/2 is dependent on dephosphorylation of Ser 218 and Ser 222 by protein phosphatase 2 (PP2A). Activated MEKs function as tyrosine/threonine (Tyr/Thr) kinases with ERK being their only known physiological substrate. The ERK proteins ERK1 and ERK2 are products of two different

genes (*ERK1* and *ERK2*) and are also evolutionary conserved. They are composed of a catalytic kinase domain, regulatory elements containing Tyr and Thr residues and a C-terminal docking domain responsible for interaction with MEK and other regulatory proteins. MEKs bind to the C-terminus of ERKs and phosphorylate their Tyr and Thr residues. This double phosphorylation seems to be exclusively exerted by MEKs. Inactivation of ERKs relies on Tyr/Thr dephosphorylation, which can be accomplished by different phosphatases. Activated ERKs are potent Ser/Thr kinases which phosphorylate Ser and Thr residues within specific consensus sequences of many different substrates both in the cytoplasm and the nucleus. Most of these substrates are transcription factors such like Elk-1, c-Myc, c-Fos, p53 or c-Jun, which drive the expression of target genes involved in proliferation, differentiation and apoptotic processes (reviewed in (Shaul and Seger, 2007)). On the other hand, ERKs can also further activate other kinases including ribosomal kinase S6K1, which then drives the transcription of other subset of genes. Specificity of ERK kinases is regulated on many different levels and depends on strength and duration of the cascade signaling, their subcellular localization as well as crosstalk with different scaffold proteins and other signaling pathways (reviewed in (Shaul and Seger, 2007)). A simplified representation of RAS/RAF/MEK/ERK activation by RTKs is depicted in Figure 3.
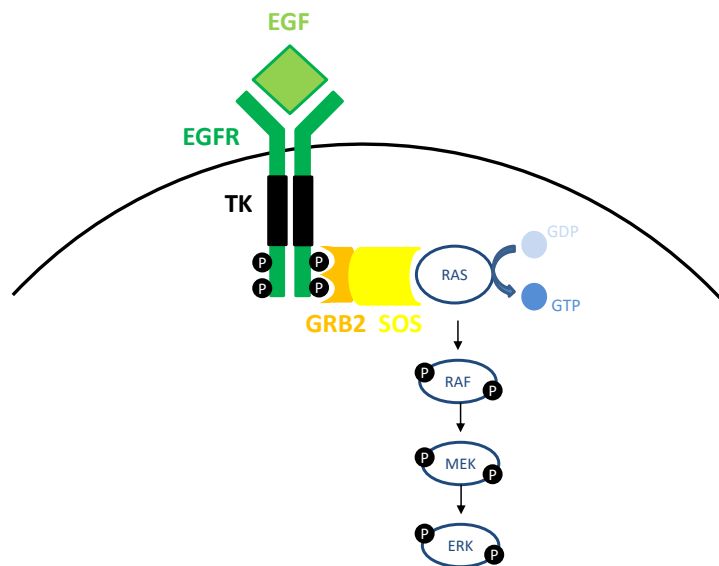
Figure 3: Schematic representation of RAS/RAF/MEK/ERK activation by EGFR. Upon binding of the EGF ligand, monomeric EGFR receptors dimerize leading to tyrosine kinase (TK) domain activation. Phosphorylated residues in the receptor's cytoplasmic domain are bound by the GRB2 docking protein. GRB2 is recognized by the SOS protein, which subsequently activates RAS via induction of GDP to GTP exchange. Activated GTP-bound RAS initiates downstream RAF/MEK/ERK kinase cascade.

2.3.2. Activation of PI3K/AKT and mTOR signaling pathways

Another important pathway regulated by RTKs is PI3K/AKT, which is known to inhibit caspase-mediated apoptosis or stimulate proliferation and cell metabolism (H. Zhou *et al.*, 2000b). The most commonly described way of PI3K activation is based on ligand binding to insulin-like growth factor 1 receptor (IGF1R) (Myers *et al.*, 1994). Phosphorylated Tyr residues of the receptor are recognized and bound by insulin receptor substrate 1 (IRS-1) protein, which constitutes a docking site for PI3K. Nevertheless, PI3K can also directly recognize phosphorylated Tyr residues at the C-terminus of other RTKs such as EGFR. The third way of PI3K activation is exerted by GTP-bound RAS protein. Regardless of the way of activation, activated PI3K is recruited to the cell membrane where it binds and phosphorylates phosphatidylinositol 4,5-bisphosphate (PIP2), which is a regular component of the cell membrane. Phosphorylated PIP2 forms a second messenger called phosphatidylinositol (3,4,5)-trisphosphate (PIP3), which is able to activate the Ser/Thr kinase AKT. Upon binding to PIP3 via its plextrin homology domain (PH), AKT becomes activated in a two-step phosphorylation exerted by two different kinases. These are the phosphoinositide dependent kinase 1 (PDK1) and the mammalian target of rapamycin (mTOR) within complex 2 (mTORC2) (Alessi *et al.*, 1997; Sarbassov *et al.*, 2005). Fully activated AKT regulates important processes in the cell i.e. proliferation, cell survival and protein synthesis. One of the well-known effectors of AKT is the mammalian target of rapamycin complex 1 (mTORC1). The activation of mTORC1 is a multistep process involving inactivation of the tuberous sclerosis 2 (TSC2) complex, which results in activation of the Ras homolog enriched in brain (RHEB). Activated RHEB binds to a catalytic domain of mTORC1 driving thereby the kinase function of mTOR. The two major substrates of mTORC1 are S6K1 kinase and eIF4E-binding protein 1 (4E-BP1) that are involved in protein synthesis (reviewed in (Laplante and Sabatini, 2012)). Thus, the PI3K/AKT/mTOR axis is very important for cell survival. In addition, it is frequently overactivated in tumor cells. This cascade is negatively regulated by phosphatase and tensin homolog (PTEN), which is a well-known tumor suppressor that dephosphorylates PIP3 to PIP2. In fact, inactivating mutations in PTEN are commonly found in a variety of cancers (Chalhoub and Baker, 2009). The exemplary activation of PI3K/AKT signaling pathway via EGFR is depicted in Figure 4.
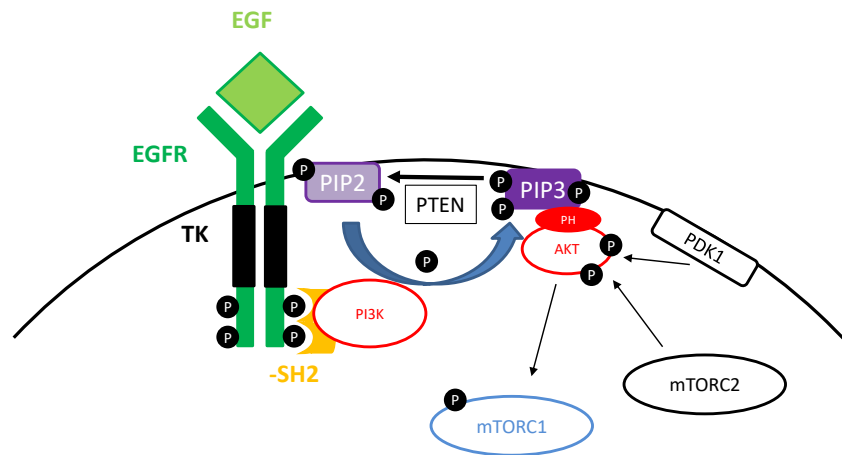
Figure 4: Schematic representation of PI3K/AKT pathway activation by EGFR. Upon RTK activation, PI3K binds to phosphorylated tyrosine residues via its SH2 domain. PIP2, which is a component of the cell membrane, becomes phosphorylated via activated PI3K to form PIP3. PIP3 is recognized by AKT via its PH domain. This results in phosphorylation and activation of AKT by two different kinases i.e. PDK1 and mTORC2.

2.3.3. Epidermal growth factor/epidermal growth factor receptor signaling in cancer

EGF has been shown to stimulate growth of various cell types *in vitro* including rodent and human mammary epithelium, murine neocortical cells with stem cell properties and rat thyroid cells (Asmis *et al.*, 1995; Osborne *et al.*, 1980; Palma and Ruiz i Altaba, 2004). In cancer, EGF has been revealed to stimulate growth, invasion and metastasis of breast cancer cells (Lu *et al.*, 2001; Osborne et al., 1980). In cervical cancer cells, EGF-mediated EGFR signaling promotes epithelial-to-mesenchymal (EMT) transition and thus tumor progression (Lee *et al.*, 2008). Moreover, autocrine EGF signaling has been shown to promote the growth of prostate cancer cells (Tillotson and Rose, 1991). It was also shown *in vivo* that EGF production by NSCLC is required for EGFR activation and tumor growth in mice (W. Wu *et al.*, 2007). Another study showed that co-expression of EGF and EGFR is correlated with progression of colon carcinoma (Iqbal and Lenz, 2004).

However, the great majority of studies focus on EGFR itself. Thus, constitutive activation of the EGFR is detected in many tumors. Most frequently these cancers are of epithelial origin and include head and neck squamous cell carcinoma (HNSCC) (Weichselbaum *et al.*, 1989), NSCLC (Veale *et al.*, 1987) or breast cancer (Masuda *et al.*, 2012; Sainsbury *et al.*, 1987). Nevertheless, pathological activation of EGFR signaling is not restricted to epithelial tumors and is also observed e.g. in glioblastoma (Libermann *et al.*, 1985). There are different

mechanisms resulting in constitutive activation of EGFR signaling i.e. excess of ligand production in autocrine or paracrine way (Sizeland and Burgess, 1992), amplification of the EGFR receptor or activating mutations within the receptor. In case of EGFR amplification in tumors such as breast cancer and malignant glioma (Al-Kuraya *et al.*, 2004; Sainsbury et al., 1987; Wong et al., 1987), the monomeric receptors on the cell membrane may spontaneously dimerize leading to the activation of downstream signaling pathways independently of ligand binding. Besides, overexpression of EGFR receptors without any mutations or amplification is observed in many different tumor entities including pancreatic cancer (Korc *et al.*, 1992), anaplastic thyroid cancer (Schiff *et al.*, 2004) and also cSCC (G. B. Fogarty *et al.*, 2007a; Mauerer *et al.*, 2011) (see below for more detailed information). Constitutive activation may also be conferred by mutations in the extracellular, transmembrane or cytoplasmic domains of EGFR. Thus, EGFR is quite often a target for therapy in cancer. Two distinct groups of drugs targeting EGFR have been developed. The first is a group of small molecule tyrosine kinase inhibitors (TKI), which inhibit the cytoplasmic tyrosine kinase activity via occupying the binding site for ATP (Busse *et al.*, 2001). There are three TKI that have been already approved by FDA. These are erlotinib for treatment of NSCLC and pancreatic cancer, gefintinb for NSCLC and lapatinib for breast cancer. The second group is composed of monoclonal antibodies, which block ligand binding to the extracellular domain of the receptor (reviewed in (Martinelli *et al.*, 2009)) with Cetuximab being approved by the FDA for the treatment of HNSCC as well as colorectal cancer. However, small molecules as well as anti-EGFR monoclonal antibodies do not work in patients bearing the mutations in downstream proteins such as e.g. KRAS (Soeda *et al.*, 2013).

2.3.4. Epidermal growth factor/epidermal growth factor receptor signaling in cSCC

In the literature, there are not many reports showing the importance of EGF ligand in cSCC. One study shows that EGF treatment of cSCC cell lines induces EGFR signaling as shown by increase in the levels of pEGFR (Galer *et al.*, 2011). However, the authors did not investigate the role of the ligand in tumor growth but rather focused on EGFR inhibition. The EGFR is indeed an interesting target for cSCC therapy. This is due to the fact that it is overexpressed in 43% of cSCC, whereby half of them show positivity for the phosphorylated form of the receptor (G. B. Fogarty et al., 2007a). This is in contrast to BCC or normal skin. Apparently, the number of cSCC showing mutations in the *EGFR* gene is quite low (3%) (Mauerer et al., 2011). On the other hand, numerical aberrations of EGFR are detectable in 77% of cSCC

(Toll *et al.*, 2010). Interestingly, EGFR overexpression might be correlated with disease progression as metastatic tumors show stronger staining signal when compared to the primary counterparts (Shimizu *et al.*, 2001). Currently, the EGFR monoclonal antibody Cetuximab is in phase 2 in clinical trials for cSCC with promising results for patients with tumors that overexpress EGFR but lack RAS mutations. Indeed, the RAS mutation rate in cSCC is very low (Uribe and Gonzalez, 2011). Out of the three RAS forms in humans i.e. NRAS, KRAS and HRAS, the latter one is most frequently mutated in non-melanoma skin cancers (Pierceall *et al.*, 1991). Finally, EGFR phosphorylation in cSCC is frequently accompanied by an increase in phosphorylated forms of AKT and ERK1/2 (Rittie *et al.*, 2007). However, the importance of AKT and/or ERK1/2 for cSCC needs to be validated prior to clinical trials applying inhibitors of the respective proteins.

2.4. Crosstalk between Hedgehog and epidermal growth factor/epidermal growth factor receptor signaling in tumors

Interestingly and as already mentioned in section 2.2.5., several studies identified a cross-talk between EGFR and HH signaling. For example, a synergistic effect of both pathways was discovered in human keratinocytes and BCC (Schnidar et al., 2009). Thus, simultaneous activation of EGFR and HH signaling induced oncogenic transformation of the human keratinocyte HaCaT cell line. Furthermore, co-inhibition of EGFR with Gefitinib and GLI activity with GANT61 significantly reduced viability and proliferation of murine BCC cell lines (Schnidar et al., 2009). On the other hand, simultaneous incubation of the medulloblastoma cell line Daoy with HH and EGF inhibited the expression of canonical HH signaling target genes i.e. *PTCH*, *GLI1* and *HHIP*. The mechanism of this inhibition is unknown because HH plus EGF resulted in stabilization of GLI1 protein. Concomitantly, the authors found an extreme upregulation of typical EGF target genes involved in tumor promotion i.e. *VEGFA*, *MMP* and *IL-8*. Together, these data show that the knowledge about the interaction of EGF/EGFR and HH signaling in cancer is sparse. In addition, the data suggest that the interaction of EGF/EGFR and HH signaling is tumor type-specific and should be thoroughly studied for each single tumor entity.

3. Aim of the study

The aim of this thesis was to evaluate the role of canonical and putative noncanonical HH signaling in cSCC. For this purpose, *GLI1* as well as EGF, PI3K/AKT, MEK/ERK and mTOR activity was assessed in human tumor cSCC tissue samples as well as in cSCC cell lines.

To investigate the relevance of canonical and noncanonical HH signaling *in vitro*, changes in *GLI1* expression were measured upon treatment of cSCC cells with HH inhibitors (that inhibit the HH pathway at the level of SMO), specific inhibitors of PI3K, AKT, mTOR and MEK1/2 signaling pathways or with EGF and IGF1 ligands. In addition, cells were treated with EGF ligand in combination with the specific inhibitors in order to unravel the mechanism of the interaction between EGF signaling and its downstream effector pathways in *GLI1* regulation. Furthermore, the putative influence of the tumor microenvironment on *GLI1* expression within tumor cells was evaluated.

Finally, the impact of HH, PI3K/AKT, mTOR and MEK/ERK signaling on metabolic activity, proliferation and apoptosis of the cSCC cells was assessed. Moreover, the role of *GLI1* in proliferation of cSCC cell lines was elucidated by taking advantage of overexpression and a siRNA knockdown approach.

4. Materials

4.1. Technical equipment

Table 1: Laboratory equipment

Equipment	Supplier
Accu-jet	Brand GmbH & Co. KG, Wertheim
Agarose gel electrophoresis chamber	Peqlab Biotechnology GmbH, Erlangen
Arium® 611 VF water purification system	Sartorius, Göttingen
Autoclave (sanoclav)	W. Krannich GmbH & Co. KG, Göttingen
Autoclave (Systec DX-150)	Systec GmbH & Co. KG, Linden
Biophotometer (6131)	Eppendorf AG, Hamburg
Bunsen burner (Gasprofi 2 scs)	WLD-TEC GmbH, Göttingen
Centrifuges (Biofuge pico, fresco, primo, Multifuge 3LR)	Kendro Laboratory Products GmbH, Hanau, Germany
Digital Monochrome Printer P91D	Mitsubishi, Ratingen
Digital Photocamera (PowerShot G2)	Canon Deutschland GmbH, Krefeld
FACS Calibur	BD Biosciences GmbH, Heidelberg
Fluorchem Q	Fisher Scientific GmbH, Schwerte
Freezer (-20°C)	Liebherr GmbH, Ochshausen
Freezer (-80°C) (MDF-U71V)	Sanyo Electric Co., Ltd., Japan
Fridge (4°C)	Robert Bosch GmbH, Stuttgart
Heating block (Thermomixer)	Eppendorf AG, Hamburg
Heating stirrer (MR 3000/3001)	Heidolph Instruments, Schwabach
High-precision scales (Sartorius Basic plus)	Sartorius AG, Göttingen
Hybridization oven (HB-1000 Hybridizer)	UVP, Inc., Upland, USA
Inverted tissue culture fluorescence microscope (Axiovert 25)	Carl Zeiss Jena GmbH, Jena
Liquid nitrogen tank	L'air liquid S.A., Paris, France
Luminometer (Synergy Mx)	BioTek Instruments, Inc., Bad Friedrichshall
Mastercycler ep gradient S	Eppendorf AG, Hamburg

Microscope (Olympus BX 60)	Olympus Deutschland GmbH, Hamburg
Microtome (HN 40)	New Brunswick Scientific GmbH, Nürtingen, Germany
Microwave (Dimension 4)	Panasonic, Hamburg
Mini centrifuge	Carl Roth GmbH & Co. KG, Karlsruhe
Multipette	Eppendorf AG, Hamburg
Paraffin tissue floating bath	Medax GmbH & Co. KG, Rendburg
pH-meter (inoLab pH Level 1)	WTW GmbH, Vienna, Austria
Pipettes (one-channel)	Eppendorf AG, Hamburg
Power supply for electrophoresis	Peqlab Biotechnology GmbH, Erlangen
Real-Time PCR System (ABI Prism 7900HT)	Life Technologies GmbH, Darmstadt
Sequencer (ABI 3500 XL)	Life Technologies GmbH, Darmstadt
Scale (Sartorius Basic plus)	Sartorius AG, Göttingen
Spectrophotometer (NanoDrop 8000)	Thermo Scientific, Wilmington, USA
Shaker (Unimax 1010)	Heidolph Instruments GmbH & Co. KG, Schwabach
Stereo microscope (Stemi 2000)	Carl Zeiss Jena GmbH, Jena
Sterile bench (Euroflow class IIA)	Clean Air Techniek bv, Woerden, Netherlands
Thermocycler	Eppendorf, Hamburg
Thermoprinter (DPU-414)	Eppendorf AG, Hamburg
Trans-Blot SD semi-dry transfer cell	Bio-Rad Laboratories GmbH, Munich
UV transilluminator	Intas Science Imaging Instruments GmbH, Göttingen
Vacuum pump	Schütt Labortechnik, Göttingen, Germany
Vortexer-Genie 2	Scientific Industries, Inc., Woburn, USA
Water bath (1083)	GFL mbH, Burgwedel

4.2. Consumables

Table 2: List of consumable materials

Consumer good	Supplier
1.5 ml reaction tubes	Ochs GmbH, Bovenden/Lenglern
1.5 ml safeseal microtubes	Sarstedt AG & Co., Nürnberg
2.0 ml reaction tubes	Sarstedt AG & Co., Nürnberg
13 ml falcon tubes	Sarstedt AG & Co., Nürnberg
15 ml falcon tubes	Greiner Bio-One GmbH, Frickenhausen
50 ml falcon tubes	Greiner Bio-One GmbH, Frickenhausen
6-well tissue culture plate	Sarstedt AG & Co., Nürnberg
24-well tissue culture plate	Corning Inc., Corning, USA
96-well assay plate (transparent)	Costar, Corning Incorporated, Corning,
96-well assay plate (black)	Life Technologies GmbH, Darmstadt
384-well PCR plate (Framestar)	4titude Ltd., Berlin
BD DiscarditTM II (2, 10, 20 ml)	BD Biosciences GmbH, Heidelberg
BD Microfine + Demi	BD Biosciences GmbH, Heidelberg
BD Plastipak	BD Biosciences GmbH, Heidelberg
BD Plastipak 1 ml Sub-Q	BD Biosciences GmbH, Heidelberg
Blotting paper (GB 33 B003)	Heinemann Labortechnik GmbH,
Cell culture dishes (100 mm) (Nuclon)	Nunc GmbH & Co.KG, Wiesbaden
Cell culture inserts, 24 well, 0.4 μm	Corning Inc., Corning, USA
Cell scraper	Sarstedt AG & Co., Nürnberg
Cell strainers (70 μm)	BD Biosciences GmbH, Heidelberg
Combitips (0.2, 0.5, 2.5, 5, 10, 25, 50 ml)	Eppendorf AG, Hamburg
Coverslips	Menzel GmbH & Co.KG, Braunschweig
CryoPure tubes	Sarstedt AG & Co., Nürnberg
Cuvettes (UVette)	Carl Roth GmbH & Co. KG, Karlsruhe
Filter tips (10 μl)	Sarstedt AG & Co., Nürnberg
Filter tips (100 μl, 200 μl, 1000 μl)	Kisker Biotech GmbH & Co. KG, Steinfurt

Flow cytometry tube	Sarstedt AG & Co., Nürnberg
Fluted filters	Sartorius AG, Göttingen
Glassware	Schott AG, Mainz
Hyperfilm ECL	Amersham Biosciences Europe GmbH,
Microspin G-50 Columns	GE Healthcare Europe GmbH, Freiburg
Milliporefilter (Nuclepore Track-Etch)	Whatman GmbH, Dassel
Miscroscope slides (SuperFrost Plus)	Menzel GmbH & Co.KG, Braunschweig
Neubauer counting chamber	Brand GmbH & Co KG, Wertheim
Nitrocellulose membrane (Hybond ECL)	GE Healthcare Europe GmbH, Freiburg
NuPAGE Novex 4 – 12% Bis-Tris Midi Gel	Invitrogen GmbH, Karlsruhe
NuPAGE Novex 3-8% Tris-Acetate Midi	Invitrogen GmbH, Karlsruhe
Nylonmembran: Hybond-XL	GE Healthcare Europe GmbH, Freiburg
Pasteur pipettes	Brand GmbH & Co.KG, Wertheim
Petri dishes	Ochs GmbH, Bovenden/Lenglern
Pipette tips (10 µl, 200 µl)	Ochs GmbH, Bovenden/Lenglern
Pipette tips (20 µl, 1000 µl)	Sarstedt AG & Co., Nürnberg
QPCR Adhesive Clear Seal	4titude Ltd., Berlin
Scalpel blade #10, #24	Aesculap AG & Co.KG, Tuttlingen
Serological pipettes (2 ml, 5 ml, 10 ml, 25	Sarstedt AG & Co., Nürnberg
SOC Medium	Invitrogen GmbH, Karlsruhe
Sterile filter	Omnilab-Krannich, Göttingen
Syringe (30 ml, 50 ml)	Terumo Medical Corp., Elkton, MD, USA

4.3. Reagents and chemicals

The chemicals or reagents that are not listed below were purchased from AppliChem GmbH, Darmstadt, Carl Roth GmbH & Co. KG, Karlsruhe, or from Sigma-Aldrich Chemistry GmbH, Steinheim.

Table 3: List of chemicals and reagents

Chemicals and reagents	Supplier
Acetic acid	Carl Roth GmbH & Co. KG, Karlsruhe
Acetic acid anhydride	Carl Roth GmbH & Co. KG, Karlsruhe
Agarose	Bio-Budget Technologies GmbH, Krefeld
Ampuwa	Fresenius Kabi Deutschland GmbH, Bad Homburg
AnnexinV-FITC	BD Biosciences GmbH, Heidelberg
BM Purple substrate	Roche Diagnostics GmbH, Mannheim
Boric acid	MP Biomedicals LLC, Illkirch, France
Bovine serum albumin (BSA)	Carl Roth GmbH & Co. KG, Karlsruhe
Chloroform	Carl Roth GmbH & Co. KG, Karlsruhe
Citric acid	Carl Roth GmbH & Co. KG, Karlsruhe
DAPI mounting medium	Vector Laboratories, Inc., Burlingame, CA, USA
Denhardt's solution, lyophilised powder (50x)	Carl Roth GmbH & Co. KG, Karlsruhe
Deoxyribonucleotide triphosphate (dNTP)	Roche Diagnostics GmbH, Mannheim
Diethyl pyrocarbonate (DEPC)	Carl Roth GmbH & Co. KG, Karlsruhe
Dextransulphat	Carl Roth GmbH & Co. KG, Karlsruhe
Dithiothreitol, 100 mM (DTT)	Invitrogen GmbH, Karlsruhe
DNA ladder (100 bp plus)	Fermentas GmbH, St. Leon-Rot
DNase/RNase-free water	GIBCO Invitrogen GmbH, Karlsruhe
Eosin Y	Merck KGaA, Darmstadt
Ethanol (EtOH) 99%	J.T. Baker B.V., Deventer, Netherlands
Ethanol (EtOH) 99% denatured	CVH Chemie-Vertrieb GmbH & Co. Hannover KG, Hannover
Ethidium bromide (0.07%)	inna-TRAIN-Diagnostics, Kronberg
Ethylenediaminetetraacetic acid (EDTA)	ICN Biochemicals Inc., Aurora, USA
Formamide	Acros Organics b.v.b.a, Geel, Belgium

Formamide	Carl Roth GmbH & Co. KG, Karlsruhe
Glutaraldehyde solution 25%	Merck KGaA, Darmstadt
Glycergel mounting medium	Dako GmbH, Hamburg
Haematoxylin, Mayer's	Medite GmbH, Burgdorf
Hydrogen peroxide	Carl Roth GmbH & Co. KG, Karlsruhe
I-Block	Tropix, Bedford, USA
Levamisole	Merck KGaA, Darmstadt
Liquid Barrier Marker	Carl Roth GmbH & Co. KG, Karlsruhe
Methanol	Carl Roth GmbH & Co. KG, Karlsruhe
Milk powder	Carl Roth GmbH & Co. KG, Karlsruhe
NuPAGE MES SDS Running Buffer, 20x	Invitrogen GmbH, Karlsruhe
NuPAGE Tris-Acetate SDS Running Buffer, 20x	Invitrogen GmbH, Karlsruhe
Orange G	Carl Roth GmbH & Co. KG, Karlsruhe
Paraformaldehyde	Carl Roth GmbH & Co. KG, Karlsruhe
PBS-Tablets	GIBCO Invitrogen GmbH, Karlsruhe
Pertex mounting medium	Medite Medizintechnik GmbH, Burgdorf
Phosphatase inhibitor cocktail tablets (PhosSTOP)	Roche Diagnostics GmbH, Mannheim
Propidium Iodide (PI)	Miltenyi Biotec, Bergisch Gladbach
Protease inhibitor cocktail tablets (Complete, mini)	Roche Diagnostics GmbH, Mannheim
Random Hexamer-Oligonucleotides	Invitrogen GmbH, Karlsruhe
SeeBlue® Plus2 Pre-Stained Standard	Invitrogen GmbH, Karlsruhe
Triethanolamine	Merck KGaA, Darmstadt
Sodiumdodecylsulfate (SDS)	Carl Roth GmbH & Co. KG, Karlsruhe
Triton-X100	Merck KGaA, Darmstadt
TRIzol Reagent	Invitrogen GmbH, Karlsruhe
Tween-20	Scharlau Chemie S.A., Barcelona, Spain
Water soluble tetrazolium salt-1 (WST-1)	Roche Diagnostics GmbH, Mannheim

reagent	
Xylene	J.T. Baker B.V., Deventer, Netherlands
Yeast tRNA	Merck KGaA, Darmstadt

4.4. Enzymes

Table 4: List of enzymes

Enzyme	Supplier
Apa1	Invitrogen GmbH, Karlsruhe
BamH1	Invitrogen GmbH, Karlsruhe
Dispase	Corning Inc., NY, USA
EcoRI	Invitrogen GmbH, Karlsruhe
Hind III	Invitrogen GmbH, Karlsruhe
Kpn1	Invitrogen GmbH, Karlsruhe
Not1	Invitrogen GmbH, Karlsruhe
Proteinase K	Carl Roth GmbH & Co. KG, Karlsruhe
RNase A	Carl Roth GmbH & Co. KG, Karlsruhe
SuperScriptII Reverse Transcriptase	Invitrogen GmbH, Karlsruhe
T3-RNA Polymerase	Promega GmbH, Mannheim
T7-RNA Polymerase	Promega GmbH, Mannheim
Thermolysin	Sigma-Aldrich Inc., St. Louis, MO, USA
Xba1	Invitrogen GmbH, Karlsruhe

4.5. Kits and Ready-to-use reaction Systems

If not otherwise stated all kits and ready-to-use reaction systems were used according to the manufacturer's instructions.

Table 5: List of used kits and ready-to-use reaction systems

Reaction system	Supplier
Amersham ECL Plus™ Western Blotting Detection Reagents	GE Healthcare Europe GmbH, Freiburg
AnnexinV binding buffer (10 x)	BD Biosciences GmbH, Heidelberg

BigDye Terminator v3.1 Cycle Sequencing kit	Life Technologies GmbH, Darmstadt
Cell Proliferation ELISA, BrdU (chemiluminscent)	Roche Diagnostics GmbH, Mannheim
Dako EnVisionTM detection System	Dako Denmark A/S, Glostrup, Denmark
DIG RNA Labeling Mix	Roche Diagnostics GmbH, Mannheim
Dual-Luciferase® Reporter Assay System	Promega GmbH, Mannheim
HiPerFect transfection Reagent	Qiagen GmbH, Hilden
HiPure Plasmid DNA Purification Kit	Invitrogen GmbH, Karlsruhe
Pierce BCA Protein Assay kit	Fisher Scientific GmbH, Schwerte
Pierce ECL western blot substrate	Fisher Scientific GmbH, Schwerte
Platinum SYBR Green qPCR SuperMix	Invitrogen GmbH, Karlsruhe
Platinum SYBR Green qPCR SuperMix-UDG with ROX	Invitrogen GmbH, Karlsruhe, Germany
PureLink®HiPure Plasmid Midiprep	Invitrogen GmbH, Karlsruhe
Roti-Fect transfection reagent	Carl Roth GmbH & Co. KG, Karlsruhe
QuantiTect SYBR Green RT-PCR	Qiagen GmbH, Hilden
Taq-Polymerase (MolTaq)	Molzym GmbH & Co. KG, Bremen

4.6. Buffers and solutions

If not otherwise stated, all buffers and solutions were prepared using double distilled water (ddH$_2$O).

Table 6: List of buffers and solutions

Buffer	Composition
AEC chromogen, pH 5.2	70 mM Sodium acetate trihydrate 30 mM Acetic acid 16 mM 3-Amino-9 Ethylcarbazole in dimethylformamide
Blotting buffer	20% (v/v) Methanol 6% (w/v) Tris 3% (w/v) Glycine

	0,0375% (v/v) SDS
Boric acid, pH 5.1	0.2 M Boric acid
BSA/sodium azide solution	0.02% Sodium azide 2% BSA in PBST
Buffer 1	100 mM Tris/HCl pH 7.5 150 mM NaCl
Buffer 2	100 mM Tris/HCl pH 9.5 100 mM NaCl 50 mM $MgCl_2$
Buffer 3	10 mM Tris/HCl pH 8 1 mM EDTA
Casein (0.2%)	0.2% (w/v) I-Block 0.1% (v/v) Tween 20 in PBS
Citric acid buffer, pH 3.0	10 mM Sodium Citrate
Citric acid buffer, pH 6.0	10 mM Sodium Citrate
Cresol	0.1% (w/v) Cresol in saturated sucrose-solution
DEPC H_2O	0.1% DEPC in ddH_2O
dNTP-Mix	10 mM dATP 10 mM dCTP 10 mM dGTP 10 mM dTTP
EDTA, pH 8.0	0.5 M EDTA in DEPC-ddH_2O
Eosin solution	80% (v/v) EtOH 1% (w/v) Eosin y (water soluble)
Formamide/2x SSC	50% formamide, 2x SSC
Haematoxylin solution, Mayer's	5% (w/v) Potassium aluminum sulfate 5% (w/v) Trichloro acetaldehyde hydrate 1% (w/v) Citric acid 0.1% (w/v) Haematoxylin

	0.015% (w/v) Sodium iodate
Hybridization Buffer with tRNA (Hyb M)	10% dextrane sulfate
	50% formamide
	0.3 M NaCl
	20 mM Tris/HCl pH 8,0
	5 mM EDTA
	10 mM „NaPO$_4$"*
	1 x Denhardts solution
	0.5 mg/ml tRNA
	In RNase-free H$_2$O
Lysogeny broth medium (LB medium)	1% (w/v) bacto-tryptone
	0.5% (w/v) yeast extract
	1% (w/v) NaCl (pH7.0)
Lysogeny broth medium (LB-agar)	LB-medium
	1.5% (w/v) agar
Magnesium chloride (MgCl$_2$) - DEPC	1 M in DEPC-H$_2$O
MBSTL Buffer pH 7.5	100 mM maleic acid
	150 mM NaCl
	5.7 M NaOH
	0.1% Tween-20
	2 mM Levamisol
Modified RIPA buffer	50 nM Tris/HCl pH 7.4
	1% NP-40 0.25% Na-Deoxycholat
	150 mM NaCl
	1 mM EDTA
	1 protease inhibitor cocktail tablet per 10ml
	1 PhosSTOP tablet per 10ml
NT Buffer	0.15 M NaCl
	0.1 M Tris pH 7.5
NTMLT Buffer	100 mM NaCl
	100 mM Tris pH 9.5

	50 mM MgCl$_2$
	2 mM Levamisol
	0.1% Tween-20
Paraformaldehyde	4% (w/v) paraformaldehyde
	In PBS
PBS (cell culture)	1 PBS tablet in 500 ml ddH$_2$O
PBS-Tween 20 (PBST)	0.1% Tween-20 in PBS
PFA/glutaraldehyde	0.2% glutaraldehyde in 4% PFA
Phosphate buffered saline solution, 10 x, pH 7,4 (PBS, stock solution)	1.4 M NaCl
	27 mM KCl
	15 mM KH2PO4
	65 mM Na2HPO4
Proteinase K, pH 8.0	50 mM Tris/HCl
	5 mM EDTA
	10 mg/ml Proteinase K
Saline, 20 x	2.85 M NaCl in DEPC-H$_2$O
SSC 20 x, pH 6.4	3 M NaCl, 0.3 M Trisodium Citrate Dihydrate in DEPC-H$_2$O
SDS loading buffer, 6 x	35% (v/v) Glycerol
	9% (w/v) SDS
	8.5% (w/v) DTT
	0.1% (w/v) Bromphenolblue
	in Upper gel buffer
Sodium chloride (NaCl) - DEPC	5 M in DEPC-H$_2$O
STE Buffer	0.5 M NaCl
	10 mM Tris pH 8
	5 mM EDTA pH 8
STOP Buffer	1% SDS
	0.1 M Tris pH 8
	10 mM EDTA pH 8
	0.5% Orange G
Stripping Buffer	62.5 mM Tris pH 6.7

	2% SDS
	100 mM ß-Mercaptoethanol
Triethanolamin	0.8 M in ddH$_2$O
Tris pH 7.5; pH 8.0; pH 9.5	1 M Tris in DEPC H$_2$O
Tris-EDTA buffer pH 9.0; pH 8.0 (TE)	10 mM Tris
	1 mM EDTA
Tris-boric acid-EDTA solution, 10 x (TBE)	890 mM tris/HCl pH 8.0
	730 mM boric acid
	12.5 mM EDTA
Tris-buffered saline solution, 10 x (TBS)	0.5 M tris/HCl pH 7.4
	1.5 M NaCl
TBS-Triton X-100	0.1% Triton X-100 in TBS
TBS-Tween 20	0.1% (v/v) Tween-20 in TBS

*NaH$_2$PO$_4$ and Na$_2$HPO$_4$ were prepared at 0.5 M concentration, pH 8.0 and mixed as follows: 6,7 ml NaH$_2$PO$_4$ + 93,3 ml Na$_2$HPO$_4$ to prepare 10 mM „NaPO$_4$" solution.

4.7. Media

4.7.1. Media for culture of prokaryotic cells.

For cultivation of bacterial cells LB and LB-agar media were prepared as listed in Table 6. After autoclaving and cooling down, Ampicillin or Kanamycin were added at a concentration of 100 µg/ml or 50 µg/ml, respectively. Both, LB-agar plates and liquid LB medium were stored at 4°C.

4.7.2. Media and reagents for culture of eukaryotic cell.

Table 7: List of cell culture media and reagents

Medium or reagent	Supplier
Accutase	PAA Laboratories GmbH, Pasching
Amphotericin B	Sigma-Aldrich Inc., St. Louis, MO, USA
Dulbecco's Modified Eagle Medium (DMEM)	Gibco, Invitrogen GmbH, Karlsruhe
F-12 Nutrient Mixture (Ham) plus GlutaMAX	Gibco, Invitrogen GmbH, Karlsruhe

Fetal calf serum (FCS)	Gibco, Invitrogen GmbH, Karlsruhe
G 418 disulfate salt solution (50 mg/ml)	Sigma-Aldrich Chemistry GmbH, Steinheim
Gelatin	Sigma-Aldrich Chemistry GmbH, Steinheim
Hank's balanced salt solution (HBSS) without Ca^{2+} and Mg^{2+}	Gibco, Invitrogen GmbH, Karlsruhe
Human keratinocyte growth supplement (HKGS)	Gibco, Invitrogen GmbH, Karlsruhe
L-Glutamine	PAN Biotech GmbH, Aidenbach
Minimum essential medium, Non-essential Amino Acids (MEM NEAA)	Gibco, Invitrogen GmbH, Karlsruhe
Mitomycin C	Sigma-Aldrich Chemistry GmbH, Steinheim
Penicillin (10.000 U/ml)/Streptomycin (10 mg/ml) (P/S)	PAN Biotech GmbH, Aidenbach
RPMI 1640 (RPMI)	Gibco, Invitrogen GmbH, Karlsruhe
TrypLE Express	Gibco, Invitrogen GmbH, Karlsruhe
Trypsin-EDTA (0.05%, 0.25%)	Gibco, Invitrogen GmbH, Karlsruhe

4.8. Biological material

4.8.1. Bacterial strains

For the transformation protocol, the competent *Escherichia coli (E. coli)* strain DH5α was used.

4.8.2. Eukaryotic cell lines and primary cells

Eukaryotic cell lines used in this work are listed in Table 8.

Table 8: List of eukaryotic cells with corresponding media and supplements

Cell line	Description	Medium	Supplements	Reference
A-431	Epidermoid carcinoma cell line	DMEM (+++)	10% FCS, 1% P/S	ATCC® CRL-1555™
B9	Murine adult fibroblasts cell line	DMEM (+++)	10% FCS, 1% P/S	(Nitzki, 2008)
HaCaT	Human keratinocyte cell line	DMEM (+++)	10% FCS, 1% P/S	(Boukamp *et al.*, 1988)
HaCaT-ras II-4	HaCaT cells transfected with Ras oncogene, resemble human cSCC phenotype	DMEM (+++)	10% FCS, 1% P/S	(Boukamp *et al.*, 1990)
HEK293	Human embryonic kidney cell line	DMEM (+++)	10% FCS, 1% P/S	ATCC LGC Promochem, Wesel; CRL1573
HEK293-Shh	HEK293 cells secreting Shh-N	DMEM (+++)	10% FCS, 1% P/S	(J. K. Chen *et al.*, 2002b)
MCF-7	Breast cancer cell line	DMEM (+++)	10% FCS, 1% P/S	(Soule *et al.*, 1973)
MET-1	Human cSCC cell line, primary tumor	DMEM (+++)	10% FCS, 1% P/S	(Popp *et al.*, 2000)
MET-4	Human cSCC cell line, metastasis	DMEM (+++)	10% FCS, 1% P/S	(Popp et al., 2000)
MEFs	Mouse embryonic fibroblasts (E12.5)	DMEM (+++)	10% FCS, 1% P/S	-
NIH/3T3	Adult murine fibroblast cell line	DMEM (+++)	10% FCS, 1% P/S	ATCC LGC Promochem, Wesel; CRL-1658

Primary human fibroblasts	-	DMEM (+++)	10% FCS, 1% P/S	-
Primary human keratinocytes	-	DMEM (+++) + F-12 Nutrient Mix (3:1)	10% FCS, 1% P/S, 1% Amphotericin B, 1% HKGS	-
SCC-12	Human cSCC cell line	DMEM (+++)	10% FCS, 1% P/S	(Rheinwald and Beckett, 1981)
SCC-13	Human cSCC cell line	RPMI	10% FCS, 1% P/S, 2 mM L-Glutamine, 1% NEAA	(Rheinwald and Beckett, 1981)
SCL-I	Human cSCC cell line	RPMI	10% FCS, 1% P/S, 2 mM L-Glutamine, 1% NEAA	(Boukamp *et al.*, 1982)
SCL-II	Human cSCC cell line	RPMI	10% FCS, 1% P/S, 2 mM L-Glutamine, 1% NEAA	(Tilgen *et al.*, 1983)

4.8.3. Mouse lines

C57BL/6N inbred mice were bred in house and used for MEFs isolation. All the experiments were done in compliance with ethical and legal regulations.

4.8.4. Patient samples

Patient skin samples were obtained from the breast reduction surgery performed in the Evangelical Hospital Goettingen-Weende in the Plastic, Aesthetic and Reconstructive Surgery Department. All experiments were done in compliance with ethical and legal regulations (23/4/13). All patients signed a written consent.

4.9. Synthetic oligonucleotides

4.9.1. Synthetic DNA-oligonucleotides

All synthetic DNA-oligonucleotides were purchased from Eurofins MWG Operon. 100 µM stock and 10 µM working solutions were prepared with ddH$_2$O and stored for a long term at -80˚C or for a short term at -20 ˚C.

Table 9: List of synthetic DNA-oligonucleotides used for qPCR

Transcript	Primer name	Primer sequence (5'-3')	Control cDNA
18S	18S forw 18S rev2	CGCAAATTACCCACTCCCG TTCCAATTACAGGGCCTCGAA	Mouse embryo E12.5
hEGF	hEGF F hEGF R	GAGGTTCTGTCCACATTAGT GTGCAAGTGGATGCACTACTT	MCF-7
hEGFR	hEGFR F hEGFR R	AAGGAGCTGCCCATGAGAAAT ATTGGGACAGCTTGGATCACA	MCF-7
mGli1	mGli1-tq-f mGli1-tq-r	TACATGCTGGTGGTGCACATG ACCGAAGGTGCGTCTTGAGG	Mouse embryo E12.5
hGLI1	hsaGLI1 tq F hsaGLI1 tq R	AGCTACATCAACTCCGGCCA GCTGCGGCGTTCAAGAGA	RMS-13
hGLI2	hsGli2F.1 hsGli2R.1	AAGCCCTTCAAGGCGCAGTA TCGTGCTCACACACATATGGCTT	RMS-13
hGLI3	hsGli3F.1 hsGli3R.1	GCCAGCGCAGCCCCTAT CGGCCTGGCTGACAGCCT	RMS-13
hIGF1	hIGF1-F hIGF1-R	GCTGAGCTGGTGGATGCTCTT AGATCACAGCTCCGGAAGCA	RUCH-2
hIGF1R	hIGF1R-F hIGF1R-R	GAGTACAACTACCGCTGCTG TACACAGGCCGTGTCGTTGT	RMS-13
hHPRT	HPRT F HPRT R	GCTGGTGAAAAGGACCTCT CACAGGACTAGAACACCTGC	RMS-13

hSMO	hSMO-F1	CAAGAACTACCGATACCGTGC	RMS-13
	hSMO-R1	AGCATGGTCTCGTTGATCTTGC	
hSHH	hSHH F	CAGCGACTTCCTCACTTTCC	MET-4
	hSHH R	GGAGCGGTTAGGGCTACTCT	
hPTCH	hsPtc1F.2	GAGGTTGGTCATGGTTACATGGA	RMS-13
	hsPTC1R.2	TGCTGTTCTTGACTGTGCCACC	

Table 10: List of synthetic DNA-oligonucleotides used for sequencing PCR

Transcript	Primer name	Primer sequence
mTOR	mTOR-seq-F	GCCATCCTCTGGCATGAGAT
	mTOR-seq-R	AATGACGGCGTATCTCTGGAT

4.9.2. Preparation of riboprobes

Riboprobes were synthesized in RNase-free conditions. All probes were diluted in 50% formamide/RNase-free H_2O, aliquoted and stored at -80˚C.

For *hGLI1* mRNA detection, 2 different riboprobes were designed, one recognizing 5' end (hGLI1 5') and the other one detecting 3´end (hGLI1 3') of *hGLI1* mRNA to increase the efficiency. Both probes were used in combination.

Table 11: List of synthetic RNA-oligonucleotides (riboprobes) used for ISH

Gene	Plasmid template	Probe orientation	Polymerase	Dilution
hGLI1 5'	pBS-hGli1 5' (#26)	Sense	T7	1:500
		Anti-sense	T3	1:500
hGLI1 3'	pBS-hGli1 3' (#27)	Sense	T7	1:500
		Anti-sense	T3	1:500

4.10. siRNA

siRNAs used in this study are listed in Table 12.

Table 12: List of siRNA

siRNA	Target sequence	Supplier
GLI1 (ON-TARGETplus SMARTpool)	GCAAAUAGGGCUUCACAUA AGGCUCAGCUUGCUUGUGUGUAA GGACGAGGGACCUUGCAUU CAGCUAGAGUCCAGAGGUU	Dharmacon
MAPK1	AATGCTGACTGGAAACGTCTG	Qiagen
Scrambled siRNA (AllStars negative)	proprietary	Qiagen

4.11. Plasmids

The plasmids listed below were used for the chemical transfection of eukaryotic cell lines.

Table 13: Plasmids used for transfection of eukaryotic cells

Plasmid name	Application	Reference or supplier
9xGli BS	Gli reporter assay (plasmid contains firefly luciferase under control of Gli1 responsive elements)	(Beer *et al.*, 2003)
HA-Akt-DN (K179M)	blocking the function of endogenous AKT	(B. P. Zhou *et al.*, 2000a), Addgene (plasmid # 16243)
myrAkt delta4-129	overexpression of AKT	(Kohn *et al.*, 1996; H. Zhou et al., 2000b), Addgene (plasmid # 10841)
pcDNA3	control plasmid for AKT overexpression	Invitrogen
pcDNA3-AU1-mTOR-S2215Y	overexpression of constitutively active mTOR	(Sato *et al.*, 2010), Addgene (plasmid #

		26037)
pcDNA3-Flag mTOR S2035T	overexpression of rapamycin resistant mTOR	(Vilella-Bach *et al.*, 1999), Addgene (plasmid # 26605)
pcDNA3-Flag mTOR wt	overexpression of WT mTOR	(Vilella-Bach et al., 1999), Addgene (plasmid # 26603)
pcDNA4/TO	control plasmid for *GLI1* overexpression	Qiagen Inc., Valencia, CA, gift from Prof. Fritz Aberger
pcDNA4NLSMT-Gli1	overexpression of human *GLI1*	gift from Prof. Fritz Aberger
pCR3.1	Gli reporter assay, Gli1 overexpression	Invitrogen GmbH, Karlsruhe
pCR 3.1-mGli1	positive control for Gli reporter assay	(Fritsch, 2014)
pEGFP-N1	transfection efficiency control	BD Bioscience Clontech, Heidelberg
pGL-TK	Gli reporter assay, positive control (plasmid contains firefly luciferase under constitutively active promoter)	Promega GmbH, Mannheim
pRL-CMV	Gli reporter assay, internal control (plasmid contains Renilla luciferase under constitutively active promoter)	Promega GmbH, Mannheim
pRK7-hSMO-WT	overexpression of WT SMO	Gift from Prof. Rune Toftgard
pRK7-SMO-M2	overexpression of constitutively active SMO variant	Gift from Prof. Rune Toftgard

4.12. Synthetic inhibitors and agonists

Table 14: List of inhibitors and agonists used in cell culture system

Inhibitor	Solvent	Concentration	Supplier
Cyclopamine	EtOH	1-10 µM	Sigma-Aldrich, Steinheim
EGF	0.1% BSA/10 mM acetic acid	100 ng/ml	R&D Systems, Inc., Minneapolis, MN, USA
Everolimus	EtOH	50 nM	Sigma-Aldrich, Steinheim
GANT61	DMSO	5-30 µM	Sigma-Aldrich, Steinheim
GDC-0449 (Vismodegib)	DMSO	10-60 µM	Selleckchem, Munich
GDC-0941	DMSO	10 µM	Genentech, San Francisco, USA
HhA (HhAntag691)	DMSO	10-60 µM	Genentech, San Francisco, USA
MK-2206	DMSO	5 µM	Selleckchem, Munich
PI103	DMSO	3-6 µM	Axxora Deutschland GmbH, Lörrach
Rapamycin	DMSO	100 nM	Calbiochem, Merck KGaA, Darmstadt
Recombinant human IGF protein	PBS	50 ng/ml	R&D Systems, Inc., Minneapolis, MN, USA
SAG (SMO agonist)	DMSO	10 nM – 1 µM	Cayman chemicals, Ann Arbor USA
UO126	DMSO	20 µM	Cell signaling, Danvers, MA, USA

4.13. Antibodies

Table 15: List of neutralizing antibodies used in cell culture experiments

Antibody	Dilution	Supplier
Human EGFR, clone LA1	10 µg/ml	Merck Millipore
Human IGF-IR, clone #33255	10 µg/ml	R&D Systems, Inc

Table 16: List of primary antibodies used for IHC

Target protein	Host	Dilution	Antigen retrieval	Supplier
Digoxigenin/AP Fab fragments*	Sheep	1:5000	-	Roche 11 093 274 910
pAKT (Ser473)	Rabbit, monoclonal	1:50	Citric acid, pH 6.0	Cell Signaling #4060
p44/42 MAPK (Erk1/2)	Rabbit, monoclonal	1:400	Citric acid, pH 6.0	Cell Signaling, #9101
pS6 (Ser240/244)	Rabbit, polyclonal	1:200	Citric acid, pH 6.0	Cell Signaling
GLI2	Rabbit, polyclonal	1:200	Citric acid, pH 6.0	LS Bioscience, LS-B2808
SHH	Rabbit, polyclonal	1:100	Citric acid, pH 6.0	Abcam, ab73958
Human EGF	Mouse, monoclonal	1:40	Boric acid	R&D System

*This Fab fragments from polyclonal anti-digoxigenin antibodies, conjugated to alkaline phosphatase, was used in ISH to detect digoxigenin-labelled RNA

Table 17: List of primary antibodies used for Western Blot

Target protein	Host	Dilution	Supplier
AKT	Mouse, monoclonal	1:1000	BD Bioscience, 610861
Flag M2	Mouse, monoclonal	1:1000	Sigma Aldrich Chemistry GmbH, Steinheim
HA tag	Rat, monoclonal	1:500	Sigma Aldrich Chemistry GmbH, Steinheim
HSC70	Mouse, monoclonal	1:5000	Santa Cruz, sc-7298
MAP Kinase (ERK1, ERK2)	Rabbit, polyclonal	1:1000	Sigma Aldrich Chemistry GmbH, Steinheim
pAKT Ser473	Rabbit, monoclonal	1:1000	Cell Signaling, 193H12

p44/42 MAPK (Erk1/2)	Rabbit, polyclonal	1:1000	New England Biolabs GmbH, Frankfurt am Main
pS6 (Ser240/244)	Rabbit, polyclonal	1:1000	Cell Signaling
S6	Mouse, monoclonal	1:1000	Cell Signaling, 54D2

Table 18: List of secondary antibodies for IHC and Western Blot

Antibody	Host	Dilution	Supplier
Anti-Mouse/HRP	Sheep, polyclonal	1:5000	GE Healthcare, NA931
Anti-Rabbit/HRP	Goat, polyclonal	1:5000	Sigma-Aldrich, A0545
Anti-Rat/HRP	Goat, polyclonal	1:400	Dianova
Dako Envision/HRP (anti-mouse/rabbit)	-	1:1 in TBS	Dako

4.14. Software

Table 19: Software used for data analysis

Name	Developer
AlphaView Q SA 3.2.2	Cell Bioscience, California, USA
CellSens Dimension	Olympus GmbH, Hamburg
Endnote X5	Thomson ISI ResearchSoft, California, USA
FlowJo	Tree Star Inc., Oregon, USA
GraphPad Prism 6	GraphPad Software, Inc., La Jolla, CA, USA
Gen5 1.11	BioTek Instruments, Inc., Bad Friedrichshall
Microsoft Office	Microsoft Co., Redmont, USA
SDS 2.2	Applied Biosystems, Darmstadt

4.15. Databases

Table 20: Databases

Database	Webpage
Basic Local Alignment Search Tool_BLAST (NCBI)	http://blast.ncbi.nlm.nih.gov/Blast.cg
COSMIC	http://cancer.sanger.ac.uk/cosmic
Ensembl	http://www.ensembl.org/index.html
National Center for Biotechnology Information	http://www.ncbi.nlm.nih.gov/
Reverse complement	http://www.bioinformatics.org/sms/rev_comp.html
The Human Protein Atlas	http://www.proteinatlas.org

5. Methods

5.1. Molecular biology methods

5.1.1. RNA isolation

Total RNA was isolated from cultured eukaryotic cells using TRIzol reagent according to the manufacturer's instructions. If not otherwise stated the entire procedure was performed on ice to maintain RNA integrity and avoid its degradation. Briefly, cells were washed once with PBS and 1 ml of TRIzol was added to the cells. Cell suspension was transferred to RNase-free 2.0 ml reaction tubes and vortexed for 2 min at the highest speed. After 5 min of incubation at room temperature (RT) 200 µl of chloroform was added to each sample and vortexed for 15 sec. To separate less dense aqueous phase containing RNA from heavier organic phase samples were incubated at RT for 3 min and then centrifuged for 10 min at 4°C with the speed of 13.000 rpm. Afterwards, the upper aqueous phase (~450-500 µl) was transferred into new RNase-free 1.5 ml reaction tube and gently mixed with equal amount of ice-cold 100% isopropanol by inverting. Remaining organic and protein phases were discarded. Precipitation of RNA was performed overnight (O/N) at -20°C and accomplished by centrifugation (10 min, 13.000rpm, 4°C). Obtained RNA pellets were washed twice with 1 ml of ice-cold 70% ethanol (EtOH), each round followed by centrifugation (15 min, 13.000 rpm, 4°C). Finally, RNA was dried at 56°C for 2-5 min, resuspended in desired amount of DNase/RNase-free water (10-30 µl) and stored at -80°C.

5.1.2. Photometric quantification of nucleic acids

DNA and RNA concentration was assessed using spectrophotometer (NanoDrop 8000). 1 µl of undiluted sample was loaded into the instrument and optical density at 260 nm (OD_{260}) and 280 nm (OD_{280}) was measured to determine nucleic acid concentration and sample purity, respectively. Since OD_{260} equal to 1.0 corresponds to 50 µg/ml of pure DNA and 40 µg/ml of RNA, the final concentration was calculated according to the formula below:

Concentration (µg/ml) = OD_{260} x 50 (for DNA) or x 40 (for RNA).

Additionally, OD_{280} was measured to determine protein content in the sample and the ratio between OD_{260} and OD_{280} (OD_{260}/OD_{280}) was calculated to assess the purity of isolated

nucleic acids. All samples with OD_{260}/OD_{280} ~1.8 (for DNA) and ~2.0 (for RNA) were considered as pure.

5.1.3. Reverse transcription (cDNA synthesis)

cDNA was reverse-transcribed from 2 µg of RNA diluted with RNase/DNase-free water to the volume of 7 µl. Each RNA sample was incubated with 250 ng of random hexamers for 10 min at 70°C to allow binding of complementary sequences. Subsequently, 0.5 mM deoxynucleotides (dNTPs) and 10 mM dithiothreitol (DTT) in 1st strand buffer were added to reaction tubes and incubated at RT for 10 min. Reverse transcription was performed using 100U of SuperScript II reverse transcriptase for 1 h at 42°C in the final reaction volume of 20 µl. Finally, the enzyme was inactivated by the incubation at 70°C for 10 min and obtained single stranded cDNA was stored at -20°C. Based on the common assumption that the reaction efficiency is ~50% the concentration of synthesized cDNA was ~50 ng/µl.

5.1.4. Quantitative polymerase chain reaction (qPCR)

Quantity of target gene expression was assessed using the fluorescently labeled, double-strand DNA intercalating dye SYBR Green. The reaction was performed in a volume of 10 µl using the components listed below:

SYBR Green (Qiagen or Invitrogen)	4 µl
Forward primer	0.4 µM (in 0.4 µl ddH$_2$O)
Reverse primer	0.4 µM (in 0.4 µl ddH$_2$O)
ddH$_2$O	3.2 µl
cDNA template	50 ng (0.35 pg for *18S*)

Each PCR reaction was performed in 40 cycles, each composed of 3 or 2 major steps depending on the SYBR Green used:

Table 21: Thermal profile of qPCR reaction

	SYBR Green (Qiagen)	SYBR Green (Invitrogen)
Denaturation	95°C; 15 sec	95°C; 15 sec
Annealing of specific primers	60°C; 30 sec	72°C; 1 min
Elongation of the product	72°C; 30 sec	

The specific primers used to amplify target genes are listed in the Table 9. At the end of every reaction a melting curve was generated to assess the specificity of the product.

Quantity of the gene expression was calculated using the standard curve method. Thus, cDNA from cell line or tissue known to express the gene of interest served to prepare serial 5-fold dilutions starting from a concentration of 10 ng/µl for all transcripts and also for the housekeeper *HPRT*. For the *18S* housekeeping gene the first concentration equaled 35 pg/µl. Based on the logarithm of the cDNA amount plotted against the cycle threshold values for each dilution, a trendline with corresponding formula (y=mx+b) was established and served to interpolate the cDNA content in each sample. The final transcript expression was normalized to *18S* and *HPRT*. All qPCR assays were performed in 3 biological replicates, each based on 3 technical replicates. Obtained data were analyzed using SDS 2.2.1, Microsoft Excel 2010 and GraphPad Prism 6.

5.1.5. Sequencing PCR

DNA nucleotide sequence was determined by the Sanger sequencing method. The reaction was based on Big Dye 3.1 (BD) and the corresponding BigDye buffer. The primers used for sequencing PCR are listed in Table 10.
The reaction reagents were as follow:

BigDye 3.1	1 x
BigDye Buffer	1 x
Primer	100 pmol
ddH$_2$O	up to 10 µl
pDNA	100 ng

The reaction was performed in 30 cycles in ABI3500XL sequencing device. The thermal profile for each reaction was as follows:

95°C	1 min	
95°C	30 sec	} 30 x
60°C	2.5 min	
60°C	5 min	
8°C	∞	

Obtained electropherograms and the nucleotide sequences were analyzed manually.

5.1.6. *E.coli* transformation

For transformation with plasmid DNA (pDNA), the competent DH5α *E.coli* that were stored in 50 µl aliquots at -80°C, were thawed on ice and gently mixed with 100 ng of pDNA. This mixture was incubated on ice for 20 min and subsequently subjected to a heat shock at 42°C for 45 sec. Afterwards bacteria were cooled down on ice for 2 min, mixed with 500 µl of super optimal broth with catabolite repression (S.O.C.) medium and incubated at 37°C for 1 h with 900 rpm shaking. In the end, 50 µl of the mixture containing transformed bacteria were plated on lysogeny broth (LB) agar plates containing the desired antibiotics (Ampicillin or Kanamycin) and incubated O/N upside down in a 37°C incubator. Single colonies were subsequently used for pDNA amplification and isolation.

5.1.7. Plasmid DNA amplification, isolation and purification

Single bacterial colonies transformed with desired plasmids were incubated O/N in 100 ml of LB medium with desired antibiotics in the concentration of 100 µg/ml or 50 µg/ml Ampicillin or Kanamycin. Plasmid purification (medium-scale) was performed using PureLink®HiPurePlasmid Midiprep according to the manufacturer's instruction. Briefly, the O/N culture was transferred into 50 ml falcon tubes and centrifuged at 10,000 rpm, 4°C for 10 min. The supernatant was discarded and the cell pellet was resuspended in 4 ml of ice cold Resuspension Buffer (R3) using a plastic transfer pipette. To lyse the cells, 4 ml of Lysis Buffer (L7) was added and mixed gently by inverting. Next, the suspension was again centrifuged with the same settings to discard cell debris. In the meantime, HiPure Midi Columns were equilibrated with 10 ml of Equilibration Buffer (EQ1) to optimize the affinity

of the columns to bind pDNA. Afterwards, the supernatant from the second centrifugation was applied to the equilibrated column and was drained by gravity flow. pDNA bound to the resin columns was then washed with 20 ml of Washing Buffer (W8) and finally eluted into 15 ml falcon tubes with 5 ml of 37°C pre-warmed Elution Buffer (E4). Obtained pDNA solution was then mixed with 3.5 ml of ice cold 100% isopropanol by inverting and incubated O/N at -20°C to allow precipitation. The next day, pDNA was pelleted by 30 min centrifugation at 4°C, 13,000 rpm and subsequently washed twice with 70% ethanol followed by centrifugation under the same conditions. Finally, DNA pellets were dried at 56°C for 2-3 min, resuspended in 100 µl of RNase/DNase-free water at thermomixer for 10 min and stored at -20°C.

5.1.8. Restriction enzyme hydrolysis

Diagnostic restriction hydrolysis was performed to verify plasmid size and insert orientation. In all settings two restriction enzymes known to cut the plasmid backbone at two sites but not the insert were chosen. For each reaction, buffers with different salt concentration were used according to the manufacturer's recommendation. The general reaction mixture was as follows:

Buffer	1 x
pDNA	0.5 µg
enzyme	0.1 U
ddH$_2$O	up to 20 µl

Hydrolysis was performed for 1 h at 37°C and afterwards the enzymes were heat-inactivated by incubation at 70°C for 10 min. Digested DNA fragments were separated and analyzed by agarose gel electrophoresis. All restriction enzymes (listed in Table 4) and corresponding buffers were purchased from Invitrogen or NEB.

5.1.9. Gel electrophoresis

DNA size was determined by separation in the agarose gels in a constant electric field of 120V. Agarose concentration differed within the range of 0.5%-2% depending on the expected DNA size. All gels were prepared by boiling an appropriate amount of agarose diluted in 1 x TBE buffer in a microwave. 1-2 drops of 0.07% ethidium bromide were used as DNA intercalating dye to visualize the product in the UV transilluminator.

5.1.10. Generation of digoxigenin-labeled riboprobes

5.1.10.1. Amplification and digoxigenin labelling of the RNA probes

For the amplification of human riboprobes the plasmid containing the sequence of interest was linearized by restriction hydrolysis for 2 h at 37°C. The reaction components were as follows:

Plasmid	10 µg
Buffer (10 x)	1 x
Enzyme	30-45 U
RNase-free ddH$_2$O	up to 50 µl

The linearized pDNA was precipitated with 300 µl of 100% EtOH at -20°C. The next day pDNA was pelleted by 30 min centrifugation at 13,000 rpm, 4°C and washed with 70% EtOH as described above (section 5.1.7.). The pellet was resuspended in 20 µl of RNase-free H$_2$O. 1 µl of undiluted linearized pDNA as well as 1 µl of a 1:5 dilution were loaded on the agarose gel and subjected to gel electrophoresis.

The labelling and the amplification of the probes were performed using T7 or T3 polymerase for amplification of sense and antisense probe, respectively, in the presence of DIG RNA labelling mix containing DIG-11-UTP. The reaction mix was as follows:

Linearized plasmid	1 µg
DIG RNA labelling mix (10 x)	2 µl
Transcription buffer (5 x)	4 µl
DTT (100 mM)	2 µl
RNA polymerase (T7/SP6) 20 U/µl	1 µl
Rnase-free H$_2$O	up to 20 µl

The reaction was performed for 90 min at 30°C. Afterwards DNase was added to clear the product from DNA:

DNase Buffer (10 x)	4 µl
RQ1-DNase	2 µl (1U/1 µl)
RNase-free H$_2$O	4 µl

After 8 min of incubation at 37°C, the reaction was stopped with 10 µl of Stop-Buffer containing 0.5% Orange G.

To further purify the product, the probes were loaded on Sephadex columns placed in 1.5 ml reaction tubes and centrifuged for 2 min at 3,000 rpm. This step was repeated until the eluate containing the RNA probes was colorless. 1 µl of undiluted probe was loaded on an agarose gel along with linearized plasmids and another 2 µl of undiluted probes were used for Dot-Blot (see next section). Finally, stock solutions of the probes were prepared by diluting them in total volume of 200 µl RNase-free H_2O/50% formamide then aliquoted and stored at -80°C. Working solutions were prepared always freshly and were assessed for each probe separately based on the Dot-Blot results (see the section below).

5.1.10.2. Assessment of labeling efficiency – Dot-blot

To assess the efficiency of digoxigenin labeling the serial dilutions of the probes (S1-S6) were prepared in 6x SSC and loaded on a Nylon Membrane. The RNA was fixed on the membrane by short exposure to UV light at 125 mJ. Next, the membrane was blocked with 4% BSA/Buffer 1 warmed up to 55°C (see Table 6) for 5 min on a shaker. Then it was shortly washed in Buffer 1. Anti-Digoxigenin AP-conjugated antibody was diluted 1:5000 in Buffer 1 and applied to the membrane for 7 min. Unbound antibodies were washed away by incubation with Buffer 1, 3 times for 2 min and then for 3 min in Buffer 2. The colorimetric reaction was accomplished by adding BM Purple substrate. The reaction was stopped after 10-20 min by incubation in Buffer 3 and then in ddH$_2$O. The intensity of the staining resembled the labeling efficiency for each probe.

5.1.11. Protein isolation from cultured cells

To isolate proteins from cultured cells, cells were scraped off from the culture plate using a disposable cell scraper. The plate was additionally washed with 2 ml of PBS and the cell suspension was transferred into 15 ml falcon tubes. Cells were then collected by centrifugation at 4°C, 2,000 rpm for 5 min and subsequently washed with 500 µl PBS followed by a second round of centrifugation under the same conditions. Subsequently, the supernatant was discarded while cell pellets were snap-frozen in liquid nitrogen. After thawing, cells were lysed with 20-70 µl of modified RIPA lysis buffer for 30 min on ice. In

the final step, lysed cells were centrifuged at 13,000 rpm, 4°C for 30 min and the supernatant containing soluble proteins was transferred into new reaction tube and stored at -80°C.

5.1.12. Photometric quantification of proteins (BCA assay)

Protein concentration was measured using Pierce BCA protein kit according to the manufacturer's instruction. Briefly 1 µl of each protein sample was pipetted into a transparent 96-well plate in triplicates. Serial dilutions of BSA at known concentration served to build a standard curve. 200 µl of substrate was added to each well and the plate was incubated for 30 min at 37°C. Based on the absorbance at 540 nm measured with Synergy Mx Luminometer the final protein content was calculated using Microsoft Excel 2010.

5.1.13. Western Blot

Prior to Western Blot 30-60 µg of proteins were diluted in a final volume of 24 µl, mixed with SDS-containing loading buffer and denatured by incubation at 95°C for 5 min with shaking at the speed of 450 rpm. The denatured proteins and SeeBlue Plus2 Prestained Standard were loaded on Nu PAGE Novex 4-12% Bis-Tris Protein Gels or Tris-Acetate for separation of bigger proteins. The proteins were separated according to the size in 1 x NuPAGE MES SDS or Tris-Acetate SDS Running buffer in the electric field of 160 mA, 160 V, 100 W for 2 h. Afterwards, the proteins were transferred to a nitrocellulose membrane by semi-dry blotting at 120 mA, 20 V, 100 W for 1 h 30 min in Blotting Buffer (Table 6). Bigger proteins separated in Tris-Acetate gel and corresponding buffer were subjected to a wet-blot. The blotting chamber was filled with Blotting Buffer and the proteins were transferred to a membrane in the electric field of 100 V, 500 mA, 100 W for 2 h 30 min in the cold room. The scheme of "Blotting Sandwich" is presented below:

After all proteins were transferred to the membrane, the unspecific binding was blocked with 5% milk in PBST for 1 h at RT. Afterwards the membrane was washed 3 x 10 min with PBST and incubated O/N with primary antibody (Table 17) diluted in BSA-azide/PBST solution at

4°C. The next day, the unbound antibodies were washed away by 3 x 10 min incubation in PBST on the shaker at RT and the HRP-conjugated secondary antibody (Table 18) diluted in 5% milk in PBST was applied to the membrane for 1 h at RT. During the last 3 washing steps the signal detection substrate was prepared by mixing Substrate A with Substrate B from the ECL Detection Reagents System in a 1:1 ratio. After 3 min, the excess of the substrate was removed and the signal was detected with the Fluorchem Q Imaging System and analyzed with AlphaView Q SA 3.2.2.

5.1.14. Membrane stripping

To strip off bound proteins from the Nylon membrane used for Western Blotting, the membrane was incubated with Stripping Buffer (Table 6) for 30 min at 55°C. Afterwards the membrane was washed and blocked as described above and incubated with another primary antibody.

5.2. Cell biology methods

5.2.1. Culture of adherent cells

All cell lines as well as primary cultured cells were maintained in the incubator with a stable temperature of 37°C, 5% CO_2 and 95% humidity. Depending on the cell type different culture media were used as listed in Table 8. Cells were washed every second or third day with 1 x PBS under sterile conditions.

5.2.2. Passaging of adherent eukaryotic cell lines

Cells grown up to 80-90% confluency were washed with 1 x PBS and subsequently detached from the culture plate using 1-3 ml of TrypLe Express. After incubation for 2-10 min at 37°C, the enzymatic activity was stopped by adding an equal amount of serum-containing medium. Detached cells were collected in 15 ml or 50 ml falcon tubes and the culture plates were additionally washed with ~4 ml of 1 x PBS to remove all remaining cells. Cell suspension was then centrifuged at 300 xg, 4°C for 5 min and the pellets were resuspended in fresh culture medium. Finally, cells were counted in Neumeyer chamber and seeded in desired number and type of culture vessels.

5.2.3. Cryopreservation of eukaryotic cells

For cryopreservation, the cells were typically grown in 2-3 10 cm culture dishes until they reached ~90% confluency. Next, they were subjected to the same procedure as described above in the section 'passaging of adherent eukaryotic cells'. In the final step cell pellets were resuspended in fresh culture medium containing 1% DMSO as cryoprotectant. 1 ml aliquots were gradually frozen by incubation at -20°C for 2 h, at -80°C O/N and were then transferred into liquid nitrogen for long term storage.

To restore cells, they were thawed in a 37°C water bath and immediately transferred to a 15 ml falcon containing 9 ml of culture medium. Afterwards cells were pelleted, resuspended in fresh culture medium and seeded in 10 cm culture plate. The next day cells were washed with 1 x PBS to remove remaining DMSO and dead cells.

5.2.4. Generation of Shh-N conditioned medium

For a generation of Shh-N and respective control medium, stably transfected HEK293-Shh and non-transfected HEK293 cells were incubated in a serum-depleted medium (DMEM supplemented with 2% FCS and 1% P/S) to stimulate the release of soluble N-Shh to the medium. After 24 h the medium was collected and filtered through a 0.2 µm pore size disposable filters to remove any remaining cells. The medium could be stored at 4°C for up to 4 months and was tested prior use on Shh-responsive B9 cells.

5.2.5. Feeder layer preparation

Feeder layer needed for cultivation of primary keratinocytes was prepared by isolation and inactivation of mouse embryonic fibroblasts (MEFs).

5.2.5.1. Isolation and cultivation of mouse embryonic fibroblasts

To obtain MEFs, 5 C57/B6 mice were superovulated with PMSG/hCG gonadotropins and mated. Obtained embryos were isolated from the uterus at the embryonic day E12.5. Single embryos were taken out of the yolk sack and placed in 37°C warm PBS in Petri dish. Using forceps, the head, limbs, tail and all the organs were removed under the binocular while the remaining embryo core was placed in a fresh Petri dish and cut into small pieces using scalpel or scissors. Such prepared embryos were placed in 0.05% trypsin (1 ml of trypsin per embryo)

in a flat-bottom flask containing sterile glass beads and magnetic stirrer. The suspension was then incubated at 37°C on a magnetic plate and stirred with a speed of ~300 rpm for exactly 5 min. After this time, trypsin was neutralized with FBS-containing DMEM (2 ml DMEM/1 ml trypsin) and the cells were distributed into desired number of T75 flasks (8-10 ml of cell suspension per flask). After 3-4 h cells were thoroughly washed with PBS to remove trypsin and larger tissue pieces. Cells were expanded by passaging whenever they reached 80-90% confluency and either frozen (see above) or inactivated with Mitomycin C at the passage P4, the latest.

5.2.5.2. Fibroblast inactivation with mitomycin C

90-95% confluent cells were thoroughly washed with PBS and incubated with medium containing Mitomycin C at a concentration of 10 µg/ml. After 3 h, inactivating medium was removed, cells were washed with 1 x PBS, frozen and stored in liquid nitrogen or used for further experiments.

5.2.6. Isolation and cultivation of primary keratinocytes from human skin

The entire procedure of keratinocytes isolation was performed as described in Nature Protocols (Aasen and Izpisua Belmonte, 2010).

Human skin was obtained from breast reduction surgery and cut into ~1.5 x 1.5 cm pieces using a sterile scalpel. Small pieces were then placed with the epidermal side up in a sterile 60 mm Petri dish filled with 5-6 ml of HBSS supplemented with 1% P/S and dispase to digest the tissue. The enzymatic reaction was carried out O/N (12-16 h) at 4°C. The next day the thin epidermal layer was peeled off from the dermis using forceps and placed in a fresh 60 mm Petri dish containing HBSS with antibiotics. The dermal part was preserved in HBSS with antibiotics at 4°C for fibroblasts isolation (see below). The epidermis was then cut into smaller pieces using a disposable scalpel and transferred into a 50 ml Falcon tube containing 20 ml of HBSS supplemented with 1% P/S and thermolysin. The suspension was incubated for 45 min at 37°C and mixed gently by shaking every 10 min. Subsequently, the thermolysin was inactivated with HBSS containing 10% FCS and 1% P/S and the solution was transferred into 2 plastic Petri dishes which were then stirred slowly (~100-150 rpm) on a magnetic stirrer at RT for 20 min. To discard undigested tissue the suspension was passed through a 70 µm filter and the flow-through was collected in a new 15 ml falcon tube. Afterwards cells were pelleted by centrifugation at 200 xg for 5 min at 4°C, the supernatant was discarded and the

cells were resuspended in 5 ml RM+ medium. Finally, cells were counted and seeded on 0.1% gelatin-coated culture plate containing feeder layer.

5.2.7. Isolation and cultivation of primary fibroblasts from human skin

The entire procedure of fibroblasts isolation was performed as described in Nature Protocols (Aasen, T & Belmonte, 2010).

To isolate fibroblasts, the preserved dermal part was cut into small pieces, which were then placed in a Petri dish (~10 pieces/plate) and covered with 1-2 drops of DMEM supplemented with 10% FCS and 1% P/S. The next day, when the pieces were firmly attached to the plate, 8-10 ml of medium was added and the tissue was cultured for 5 days until the outgrowth of fibroblasts appeared and for another 7-10 days until plate was 70% confluent. The cells were washed every 3 days with PBS, passaged and expanded according to the procedure described above (section 'Passaging of adherent eukaryotic cells').

5.2.8. Co-culture of eukaryotic cells

In co-culture experimental system, the cSCC cell line was grown at the bottom of 24-well plate at the number of 4-6 x 10^3 cells/well in 500 µl culture medium. The nourishing fibroblasts were seeded in 200 µl culture medium in cell culture inserts with 0.4 µm pores in diameter, which do not allow for migration of the cells. The inserts were then placed in the 24-well plate to allow exchange of secreted molecules. After the desired incubation time, inserts were discarded while the cells remaining in the plate were subjected to the desired assays.

5.2.9. Immunocytochemistry

Immunocytochemistry of cultured cells was performed on round cover slips placed at the bottom of 24-well plate. The number of seeded cells was 3 x 10^5 cells/well. First, cells were washed with PBS and fixed with 4% PFA in PBS at RT for 30-40 min followed by 10 min incubation in NH_4Cl at 37°C. After two rounds of washing with PBS cell membranes were permeabilized with 0.2% Triton X-100 in PBS (3 x 4 min). The primary antibodies were diluted 1:100 in 0.2% Triton 100-X/PBS and applied to the wells for 1 h at RT. Afterwards, cells were washed 3 x 4 min with 0.2% Triton X-100 in PBS and the secondary antibody was added for 1 h at RT followed by another round of washing with 0.2% Triton X-100/PBS and additionally 2 x 5 min with pure PBS. At the end, coverslips were air-dried, mounted with

DAPI mounting medium and placed on the slides. The staining was analyzed using Olympus BX 60 fluorescent microscope.

5.2.10. Chemical transfection of eukaryotic cells

5.2.10.1. pDNA transfection

Chemical transfection of pDNA was performed using RotiFect® as transfection reagent according to the manufacturer's instructions. Briefly, cells were seeded in a 6-well (or a 24-well) plate at the number of 1.5×10^5 (3×10^4) cells/well. Number of seeded cells, ratio between nucleic acid and transfection reagent as well as transfection time were established for each cell line based on the efficiency of pEGFP transfection. To find the best transfection conditions we varied the amount of pDNA (2 and 4 µg), the ratio between transfected pDNA and Rotifect (1:2, 1:4, 1:5 and 1:6) as well as incubation time with transfection mixture (3, 6 and 16 h). The best transfection conditions for each cell line are presented in Table 22. In some cell lines, all applied settings resulted in a great toxicity and thus, those cells were considered as not possible to transfect with this method.

Table 22: Transfection conditions for cSCC cell lines

Cell line	DNA:Rotifect	pDNA amount (µg)	Rotifect vol. (µl)	Transfection time	Efficiency	Notes
SCL-I	1:2	4	8	16 h	~75%	-
SCL-II	1:6	4	24	3-6 h	~25%	Toxic
SCC-13	1:6	2	12	3-6 h	~40%	Toxic
MET-1	1:2	2	4	3-6 h	~5%	Toxic
MET-4	1:5	2	10	6 h	~70%	-
HaCaT-ras II-4	1:2	2	4	16 h	~75%	-
SCC-12	1:2	4	8	3-16 h	~15%	-

The appropriate amount of pDNA and RotiFect was diluted in separate reaction tubes in 200 µl (or 30 µl for 24-well plate) of serum-free medium without antibiotics each. Afterwards, both components were mixed by pipetting and incubated at RT for 40 min to let the complexes form. In the meantime, cells were washed once with PBS, and the culture medium

was replaced with 1.5 ml (250 µl) antibiotic-free medium supplemented with 10% FCS. Finally, the complexes were added dropwise to the cultured cells for desired time (6-18 h), after which the transfection medium was replaced with complete culture medium.

5.2.10.2. siRNA transfection

For the transfection of siRNA HiPerFect was used according to the supplier's guidance. Briefly, 1.5×10^5 cells were seeded in each well of a 6-well plate (or 3×10^4 for a 96-well plate). 300 ng (or 25 ng) of the siRNA was mixed with 18 µl (1.5 µl) of HiPerFect in 400 µl (30 µl) of pure DMEM or RPMI in 1.5 ml reaction tubes. The mixture was incubated for 10 min at RT to let the complexes form. In the meantime, cells were washed with PBS and the medium was replaced with 1.5 ml (70 µl) of fresh DMEM or RPMI supplemented with 10% FCS and 1% P/S. Afterwards, complexes were added dropwise to each well and cells were incubated for 24 h. After this time cells were either collected for RNA isolation or re-seeded in a 96-well plate for another 24 h in the presence of BrdU for proliferation assay.

5.2.11. Dual-luciferase assay

For the dual-luciferase assay cells were transiently transfected with experimentally regulated Firefly expression vector and constitutively active Renilla expression vector that served as an internal control. The assay was performed using the Dual-Luciferase® reporter assay system according to the supplier's instructions. Shortly, 100 µl of passive lysis buffer (PLB) was added to each well of a 24-well plate and placed on the shaker at RT for 15 min at ~300 rpm to lyse cells. Afterwards the plate was frozen at -80°C for 30 min and after thawing, 20 µl of cell suspension was transferred per well of a black 96-well plate, in triplicates. 100 µl of LAR II and Stop&Glow substrates were pipetted sequentially into each well to induce the reaction conducted by Firefly and Renilla luciferases, respectively, and the luminescence was measured using a Synergy Mx luminometer at 550-570 nm and 480 nm, respectively. The data normalization and calculation were done in Microsoft Excel 2010.

5.2.12. Proliferation assay (BrdU incorporation)

The proliferation of the cells was measured based on 5-Bromo-2-Deoxyuridine (BrdU) incorporation in DNA during the S-phase. The assay was done at RT temperature using a BrdU cell proliferation kit in accordance with manufacturer's instructions. In brief, cells were seeded in a 96-well plate (6×10^3 cells/well) and cultured in the presence of 10 µM BrdU for

24 h. Afterwards the cells were fixed and DNA was denatured with 200 µl of Fix-Denat for 30 min followed by incubation with peroxidase coupled anti-BrdU antibody diluted 1:100 in Antibody-dilution-solution for 1 h. Negative controls lacking either anti-BrdU antibody or BrdU itself were included in the assay. To remove unbound antibodies, cells were thoroughly washed 3 x 5 min with 200 µl of 1 x Washing Buffer. The enzymatic reaction was started by adding 100 µl of peroxidase substrate to each well and the emitted luminescence was measured in the Synergy Mx Luminometer. Each sample was measured in triplicates and the proliferation rate was calculated in Microsoft Excel 2010.

5.2.13. Metabolic activity assay (WST-1)

Metabolic activity assay was based on tetrazolium salt WST-1, which is cleaved to a soluble formazan dye only in the presence of NAD(P)H in living cells. Shortly, cells were seeded in a transparent 96-well plate (6 x 10^3 cells/well) and incubated at 37°C with WST-1 for the last 3 h of culture time. Colorimetric reaction was then measured in a microplate reader at a wavelength of 450 nm. All samples were measured in triplicates and the data were analyzed using Microsoft Excel 2010.

5.2.14. Annexin V/Propidium iodide (PI) staining (FACS analysis)

To assess the number of early and late apoptotic as well as viable and necrotic cells, cells were seeded in a 6-well plate at a number of 1.5 x 10^5 and grown for 24 h. Afterwards, the cells were detached from the plate using 1 ml of accutase/well, collected in the 15 ml falcon tube, pelleted by centrifugation at 300 xg, 4°C for 5 min and washed once with 1 x PBS. After a second centrifugation step with the same settings, the supernatant was discarded and 2 µl Annexin V-FITC in 100 µl of Annexin V binding buffer was added to each tube. The mixture was shortly vortexed and incubated at RT for 10 min followed by 5 min incubation with PI. Prior to measurement, 300 µl of Annexin V binding buffer was added to each reaction tube. Finally, cells were sorted by flow cytometry in a FACS Calibur machine using the channel FL-1 and FL-3 for Annexin V FITC and PI, respectively, giving rise to 4 populations with the corresponding phenotype:

1. Annexin V negative and PI negative – viable cells
2. Annexin V positive, PI negative – early apoptotic cells
3. Annexin V positive, PI positive – late apoptotic cells
4. Annexin V negative, PI positive – necrotic cells

All samples were measured in triplicates and the data were analyzed using the FlowJo software, Microsoft Excel 2010 and GraphPad Prism 6.

5.3. Histological methods

5.3.1. Immunohistochemistry

For immunohistochemistry, 5 µm paraffin tissue sections were prepared on a microtome and mounted on Superfrost slides. If not otherwise stated, the entire procedure was performed at RT. Sections were first deparaffinized 2 x 10 min in Xylene and then rehydrated in serial ethanol dilutions 100%, 95%, 80%, 70%, 50%, 30% and ddH$_2$O. Depending on the antibody, different pretreatments for antigen retrieval were applied:

1. Citric acid pH 6.0 – samples were boiled in buffer in a microwave 1 x 4 min and 4 x 3 min at 600W
2. Tris/EDTA (TE) buffer pH 9.0 – the same procedure as above
3. Citric acid pH 3.0 – samples were incubated at 37°C for 30 min
4. Boric acid pH 5.1 – samples were incubated at 55°C for 30 min

Irrespective of the pretreatment, sections were cooled down and washed in TBS/0.1% Triton. To block endogenous peroxidase activity, slides were incubated with 3% H$_2$O$_2$ for 20 min. Afterwards they were washed with ddH$_2$O for 5 min and briefly rinsed in TBS/0.1% Triton. To block unspecific antibody binding, the slides were incubated with either 0.02% Casein or 5% FCS/10% BSA in 1 x PBS in a moist chamber. After 20 min, the blocking solution was discarded and the primary antibody diluted in 1 x TBS/0.1% Triton was applied onto the sections at required concentration. Incubation was carried O/N at 4°C in a moist chamber. The next day, the slides were washed 3 x with TBS/0.1% Triton to remove unbound primary antibodies. Then the secondary HRP-conjugated antibody was applied. After 30 min of incubation in a moist chamber at RT slides were washed again and the staining solution, either DAB chromogen or AEC was added. Intensity and specificity of the staining were monitored under the microscope and finally the reaction was stopped after 5-30 min with ddH$_2$O. Subsequently, counterstaining of nuclei was performed by incubation with hemalum solution for 20 sec. The excess of staining solution was removed with ddH$_2$O followed by incubation with warm tap water. In the end slides were roughly dried and mounted with Glycergel.

5.3.2. Hematoxylin & eosin (HE) staining

To visualize morphology of the tissue, paraffin sections were prepared on a microtome and fixed on SuperFrost slides. First, tissue sections were deparaffinized by incubation in Xylene (2 x 10 min) and hydrated in descending ethanol series: 100%, 96%, 70%. After washing with ddH$_2$O slides were incubated with a hemalum solution for 20 min and washed again under running warm tap water. Then the slides were transferred to a cuvette containing 1% eosin staining solution for no more than 20 sec. After a washing step with ddH$_2$O, tissues were dehydrated in a series of ascending ethanol solutions: 70%, 96%, 100% and placed in Xylene before mounting them with Pertex. In the final step, slides were dried at 55°C for 30 min.

5.3.3. *In situ* hybridization (ISH) of paraffin embedded tissue sections

ISH was performed on paraffin tissue sections using digoxigenin-labeled ribo-probes. To eliminate RNases from the working environment, all the solutions (except for TEA) were DEPC-treated and autoclaved along with all equipment. To detect mRNA within tissue samples, the 5 µm paraffin sections were prepared. Prior to ISH the sections were incubated at 65°C for 30 min. Deparaffinization with Xylene and hydration of the tissues in serial ethanol dilutions were done as described in IHC section. After incubation in 30% ethanol, the slides were washed in 1 x Saline and 1 x PBS, 5 min each and fixed in 4% PFA in PBS for 20 min. After 2 rounds of washing with 1 x PBS (5 min each) tissues were subjected to proteinase K treatment for 7.5 min on ice to digest proteins that may obstruct target mRNA. Subsequently slides were washed with 1 x PBS and re-fixed with 4% PFA in PBS for 5 min on ice to maintain tissue integrity. To reduce non-specific binding of the probes and thus background signals, the tissues were treated with acetic anhydride diluted in 0.1M triethanolamine (TEA). After 2 washing steps with 1 x PBS and 1 x Saline the slides were dehydrated with ascending ethanol dilutions (30%-100%) with prolonged incubation (5-10 min) in 70% EtOH to avoid salt deposition on dehydrated slides and air-dried. Then a liquid barrier marker from Carl Roth GmbH & Co. KG, Karlsruhe was used to separate sections placed on the same slide for application of sense (negative control) and anti-sense probes. hGLI1 riboprobes were diluted 1:1000 in HybM hybridization buffer, 65 µl were pipetted on sections and the slides were covered with coverslips. Hybridization was performed in a moist chamber soaked with 50% formamide/5 x SSC, which was tightly wrapped in a plastic bag. Incubation time was ~16 h in

a 56°C incubator. The next day, samples were subjected to high-stringency washing steps involving:

1. 20 min at 63°C in 50% formamide/2xSSC
2. 10 min at RT in STE buffer
3. 3 x 10 min at 37°C in STE buffer

To digest all unbound single-stranded riboprobes, sections were exposed to RNase A treatment for 30 min in STE buffer followed by further washing steps:

4. 15 min at 37°C in STE buffer
5. 20 min at 63°C in 50% formamide/2xSSC
6. 15 min at RT in 2 x SSC

Afterwards the slides were incubated in NT buffer for 10 min at RT and then 3 x 5min in MBSTL buffer. 0.02% Casein solution was placed on sections for 1 h at RT to block unspecific binding of the secondary antibody. AP-conjugated anti-digoxigenin antibody that was diluted 1:1000 in 0.02% Casein/MBSTL and placed on sections for O/N at 4°C in a moist chamber. On the third day, the slides were thoroughly washed 6 x 15 min in MBSTL on the orbital shaker at RT to block endogenous AP activity. Subsequently, they were placed horizontally in a moist chamber and incubated with NTMLT buffer 3 x 5 min at RT. For the final colorimetric reaction, BM-purple substrate was placed on the sections for at least 24 h. When the staining signal was strong enough, the enzymatic reaction was stopped with 10 mM Tris pH 8/1 mM EDTA solution and the tissues were fixed with 4% PFA/0.2% glutaraldehyde for 1-2 h at RT with shaking. After washing in PBS slides were mounted with Glycer-gel mounting medium and analyzed with an Olympus BX 60 microscope.

6. Results

6.1. Expression of *GLI1*, SHH, pS6, pAKT, pERK and EGF in human cSCC samples

PTCH mutations have been identified in 15% of cSCC cases (Ping et al., 2001). In addition, besides HH and PTCH1, cSCC were reported to express GLI1, the major target of active HH signaling (Celebi *et al.*, 2016). Our lab also has tested the antibodies described by Celebi and colleagues. However, in our hands the respective antibodies gave very unspecific signals. We here have used an antibody against SHH from abcam that detects the N-terminal end of SHH and stained 10 human cSCC specimens. Due to the lack of an adequate GLI1 antibody the staining for GLI1 was done by *GLI1* ISH. Using adjacent slides, the tumors were also stained with antibodies against pERK (readout for MEK/ERK pathway activation), pAKT (readout for PI3K/AKT activity), pS6 (hallmark of active mTOR signaling) and EGF.

As shown in Fig. 5 A the anti-SHH antibody showed positive staining in ductal epithelium of pancreatic adenocarcinoma that was used as a positive control (Fig. 5 A). Similar expression pattern of SHH in pancreatic cancer has been described in the literature (Thayer *et al.*, 2003). However, the antibody stained neither cSCC tumor cells nor cSCC stroma (Fig. 5 A). This shows that SHH is not expressed by cSCC. In contrast, when we measured HH signaling activity by performing a *GLI1* specific ISH on adjacent slides, we found that *GLI1* expression was high in the tumor center whereas tumor cells invading the dermis were not or only moderately positive for *GLI1* (Fig. 5 A, B). Most interestingly, this staining pattern was inverse to that using an antibody that specifically detects phosphorylation at S240/244 sites of the mTORC1/S6K-downstream target S6 (Fig. 5 B; please note that in the following the term mTORC1 will be substituted by mTOR). Thus, positivity for pS6 was frequently revealed in invading tumor cells, whereas it was low in the tumor center (Fig. 5 B, E). In contrast, the anti-pAKT antibody recognizing pSER473 of AKT did not show any positive staining in tumor cells (Fig. 5 B) and unfortunately positive control tissue (glioblastoma) raised too much background staining (picture not shown). These data question the reliability of this anti-pAKT antibody although Barrette et al. has reported a positive staining of invasive cSCC tissue samples when using it. On the other hand, pERK was mostly expressed in stromal cells surrounding neoplastic tissue with only rare and weak signals detected in single tumor cells (Fig. 5 C). Therefore, the positivity of pERK was adjacent to tumor cells that were *GLI1*

negative (Fig. 5 D). EGF was expressed all over the tumor with sometimes stronger expression in *GLI1*-negative areas of tumor cells invading the dermis (Fig. 5 E).
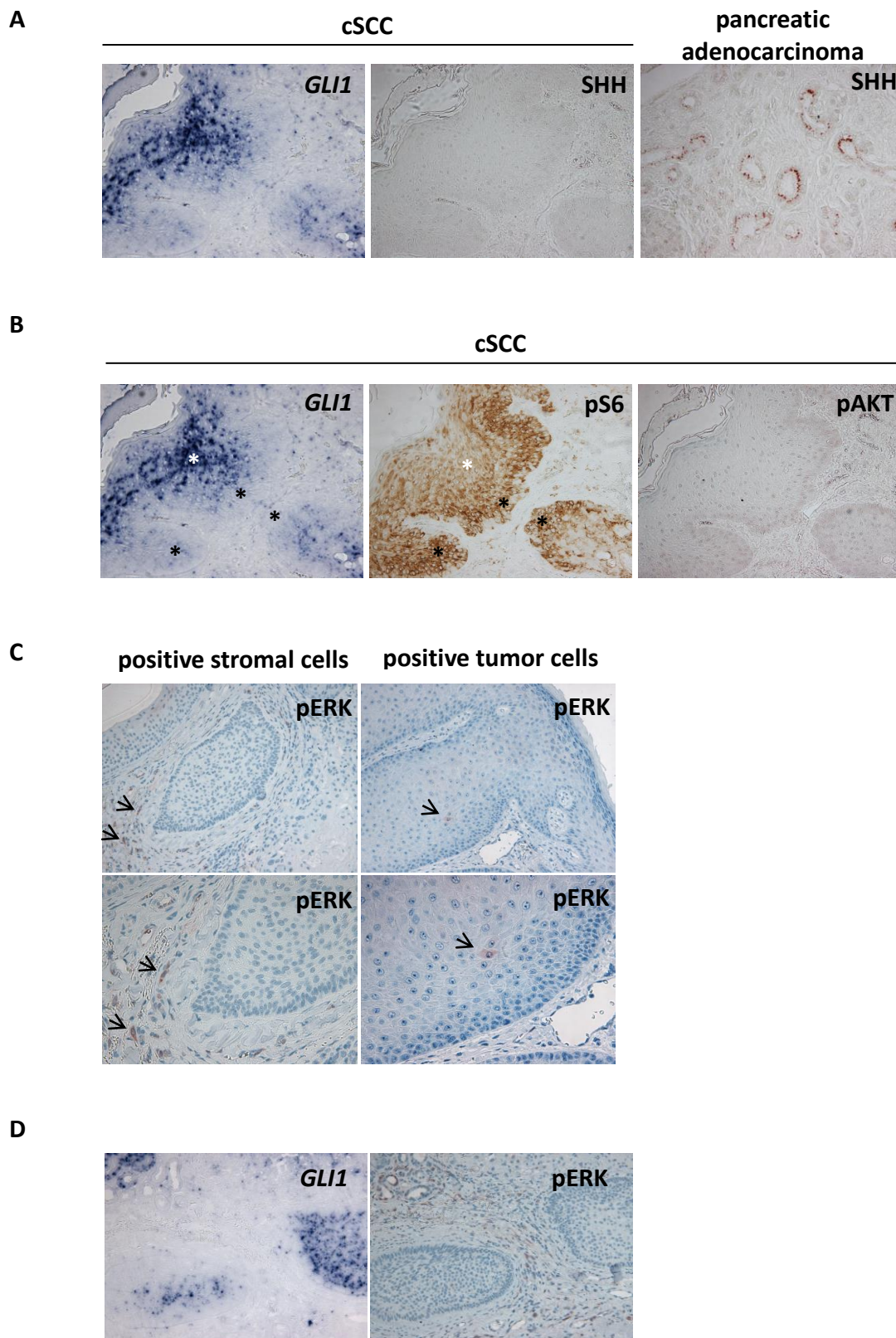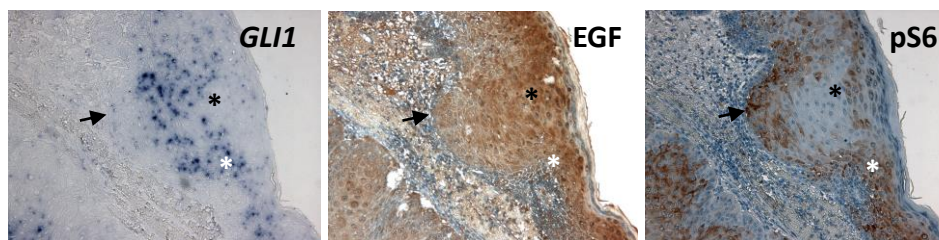
E

Figure 5: Immunohistochemical analysis of SHH, pS6, pERK, pAKT and EGF as well as *in situ* hybridization of *GLI1* of human cSCC biopsies. A. Representative pictures of adjacent sections from human cSCC (n=10) showing strong *GLI1* expression within the tumor mass (as measured by ISH) and no SHH signals (as measured by antibody staining/IHC) throughout the whole tissue. Pancreatic adenocarcinoma served as a positive control for SHH staining. The pictures are presented at 10 x magnification. **B.** *GLI1* ISH and IHC for pS6 and pAKT on adjacent cSCC sections. Inverse pattern of *GLI1* mRNA expression and pS6 protein is shown. No specific signal for pAKT was detected. Pictures are shown at 10 x magnification. Black asterisks indicate the areas strongly positive for pS6 but negative for *GLI1*. White asterisks show the regions weakly positive for pS6 but strongly expressing *GLI1*. **C.** Representative pictures showing pERK positive stromal (left) and tumor (right) cells. Upper panel 10 x and lower panel 20 x magnification. Arrows point to pERK positive cells. **D.** Representative pictures showing *GLI1* positive tumors surrounded by pERK positive stromal cells, 10 x magnification. **E.** Representative pictures of adjacent cSCC sections showing overlapping or inverse staining for *GLI1*, EGF and pS6. White asterisks indicate areas positive for *GLI1*, EGF and pS6, black asterisks indicate the regions that are EGF positive but *GLI1* and pS6 negative. Invasion front of the tumor, which is positive for EGF and pS6 but negative for *GLI1,* is indicated with an arrow. The pictures are shown at 10 x magnification. All staining reactions were performed using either AEC (red) or DAB (brown) in case of IHC and using BM-purple (blue) in case of ISH. The expression pattern and staining intensity were assessed by a pathologist.

Due to the lack of SHH staining in tumor tissue but *GLI1* positivity in the tumor center (Fig. 5 A), we hypothesized that HH/GLI signaling in cSCC might be activated in a noncanonical way. The opposing expression pattern of *GLI1* and pS6 (Fig. 5 B) also may indicate that HH/GLI and mTOR pathways may regulate each other in a negative manner. Moreover, both HH/GLI and mTOR activation may be driven by EGF signaling as EGF staining sometimes overlapped both the *GLI1* and pS6 positive areas (Fig. 5 E). On the other hand, EGF positivity overlapped *GLI1* negative areas (black asterisks and black arrows in Fig. 5 E), which may indicate a negative regulation of *GLI1* by EGF. In addition, there might also be a negative interaction between *GLI1* expressing tumor cells and pERK positive stromal cells. Thus, as shown very impressively in Fig. 5 D, pERK positive stromal cells surround the tumor areas, which are *GLI1* negative (Fig. 5 D). As already stated we were not sure about the reliability of the pAKT staining.

6.2. Basal expression of components of the HH/GLI, PI3K/AKT/mTOR and MEK/ERK pathways in cSCC cell lines

To investigate the role of HH/GLI, PI3K/AKT/mTOR (please note, mTOR is frequently activated by AKT and in the following will be sometimes combined with PI3K/AKT signaling) and MEK/ERK signaling and a putative interaction between them in cSCC, we performed *in vitro* experiments involving initially 6 different cSCC cell lines, namely, SCL-I, SCL-II, SCC-13, SCC-12, MET-1 and MET-4 as well as HaCaT ras II-4 transformed cells also resembling the cSCC phenotype (Boukamp et al., 1990).

6.2.1. Expression of canonical HH/GLI pathway components on mRNA level

We first checked to what extent the used cell lines express the major HH/GLI pathway components *GLI1*, *GLI2*, *GLI3*, *SMO*, *PTCH* and *SHH*. For this purpose, we performed qPCR. As shown in Fig. 6 almost all pathway components were expressed at a variable level in all 7 cell lines. The exception was *SHH,* which was markedly expressed only by MET-1 and MET-4 cells. In addition, *GLI3* was not expressed in SCC-13 that also expressed *SMO* at extremely low levels. *SMO* was also not expressed in SCL-II cells. We also compared the expression levels of cSCC cell lines to primary keratinocytes as well as immortalized HaCaT cells commonly used in studies on human keratinocytes, to see whether the HH/GLI pathway is upregulated in cSCC. The data show that primary keratinocytes expressed low levels of *GLI1* and *GLI2* but none of the other pathway components, whereas HaCaT cells expressed *GLI1*, low levels of *GLI2*, *PTCH* and *SMO*. These data indicate that both primary keratinocytes and immortalized keratinocyte cell line express only moderate amounts of *GLI2* and completely lack *GLI3*, which are important factors for activation of both noncanonical and canonical HH signaling. Out of all cell lines, MET-1 and MET-4 expressed the highest levels of *GLI2*, *GLI3*, *SMO* and *SHH.* Moreover, we also noted relatively high level of *GLI1* expression in these two cell lines (Fig. 6). Therefore, we chose them as representative cell lines for further analysis. Furthermore, we chose the cell line SCL-I that – as the human tumor samples – does not express *SHH*, but otherwise all components necessary for stimulation of the canonical (and noncanonical) HH pathway.
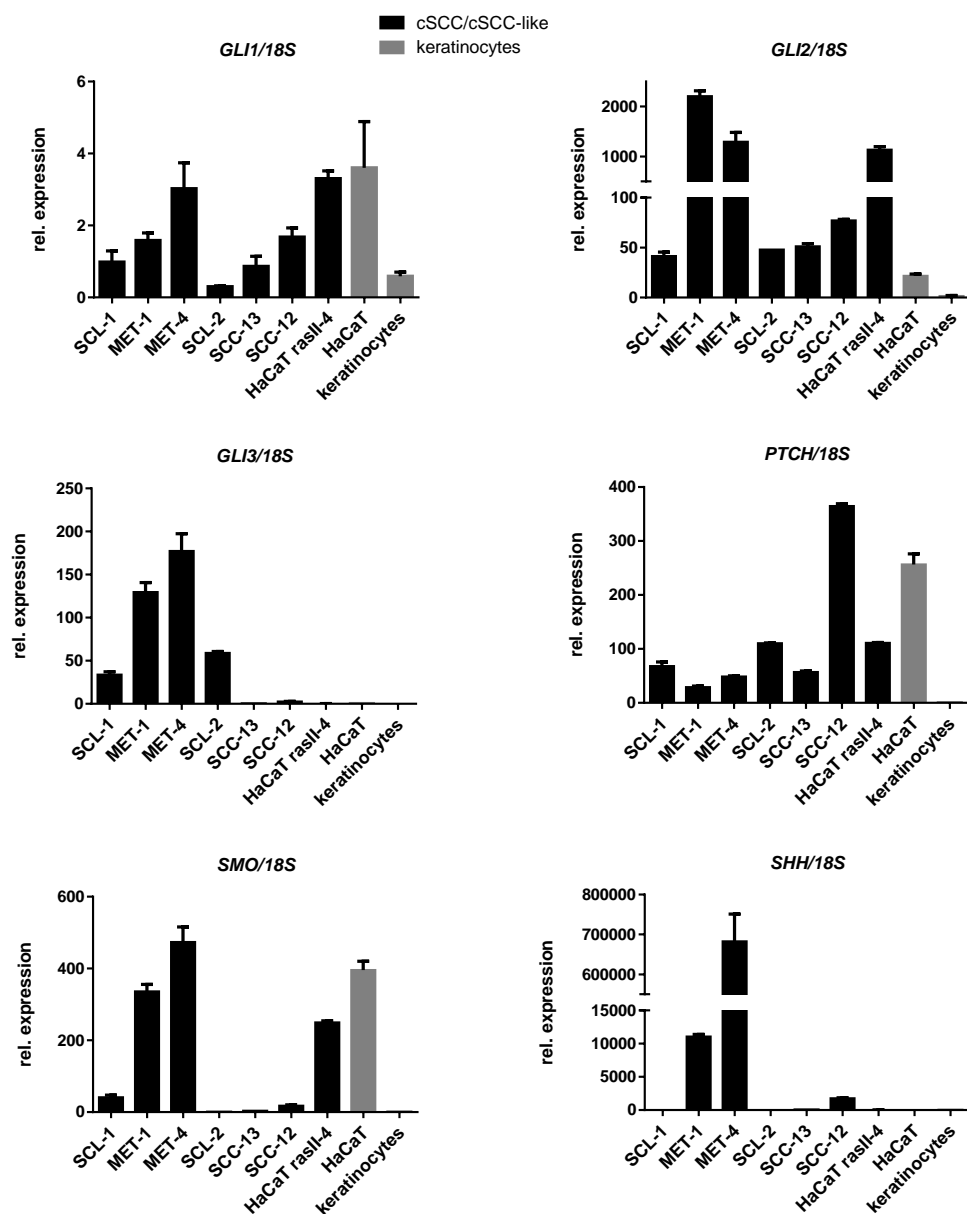
Figure 6: Basal expression of canonical HH/GLI pathway components in cSCC/cSCC-like cell lines and keratinocytes. qPCR showing relative expression levels of *GLI1*, *GLI2*, *GLI3*, *PTCH*, *SMO* and *SHH* in the cSCC cells lines SCL-I, MET-1, MET-4, SCL-II, SCC-13, SCC-12, in the cSCC-like cell line HaCaT ras II-4 cell (black bars), as well as in the keratinocyte cell line HaCaT and primary human keratinocytes (keratinocytes) (grey bars). The target gene expression was normalized to the *18S rRNA* housekeeping gene. The data are presented as mean +/- SEM of one experiment measured in triplicates.

6.2.2. Expression of pERK, pAKT and pS6 on protein level

We next checked the basal levels of pAKT, pERK and pS6 as readouts for active PI3K/AKT, MEK/ERK and mTOR signaling pathways, respectively. All examined cell lines showed high levels of phosphorylated S6 protein when compared to the total amount of S6 or HSC70

loading control. Also, all cell lines expressed pAKT and pERK, however to a variable extent. In detail, SCL-I cells highly expressed pAKT and pERK, SCL-II cells showed strong expression of only pERK while HaCaT ras II-4 and MET-1 cells displayed a moderate expression of pAKT and quite low pERK levels. In the remaining cell lines pERK and pAKT levels were rather low (Fig. 7). Interestingly, in the cell lines showing the highest level of pERK i.e. SCL-I and SCL-II (Fig. 7) we had measured the lowest level of *GLI1* by qPCR (see Fig. 6). Taken together, all cSCC cell lines seem to differ between each other, but most of them express all major components of the HH pathway and show activation of PI3K/AKT/mTOR and MEK/ERK signaling pathways, which are downstream effector pathways of RTKs.
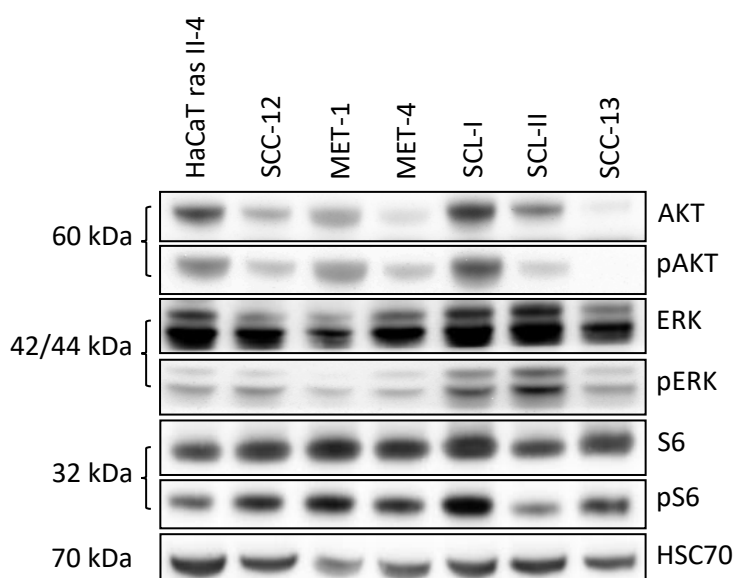

Figure 7: Basal activity of PI3K/AKT, MEK/ERK and mTOR signaling pathways in cSCC/cSCC-like cell lines. Representative Western Blot showing activity of AKT/pAKT, ERK/pERK and S6/pS6 in the cSCC-like HaCaT ras II-4 cell line and in the cSCC cell lines SCC-12, MET-1, MET-4, SCL-I, SCL-II and SCC-13. HSC70 served as a loading control. The size of the proteins (in kDa) is indicated on the left side of the blot.

6.3. Modulation of canonical HH signaling activity in cSCC cell lines

In order to investigate whether it is possible to activate HH signaling in cSCC via the canonical PTCH/SMO/GLI axis we incubated the cells with different molecules modulating PTCH or SMO activity and measured its influence on *GLI1* expression level. For this purpose, we used SCL-I, MET-1 and MET-4 cells. As already said, these cell lines all express *PTCH*, *SMO* and *GLI1-3*, which are necessary for activation of the canonical HH cascade by

SHH. Whereas MET-1 and MET-4 also express *SHH*, SCL-I, similar to cSCC tumor samples, does not (see Fig. 5 A and Fig. 6). In addition, SCL-I and MET-4 cells were easy to transfect (see Table 22 in the Material and Methods section).

6.3.1. Activation with SHH conditioned medium or SAG

To see whether *GLI1* expression level raises upon activation of canonical HH/GLI signaling we incubated the cells with either SHH conditioned medium (SHH-CM) or Smoothened agonist (SAG; at concentrations ranging from 10 nM – 1 µM) for 24 h. Control- and SHH–CM were prepared as described in the Materials and Methods (section 5.2.4). Prior to the experiment, the functionality of freshly prepared SHH-CM was always tested on the SHH-responsive murine cell line B9 (Table 8, Materials section). As shown in Fig. 8 A, SHH-CM induced at least 100-fold increase in *Gli1* expression in B9 cells, when compared to cells treated with control-CM. This was observed in all experiments. A representative graph shows a 400-fold induction in *Gli1* expression upon incubation with SHH-CM (Fig. 8 A). However, none of the three cSCC cell lines responded to SHH-CM as indicated by the lack of increased *GLI1* transcription (Fig. 8 A). When the cells were treated with SAG, *GLI1* expression was slightly increased in all three cell lines especially after incubation with 100 nM, however these changes were statistically not significant (Fig. 8 B). To further verify these data, we also performed a Dual-Luciferase GLI reporter assay in SCL-I cells due to their best transfection efficiency (Table 22, Methods section). For this purpose, the cells were transfected with a plasmid encoding firefly luciferase under the herpes simplex virus thymidine kinase (HSV TK) promoter containing 9xGli-BS and a plasmid encoding renilla firefly luciferase for normalization. The cells were then incubated with either control-CM or SHH-CM. Transfection along with a plasmid encoding Gli1 was used as a positive control. As expected, the control transfection resulted in a 3-fold increase in luciferase activity (Fig. 8 C). However, in line with the *GLI1* qPCR data, incubation with SHH–CM did not change GLI-driven luciferase activity in comparison to cells incubated with control-CM (Fig. 8 C). Therefore, we conclude that it is not possible to activate canonical HH/GLI signaling in cSCC cell lines.

A

B

C

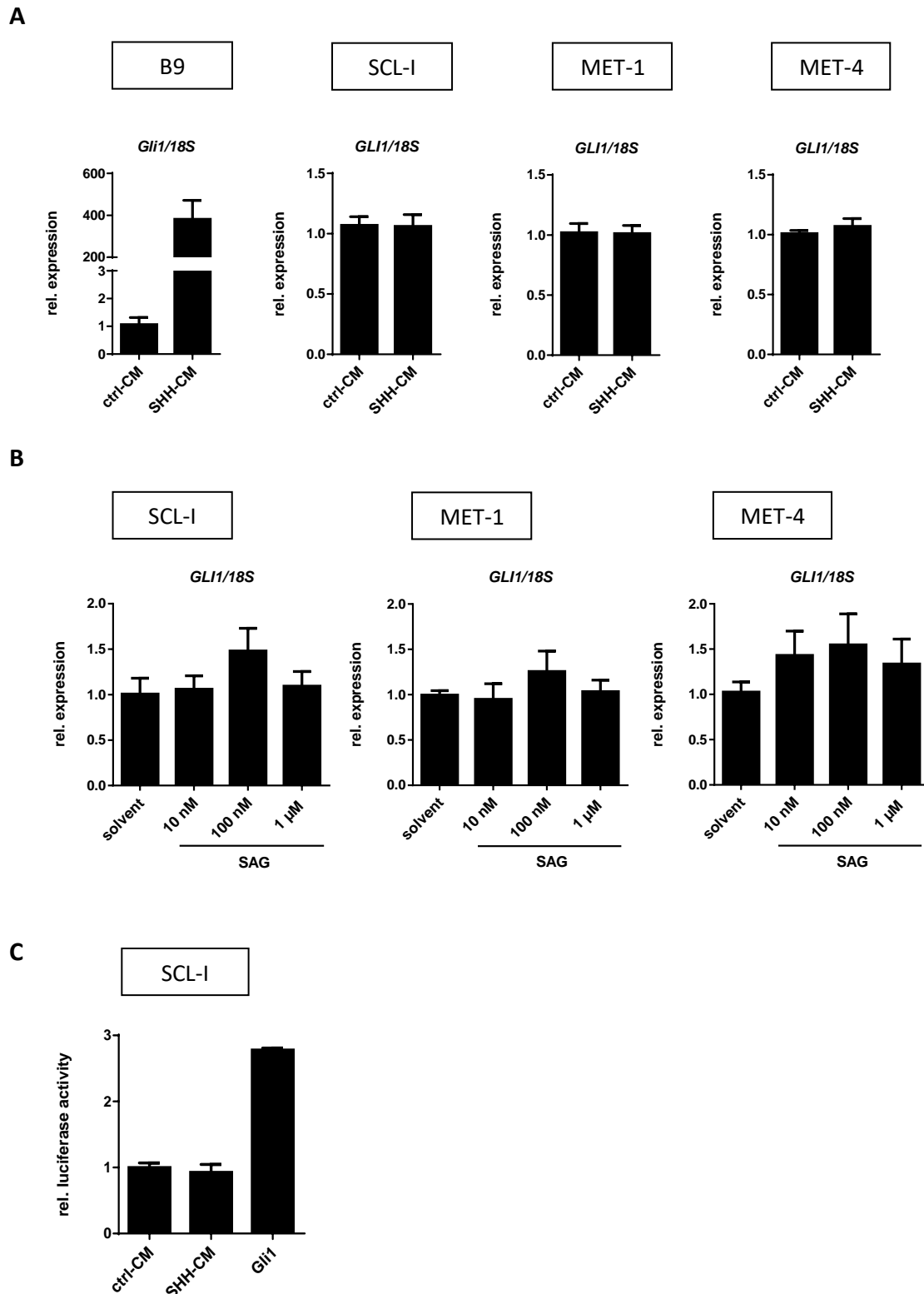**Figure 8: Impact of SHH ligand or SAG on *GLI1* expression in cSCC cell lines. A.** qPCR showing relative expression of *GLI1/18S* in SCL-I, MET-1 and MET-4 cells incubated with control- or SHH- CM for 24 h. The data represent a summary of three independent experiments, each performed in triplicates. **B.** qPCR showing relative expression of *GLI1/18S* in SCL-I, MET-1 and MET-4 cells incubated with 10 nM, 100 nM or 1 μM

SAG. The data represent the summary of three independent experiments, each performed in triplicates. **C.** Changes in relative luciferase activity upon transfection of SCL-I cells with a plasmid encoding firefly luciferase under the HSV TK promoter containing 9xGli-BS and incubation with either control-CM or SHH-CM. Co-transfection of plasmids encoding *Gli1* served as a positive control (Gli1). The graph represents one experiment performed in three technical replicates. All data are shown as mean values +/- SEM; ctrl-CM, control medium; SHH-CM, SHH conditioned medium.

6.3.2. Overexpression of SMO

In a final experimental setting, we directly overexpressed a constitutively active variant of SMO, namely SMO-M2, or wild type SMO (SMO-WT) in SCL-I cells according to the established conditions described in Table 22 in the Methods section. After 24 h the cells were collected for RNA isolation and subjected to *GLI1* expression analysis. Additionally, we transfected the cells with the SMO-M2 plasmid along with the plasmid encoding firefly luciferase under the control of HSV TK promoter containing 9xGli binding sites as well as the plasmid encoding constitutively active renilla firefly (as described in 5.2.11. in Methods section) and performed Dual-Luciferase GLI reporter assay. Also in this experiment co-transfection of *Gli1* and luciferase served as a positive control and resulted in more than 8-fold increase in luciferase activity (Fig. 9 B). In accordance with the data obtained with SHH or SAG, overexpression of SMO neither altered *GLI1* expression nor GLI activity (Fig. 9).
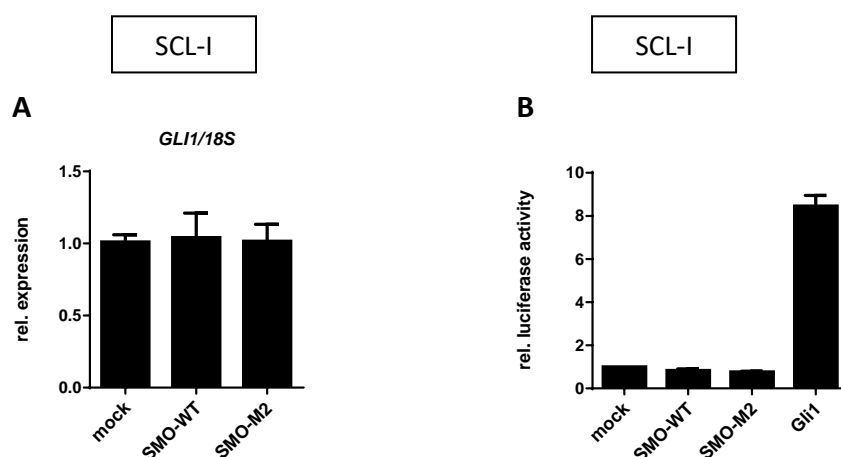
Figure 9: Effects of active SMO on *GLI1* expression and GLI activity in cSCC cell lines. A. Relative *GLI1* expression level in SCL-I cells transfected with SMO-WT or SMO-M2 (active SMO variant) plasmids normalized to the *18S rRNA* housekeeping gene. The data show a summary of four independent experiments, performed in triplicates. The *GLI1* expression in mock transfected cells was set to 1. **B.** Relative GLI-driven luciferase activity in SCL-I cells after transfection with SMO-WT and SMO-M2 compared to that in mock transfected cells, which was set to 1. Co-transfection of the 9xGli-BS-firefly luciferase plasmid and a plasmid

encoding *Gli1* served as a positive control (Gli1). The graph represents a summary of two independent experiments. All data are shown as mean +/- SEM.

6.3.3. Incubation with SMO inhibitors

In a next approach, we tried to inhibit the canonical HH/GLI axis and thus *GLI1* expression via application of three different small-molecule SMO antagonists, which were cyclopamine (CP), vismodegib and HH Antag (HhA). Although SCL-I cells do not express the ligand SHH (see Fig. 6) we incubated this cell line together with MET-1 and MET-4 cells (that express high levels of the HH ligand) for 24 h with different concentrations of the inhibitors i.e. 1 - 10 µM CP and 10 - 60 µM vismodegib or HhA. Our data show that CP did not alter *GLI1* expression in any of the cell lines at any applied concentration (Fig. 10 A). Similarly, incubation with 10 µM and 30 µM vismodegib did not affect *GLI1* expression and paradoxically resulted in a significant upregulation of *GLI1* in SCL-I and MET-4 cells at a concentration of 60 µM (Fig. 10 B). A paradox increase in *GLI1* expression was also seen in SCL-I cells that had been incubated with HhA (Fig. 10 C). However, treatment with HhA led to the expected significant decrease in *GLI1* expression in MET-1 and MET-4 cells (Fig. 10 C).
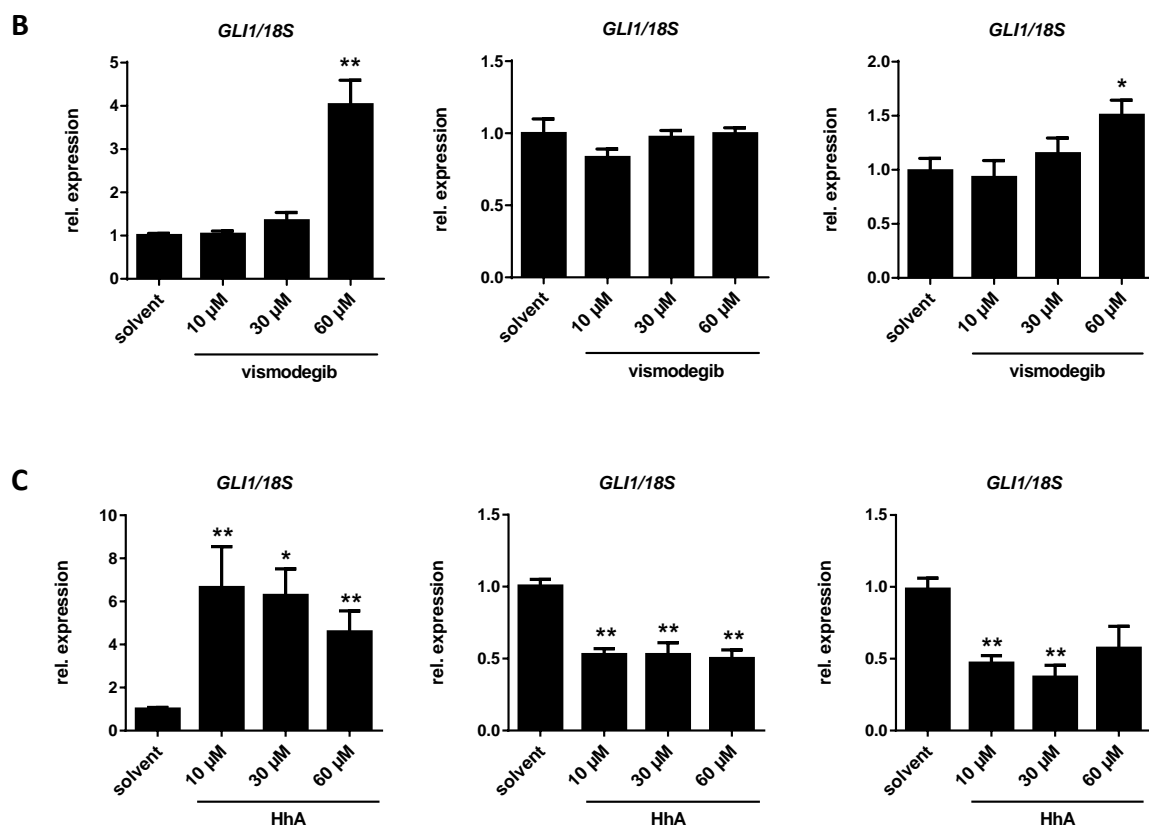
B

C
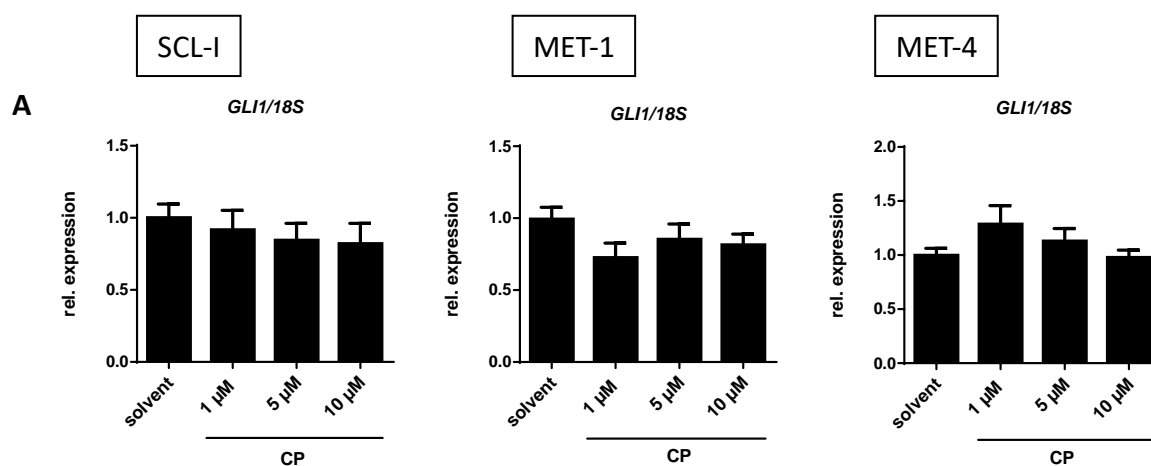
Figure 10: Impact of SMO inhibitors on *GLI1* expression in cSCC cell lines. qPCR showing relative expression of *GLI1/18S rRNA* in cells incubated with **A.** cylopamine (CP), **B.** HhA or **C.** vismodegib at the indicated concentrations for 24 h. Each graph represents a summary of two independent experiments analyzed in triplicates, with the solvent control set to 1. All data are presented as mean +/- SEM; *, $p<0.05$; **, $p<0.01$. Statistical comparisons were done with Mann-Whitney test.

Based on the lack of activation of the pathway upon stimulation with either SHH or SAG, we assume that canonical HH signaling cannot be activated in cSCC cell lines. Nevertheless, the fact that *GLI1* as a main target of canonical HH/GLI signaling pathway can in principle be up- or downregulated indicates that *GLI1* is not silenced in any of the used cell lines.

The paradoxical upregulation of *GLI1* in SCL-I cells after treatment with HhA may also indicate that this drug might regulate other signaling pathways in SCL-I cells that are not regulated in MET-1 or MET-4 cells.

Because the results from the patient samples indicated a negative crosstalk between HH/*GLI1* and mTOR or HH/*GLI1* and ERK signaling (see section 6.1., Fig. 5 B and D), we checked whether the induction of *GLI1* expression observed in SCL-I cells after treatment with HhA (see Fig. 10 C) was related to activation of one of these pathways. For this purpose, we

performed Western Blot analyses. Indeed, we noted a decrease in phosphorylation of ERK and a decrease in AKT/pAKT in SCL-I cells (Fig. 11). However, in contrast to our hypothesis of a negative regulation between *GLI1* and mTOR pathway, we observed that *GLI1* induction was accompanied by an increase in S6 phosphorylation in SCL-I cells (Fig. 11). Interestingly, in MET-1 cells, in which HhA has downregulated *GLI1* (see Fig. 10 C), we noticed an increase in pERK, whereas again the AKT/pAKT was decreased (Fig. 11). Due to these data and although no changes in the respective molecules were observed in MET-4 cells, we hypothesized that it might be the MEK/ERK axis that can negatively regulate *GLI1* expression and thus the HH/GLI axis.
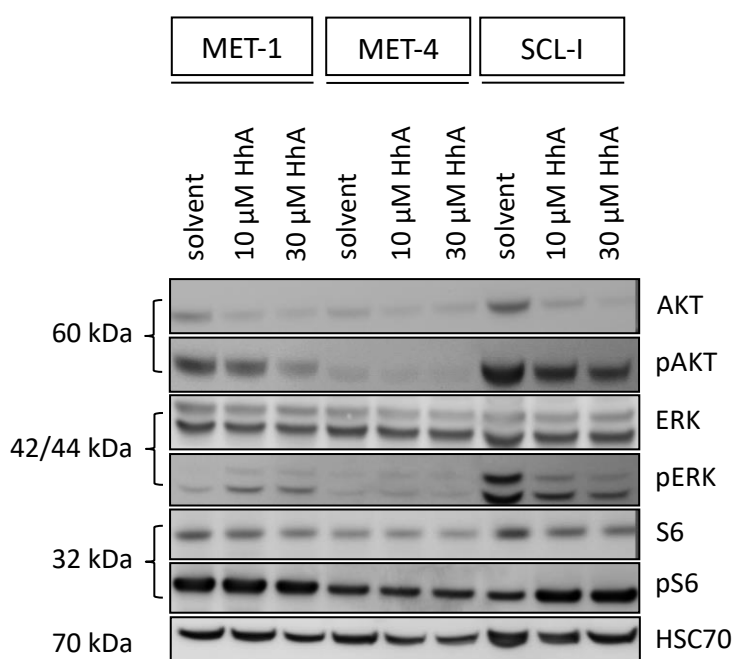
Figure 11: Influence of HhA treatment on PI3K/AKT/mTOR and MEK/ERK pathway activity in cSCC cell lines. Western Blot showing changes in phosphorylation level of AKT, ERK and S6 in cSCC cell lines after treatment with 10 µM and 30 µM of HhA. HSC70 served as a loading control. Size of the proteins (in kDa) is indicated on the left side of the blot.

6.4. Modulation of noncanonical HH signaling activity in cSCC cell lines

In the following, we focused on the interaction between HH/GLI and PI3K/AKT/mTOR and MEK/ERK signaling pathways that are known to be able to influence the activity of GLI proteins family (Eberl et al., 2012; Stecca et al., 2007; Y. Wang et al., 2012). We furthermore put into focus potential ligands that activate the respective pathways. These were EGF that we detected in the IHC analysis of cSCC samples (see Fig. 5 E) and IGF1 that besides EGF is an important factor in cSCC pathogenesis (Oh *et al.*, 2014).

6.4.1. Impact of PI3K/AKT, mTOR and MEK/ERK signaling on GLI1 expression level

To figure out whether PI3K/AKT, MEK/ERK or mTOR may regulate *GLI1* mRNA levels we treated the cells with specific inhibitors of the aforementioned pathways i.e. GDC-0941 (specific PI3K inhibitor), PI103 (dual PI3K and mTOR inhibitor), MK-2206 (specific AKT inhibitor), UO126 (MEK1/2 inhibitor) as well as everolimus and rapamycin (mTOR inhibitors). Prior to *GLI1* expression analysis we assessed efficiency and specificity of the inhibitors at given concentrations (Table 14, Materials section). The obtained results after 48 h of incubation were consistent for all 3 cell lines. Thus, everolimus and rapamycin inhibited mTOR and therefore S6K, which cannot further phosphorylate the ribosomal protein S6. GDC-0941 and MK-2206 blocked PI3K and AKT activity, respectively, which was indicated by reduction in AKT phosphorylation level. PI103 as a dual inhibitor of PI3K and mTOR decreased the level of pAKT and pS6 and UO126 as a MEK1/2 inhibitor reduced the level of pERK. One exception was MET-1 cell line, in which PI103 inhibitor did not exert expected results (Fig. 12).

Additionally, we noted that GDC-0941 and MK-2206 inhibitors also decreased the level of pS6 in SCL-I and MET-1 cells, whereas in MET-4 cells this effect was only observed after treatment with MK-2206. Furthermore, in SCL-I and MET-4 cells, the treatment with UO126 resulted not only in a decreased signal for pERK but also for pS6 (Fig. 12). This is in line with the fact that mTOR activity can be regulated by both PI3K/AKT and MEK/ERK signaling (Mendoza et al., 2011). We also observed an interaction between PI3K, AKT and mTOR signaling with MEK/ERK. Thus, treatment with GDC-0941 resulted in decreased pERK level in SCL-I and MET-1 cells. A similar effect was observed in SCL-I and MET-4 cells upon incubation with PI103 and in MET-1 and MET-4 cells after treatment with MK-2206 (Fig. 12). On the other hand, we noted an increased level of pAKT after treatment with UO126 suggesting the existence of a negative feedback loop between pERK and pAKT in MET-4 cells. Such a feedback has been described by two groups who showed that MEK1/2 inhibition leads to the activation of the PI3K/AKT pathway (Yu et al., 2002; Lehr et al., 2004). Moreover, specific inhibition of mTOR signaling with everolimus or rapamycin resulted in increased level of AKT and ERK phosphorylated forms in MET-4 cells (Fig.12).
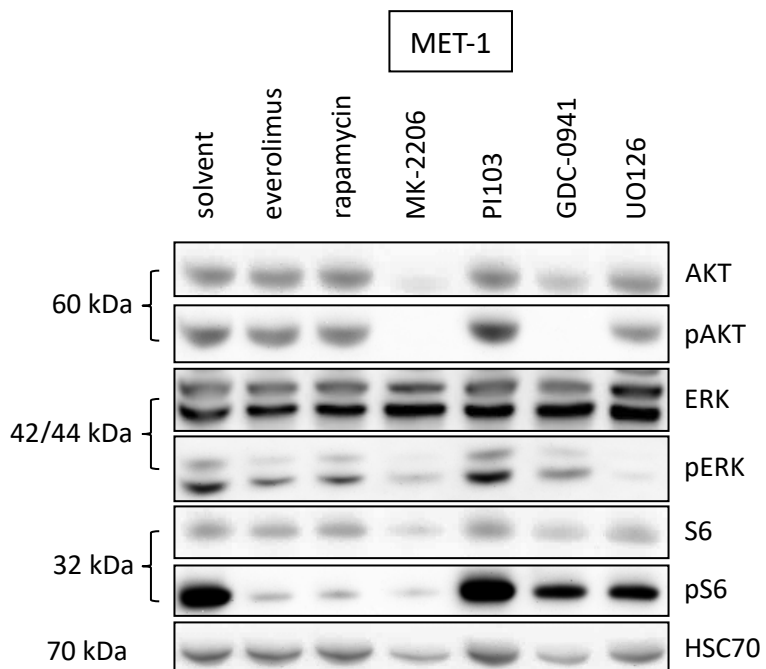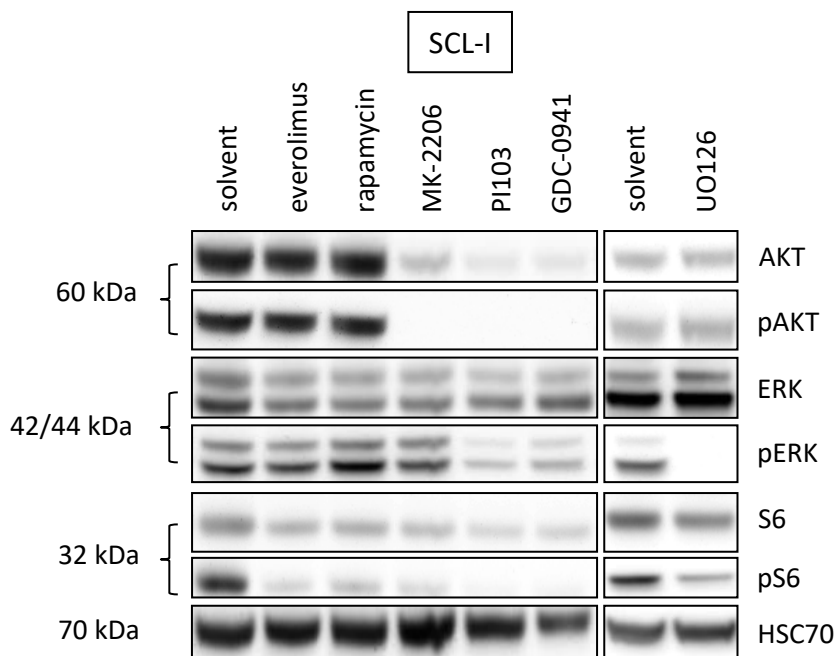
Figure 12: Effects of PI3K, AKT, mTOR and MEK1/2 inhibition on cSCC cell lines. Representative blots showing changes in pAKT, pERK and pS6 levels upon treatment of SCL-I, MET-1 and MET-4 cells with 50 nM everolimus, 100 nM rapamycin, 5 µM MK-2206, 3 µM PI103, 10 µM GDC-0941 and 20µM UO126. HSC70 expression served as a loading control. The size (in kDa) of the analyzed proteins is indicated on the left side of the blots.
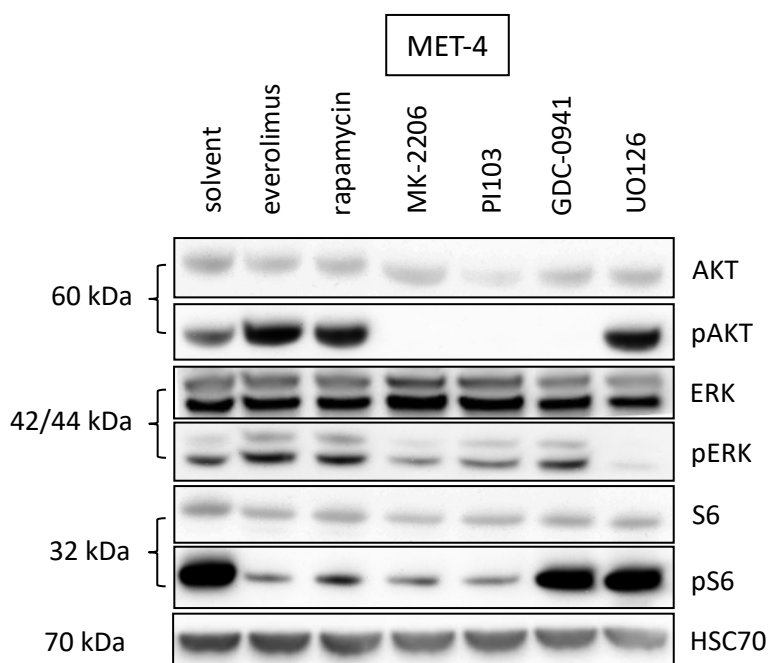
To further see whether these changes affect the *GLI1* expression level, we incubated the cells with the same set of inhibitors for 24 h and performed *GLI1*-specific qPCR analysis. Treatment with PI3K/AKT and/or mTOR inhibitors consistently inhibited *GLI1* expression. The inhibition was significant in all cell lines with the exception of MET-1 cells after treatment with rapamycin or PI103 (Fig. 13). Interestingly, *GLI1* was significantly upregulated in SCL-I cells upon treatment with UO126, whereas in MET-1 and MET-4 cells this drug did not influence *GLI1* expression level (Fig. 13). This indicates that in general inhibition of PI3K/AKT/mTOR signaling decreases *GLI1* transcription, whereas inhibition of MEK1/2 (and concomitant decrease in ERK phosphorylation) results either in activation of *GLI1* transcription (i.e. in SCL-I cells) or does not impact on *GLI1* expression (i.e. in MET-1 and MET-4 cells). In other words, whereas PI3K/AKT/mTOR signaling may in general activate *GLI1* transcription, the MEK axis can inhibit it.
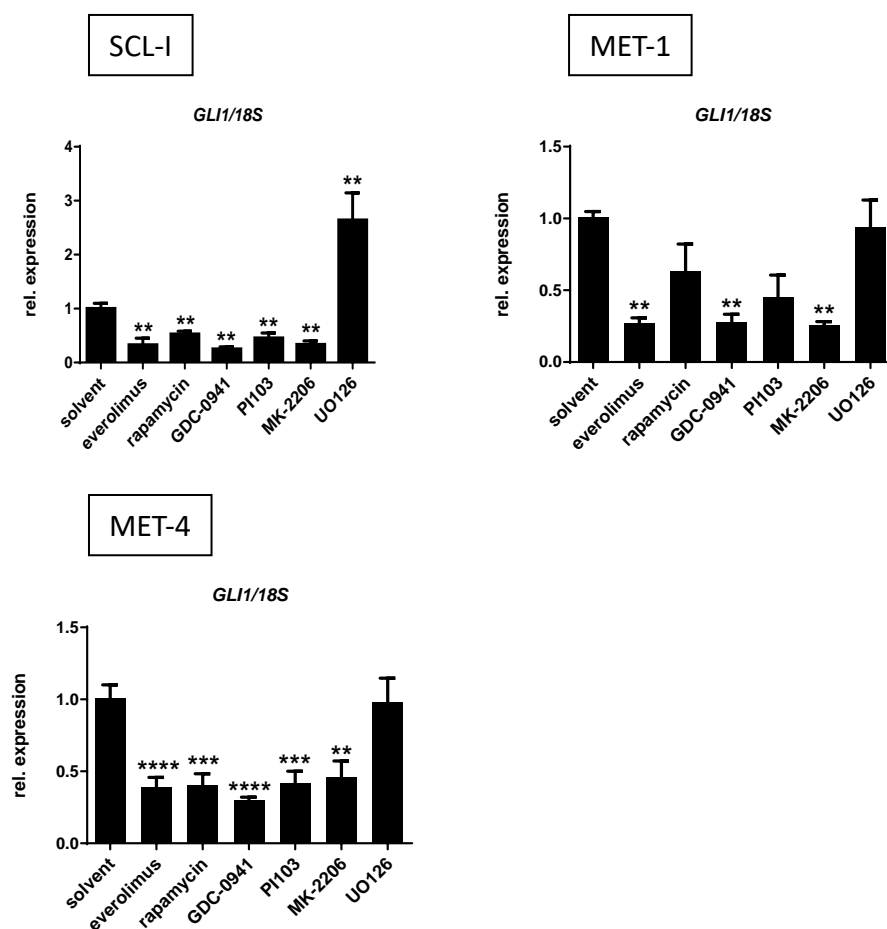
Figure 13: Impact of PI3K, AKT, mTOR and MEK1/2 inhibition on *GLI1* expression level in cSCC cell lines. Relative *GLI1/18S* expression upon 24 h treatment of SCL-I, MET-1 and MET-4 cells with 50 nM everolimus, 100 nM rapamycin, 5 μM MK-2206, 3 μM PI103, 10 μM GDC-0941, 20μM UO126 and solvent control that was set to 1. Each graph summarizes data from 3 independent experiments performed in triplicates. Data are presented as mean +/- SEM; *, $p<0.05$; **, $p<0.01$; ***, $p<0.001$; ****, $p<0.0001$. Statistical comparisons were done with Mann-Whitney test.

To further analyze the potential role of mTOR or PI3K/AKT pathway in activation of *GLI1* expression and/or its relevance for pathogenesis of cSCC we first transfected SCL-I cells with one of three mTOR plasmids expressing wild type mTOR (pcDNA3-Flag mTOR wt), a constitutively active (pcDNA3-AU1-mTOR-S2215Y) or a rapamycin-resistant (pcDNA3-Flag mTOR S2035T) variant as well as a corresponding empty vector (pcDNA3). Prior to the expression analysis we confirmed the specificity of the plasmids by sequencing the part of insert bearing the indicated mutation (data not shown). If mTOR indeed should positively regulate *GLI1*, then all three mTOR variants should increase *GLI1* expression level under full-serum conditions. Moreover, in case of wild type and constitutively active variants, *GLI1* level should be decreased upon mTOR inhibition with rapamycin because the constitutively

active mTOR variant bearing S2215Y point mutation is still sensitive to rapamycin treatment (Sato et al., 2010). However, it should not decrease in cells transfected with the rapamycin-resistant mTOR variant. Unfortunately, we were not able to detect any overexpression of mTOR, neither with anti-AU1 nor with anti-flag tag antibody (data not shown). We also checked the level of pS6 as readout for mTOR pathway activity but we did not observe any differences when compared to the empty vector control (data not shown). Therefore, we did not put more effort in this experiment.

In order to investigate the potential role of PI3K/AKT in *GLI1* activation, the cells were transfected with either a constitutively active variant of AKT1 (Akt1-CA) or its dominant negative form (Akt1-DN). If AKT indeed should positively regulate *GLI1* expression, then the transfection with constitutively active variant should result in increase, whereas the dominant negative variant should decrease the *GLI1* expression level. The constitutive activation of Akt1-CA variant is achieved by fusing src myristoylation signal (myr) to N-terminal end of Akt1 sequence. Myristoylation signal targets Akt1 to the cell membrane and results in its constitutive activation. Furthermore, Akt1-CA has a depleted PH domain and thus the protein size is smaller (~52 kDa) than the full length Akt1-DN (~60 kDa) and both plasmids contain an HA-tag (Fig. 14 A). To first assess the efficiency of the transfection and the functionality of the plasmids we performed Western Blot with an anti-HA tag antibody as well as anti-AKT/pAKT antibodies. In addition, we used HEK293 cells as a positive control due to their great transfection efficiency. The results show that the HA-tagged forms of AKT1 are expressed in HEK293 cells at the expected sizes (Fig. 14 B). As expected, the Akt-CA variant was highly phosphorylated, whereas phosphorylation of endogenous AKT did not change in HEK293 cells. Also, Akt1-DN was highly expressed as indicated by the detection of HA tag. As expected the expression of Akt1-DN was accompanied by a decrease in endogenous AKT phosphorylation confirming thereby functionality of the plasmid (Fig. 14 B). When the plasmids were expressed in the experimental SCL-I cell line we detected a band corresponding to the Akt1-CA variant with the anti-HA tag antibody, which was accompanied by a slight increase in phosphorylation of endogenous AKT detected with anti-pAKT antibody. On the other hand, only a very faint band was detected for the Akt1-DN variant with the anti-HA tag antibody. Overall, either the transfection efficiency or the expression of the plasmids in SCL-I cells was lower than in HEK293 cells. (Fig. 14 B). When *GLI1* expression in Akt1-CA and Akt-DN transfected SCL-I cells was analyzed and normalized to

either *18S rRNA* or *HPRT* expression, no significant changes in *GLI1* expression were detected when compared to untransfected cells or to cells that have been transfected with a plasmid that expresses EGFP (Fig. 14 C). Together these data suggest that i) *GLI1* expression is not regulated by AKT and ii) that the downregulation of *GLI1* upon incubation of the cells with MK-2206 and PI103 (and also with GDC-0449; see Fig. 13) must be due to other signaling molecules than AKT.

A
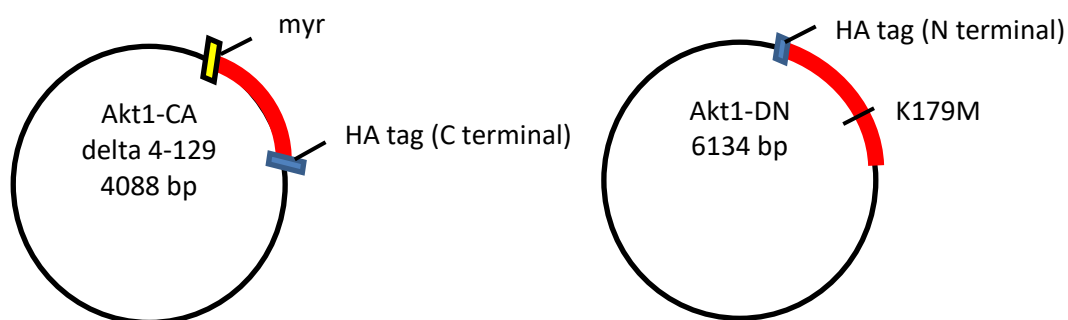
B
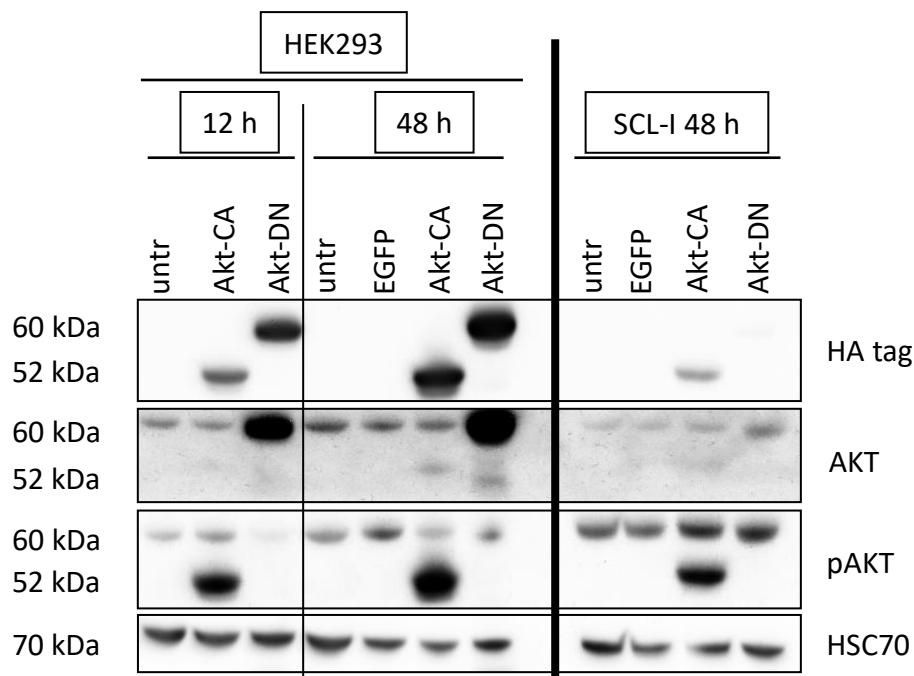
C
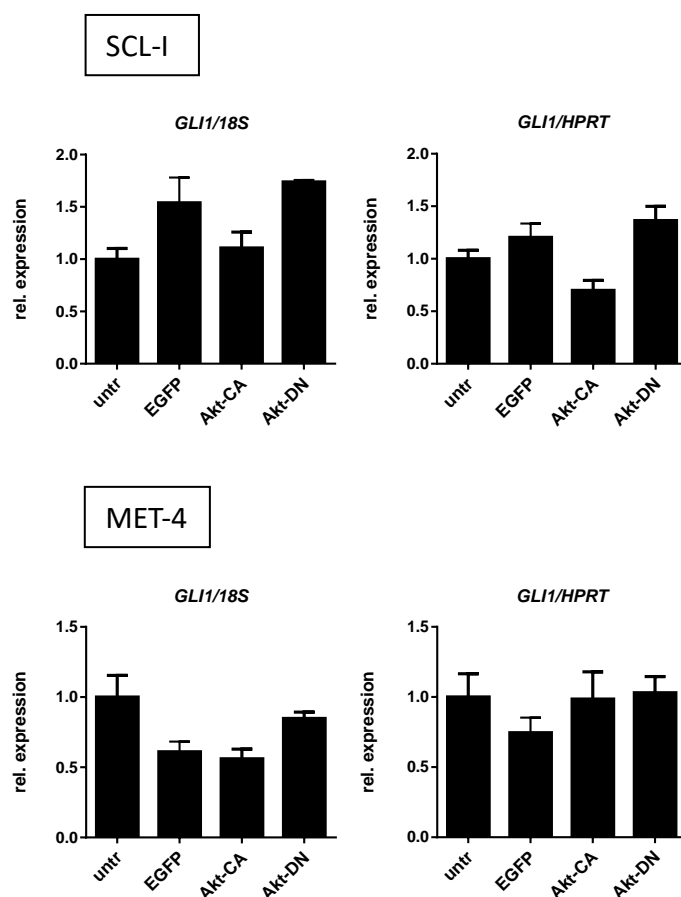
Figure 14: Expression of a constitutively active and dominant-negative form of AKT and impact on *GLI1* expression level in cSCC cells lines. A. A scheme depicting specific mutations and modifications of the constitutively active (CA) and dominant negative (DN) form of AKT within the plasmid used for transfection; myr, N-terminal myristoylation signal in the Akt1-CA plasmid; K179M, dominant negative point mutation in Akt1-DN plasmid; the HA tag is located at the C- or N- terminus of Akt1-CA and Akt1-DN plasmids, respectively. **B.** Western Blot analysis for the detection of the HA tag and total AKT/pAKT showing the efficiency of transfection and functionality of the plasmids in HEK293 control cell line and SCL-I cells at indicated time points. HSC70 served as a loading control. Protein sizes (kDa) are indicated on the left side of the blot. The 60 kDa size corresponds to the full-length Akt1-DN variant as well as endogenous AKT. 52 kDa size corresponds to the Akt1-CA variant, which has a depleted PH domain. **C.** qPCR analysis of *GLI1* in SCL-I and MET-4 cells 24 h after transfection with the AKT plasmids or EGFP control plasmid. *GLI1* expression was normalized to the expression of either *18S rRNA* or *HPRT* and compared to values of untransfected and EGFP transfected cells. The expression in untransfected cells was set to 1. Each graph summarizes three technical replicates of one experiment. The data are presented as the mean +/- SEM; untr, untransfected. Statistical comparisons were done with Mann-Whitney test.

84

To investigate the impact of MEK/ERK on *GLI1* expression we have pursued a different approach. As described in section 6.1. we observed pERK expression in stromal cells surrounding the cSCC cells that were negative for *GLI1* (see Fig. 5 D). We also described that cells located in outer parts of the tumor are strongly pS6 positive (see section 6.1, Fig. 5 B and E) and might therefore play a role in integration of the signals derived from stroma. Due to the experiments indicating that the MEK/ERK axis may indeed negatively impact on *GLI1* expression (see section 6.3.3. and 6.4.1.), we decided to check whether fibroblasts that express pERK (Wayne *et al.*, 2006) and are a common type of stromal cells may influence *GLI1* expression. For this purpose, we co-cultured SCL-I, MET-1 and MET-4 cells with the human fibroblast cell line BJ. Our co-culture system allows for clear distinction between different cell types as "feeder cells" are cultured in inserts with pore size that enables exchange of nutrients but not cell migration. We observed that co-culture of SCL-I cells with BJ cells significantly inhibited *GLI1* expression. A similar tendency was also observed in co-cultured MET-1 cells when compared to the MET-1 monoculture system, whereas in MET-4 cells this effect was not visible (Fig. 15 A). This shows that fibroblasts that express pERK can inhibit *GLI1* expression in a paracrine manner. To exclude effects of the factors included in the serum, we also performed the same experiment under serum depletion conditions (0.5% FCS). Under starved conditions we also noted the decrease in *GLI1* expression in all 3 cell lines, which however did not reach significance (Fig. 15 A). Unfortunately, we so far have not checked for pERK expression in BJ ourselves, which will be done in the future.

Based on the opposing staining pattern between pS6 and *GLI1* in human cSCC tissue sections (see Fig. 5 B), we also wanted to know whether the decrease in *GLI1* expression level was accompanied by changes in S6 phosphorylation. For this purpose, we co-cultured fibroblasts with SCL-I cells in 10% FCS-containing medium and stained the SCL-I cells via immunofluorescence with a Cy3 anti-pS6 antibody. However, we did not observe any changes in the number of pS6 positive cells between mono- and co-culture (Figure 15 B, C). Nevertheless, it remains to be said that the basal expression level of pS6 in monocultured control cells is high and reaches nearly 100%. Thus, an increase in pS6 positive cells or an upregulation of pS6 protein expression would have been hard to detect. Together, although we could neither confirm nor exclude a negative regulation between *GLI1* and pS6, the results indicate that the tumor microenvironment may play a role in *GLI1* downregulation within the tumor tissue. Whether the *GLI1* downregulation in co-culture is due to MEK/ERK activity in

the fibroblasts and whether it is independent of mTORC1 requires further validation in the future.

A

B

C
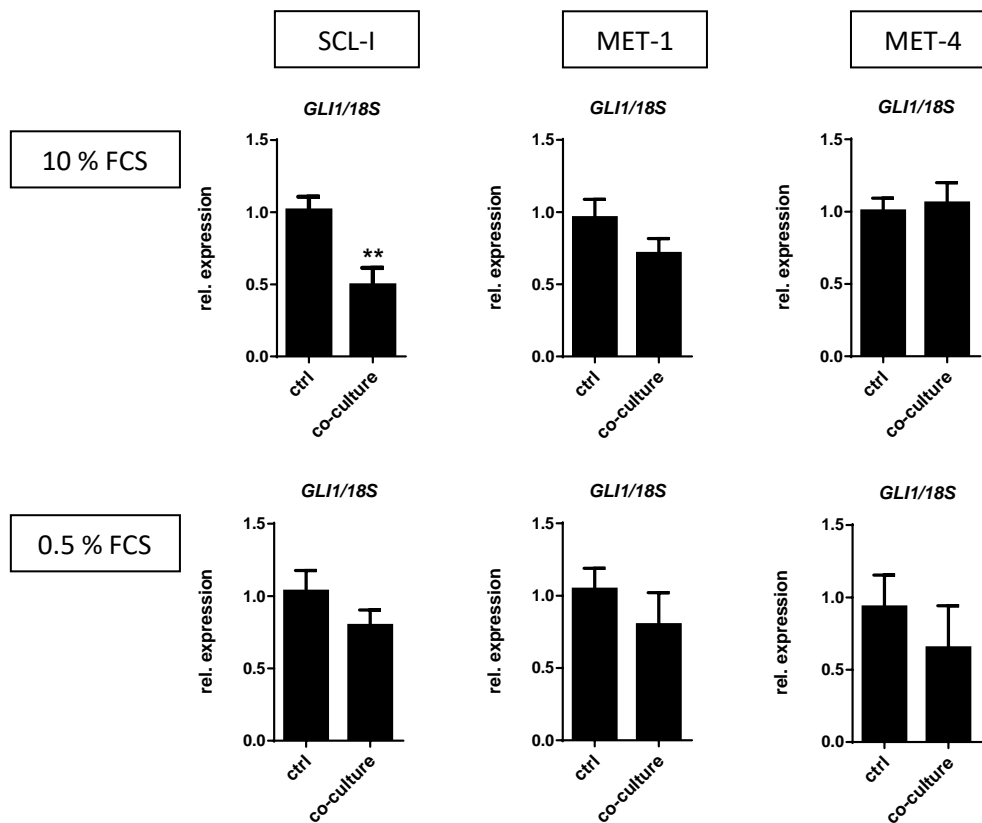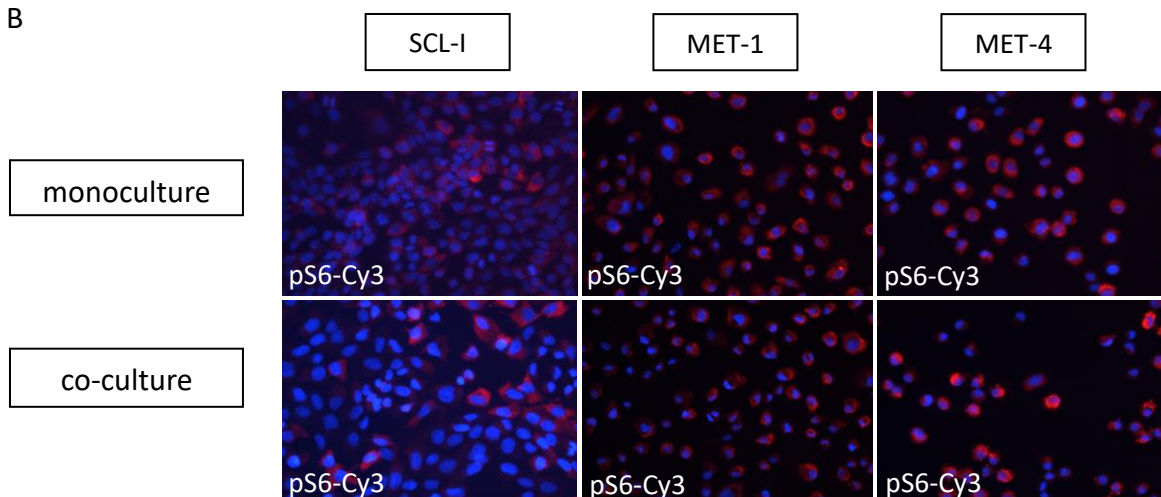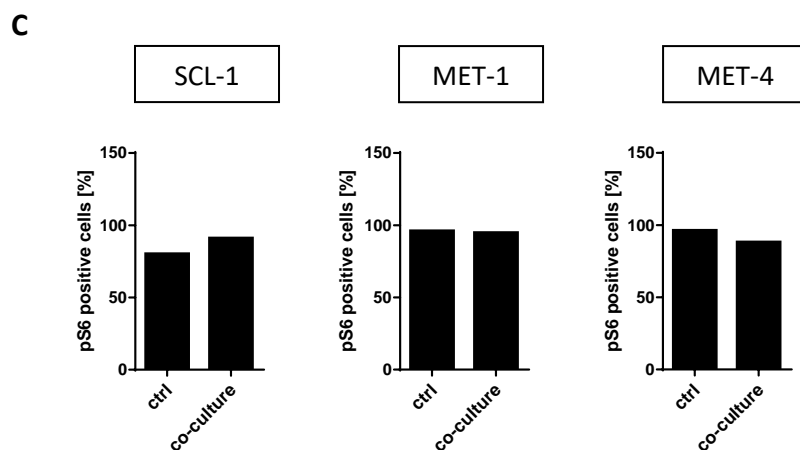
Figure 15: Impact of co-cultured human fibroblasts on *GLI1* and pS6 expression in cSCC cell lines. Analysis of the cSCC cell lines SCL-I, MET-1 and MET-4 that were co-cultured with the human fibroblast cell line BJ (co-cultured) in comparison to monocultured cells (ctrl). **A.** Comparison of *GLI1* expression levels under full-serum and serum-depleted conditions. All data are presented as the mean value +/- SEM of three independent experiments; **, $p<0.01$. Statistical analysis was performed using Mann-Whitney test; ctrl, control. **B.** Expression analysis of pS6 by immunofluorescence. Representative pictures show pS6-Cy3 expression in red and DAPI-stained nuclei in blue at a 20 x magnification. **C.** pS6-Cy3 positive cells (red) shown as the percentage of all cells visualized by DAPI staining (blue).

6.4.2. Impact of EGF/EGFR and IGF1/IGF1R on *GLI1* expression level

The RTKs EGFR and IGF1R are known to be highly expressed in a high percentage of cSCC in patients (Oh et al., 2014; Shimizu et al., 2001) and are also expressed in MET-1 and MET-4 cells (Clayburgh *et al.*, 2013).

Because RAS/MEK/ERK and PI3K/AKT/mTOR signaling are downstream of RTKs and because cSCC express high levels of at least the EGF ligand (see Fig. 5 E), we next wanted to know whether EGF or related RTK ligands are involved in the modulation of noncanonical HH/GLI signaling. Hence the cell lines were stimulated with commercially available EGF and IGF1. To exclude effects of growth factors included in the serum of the cell culture medium, all the experiments with EGF or IGF1 were done under serum depletion conditions (0.5 % FCS containing medium). To first establish the most efficient conditions for stimulation of the pathways, cells were incubated with different concentrations of the ligands and for different time durations. As revealed by Western Blot, incubation with 100 ng/µl EGF as short as for 5 min was sufficient to trigger phosphorylation of ERK1/2, the downstream target of MEK, while phosphorylation of AKT appeared after 30 min of stimulation (Fig. 16 A). These changes were also accompanied by an increase in pS6 30 min after stimulation with EGF and

thus activation of mTOR signaling. This activation was sustained throughout the experiment (Fig. 16 A). However, ERK and AKT phosphorylation was only a temporary effect as the phosphorylation of pAKT and pERK decreased after 6 h of incubation in all three cell lines and after 3 h in SCL-I and MET-4 cells, respectively (Fig. 16 A). The decrease in pS6/S6 levels after 5 min of treatment in MET-4 cells is a matter of protein loading (see fainter HSC70 signals in Fig. 16 A), and was not seen in the other 2 blots that have been done.

We next examined the changes in *GLI1* transcription. Indeed, as shown in Fig. 16 B, EGF significantly decreased the expression of this HH signaling marker in all 3 cell lines after 3 h of incubation (Fig. 16 B). This is in line with the opposing staining pattern observed for EGF and *GLI1* in some human tissue samples in invading parts of the tumors (see Fig. 5 E).

Figure 16: Effects of EGF on PI3K/AKT, MEK/ERK and mTOR downstream signaling pathways on *GLI1* expression level in cSCC cell lines. A. Representative Western Blot showing activation of PI3K/AKT, MEK/ERK and mTOR signaling pathways upon treatment with 100 ng/µl EGF in a time-dependent manner. Red frames highlight the strongest induction of phosphorylation of AKT, ERK and S6 in each cell line. HSC70 served as a loading control. Protein size in kDA is indicated on the left side of the blot. **B.** Changes in *GLI1/18S rRNA* expression level upon 3 h stimulation with EGF in SCL-I, MET-1 and MET-4 cells. Each graph represents a summary of three independent experiments measured in triplicates with solvent control set to 1. All data are displayed as a mean +/- SEM; **, $p<0.01$; ***, $p<0.001$. Statistical comparisons were done by Mann-Whitney testing.

On the other hand, 50 ng/µl IGF1 activated the downstream signaling pathways after 3-6 h with phosphorylation of AKT appearing already after 3 h of incubation in all three cell lines and less prominent phosphorylation of ERK after 6 h of incubation in SCL-I and MET-1 cells. No changes in pERK were observed in MET-4 cells (Fig. 17 A). As observed upon EGF stimulation, IGF1-mediated increase in pAKT and pERK was accompanied by increased pS6 levels occurring already after 3 h of incubation and indicating activation of mTOR signaling. Moreover, increase in pS6 expression clearly overlapped with induction of AKT phosphorylation. These data might indicate that IGF1 mainly stimulates AKT phosphorylation that further activates mTOR. Similar effects have been described in the literature, suggesting that IGF1 strongly induces PI3K/mTOR but only weakly activates RAS/ERK activity (Mendoza *et al.*, 2011). Importantly, and as seen with EGF, the incubation with IGF1 also decreased *GLI1* transcription after 6 h, which was significant for SCL-I and MET-4 cells (Fig. 17 B).

Together these data suggest a negative regulation of *GLI1* expression by EGF and IGF1 signaling in the cSCC cell lines SCL-I, MET-1 and MET-4.
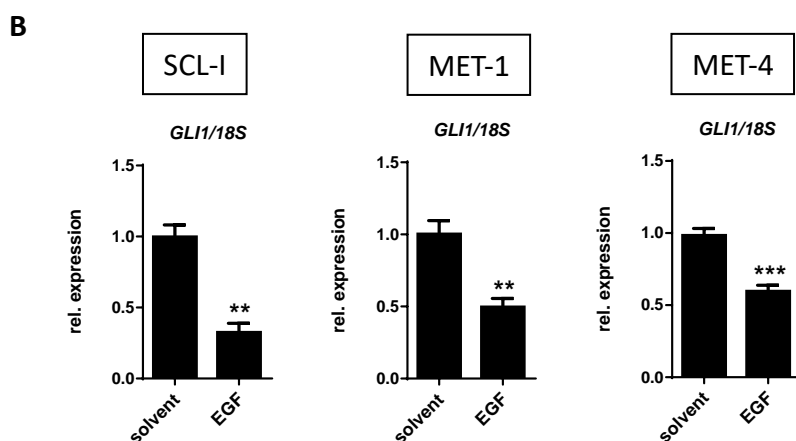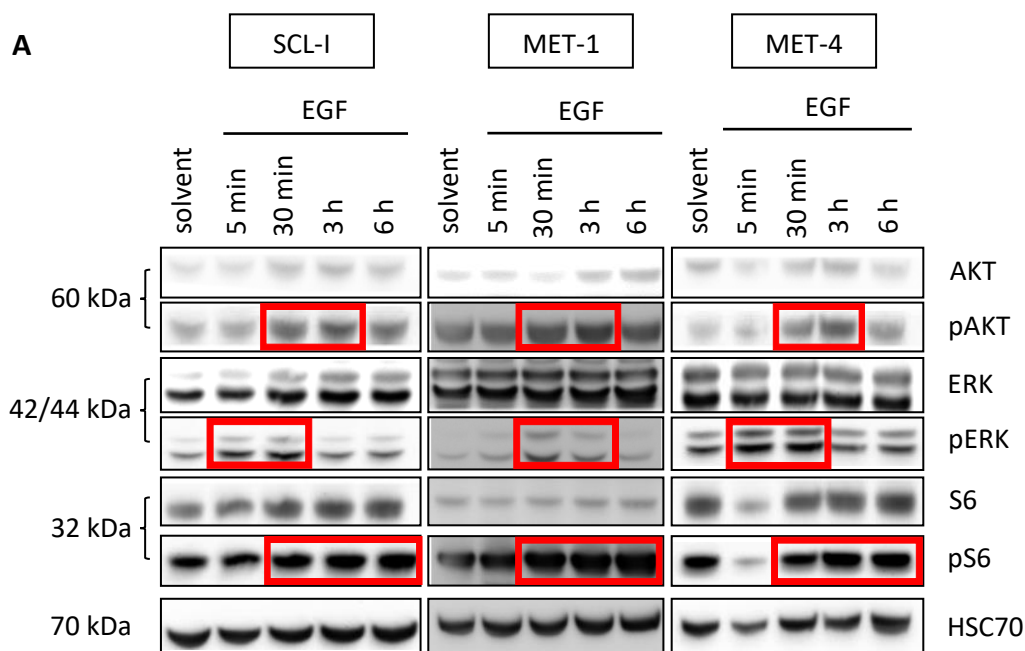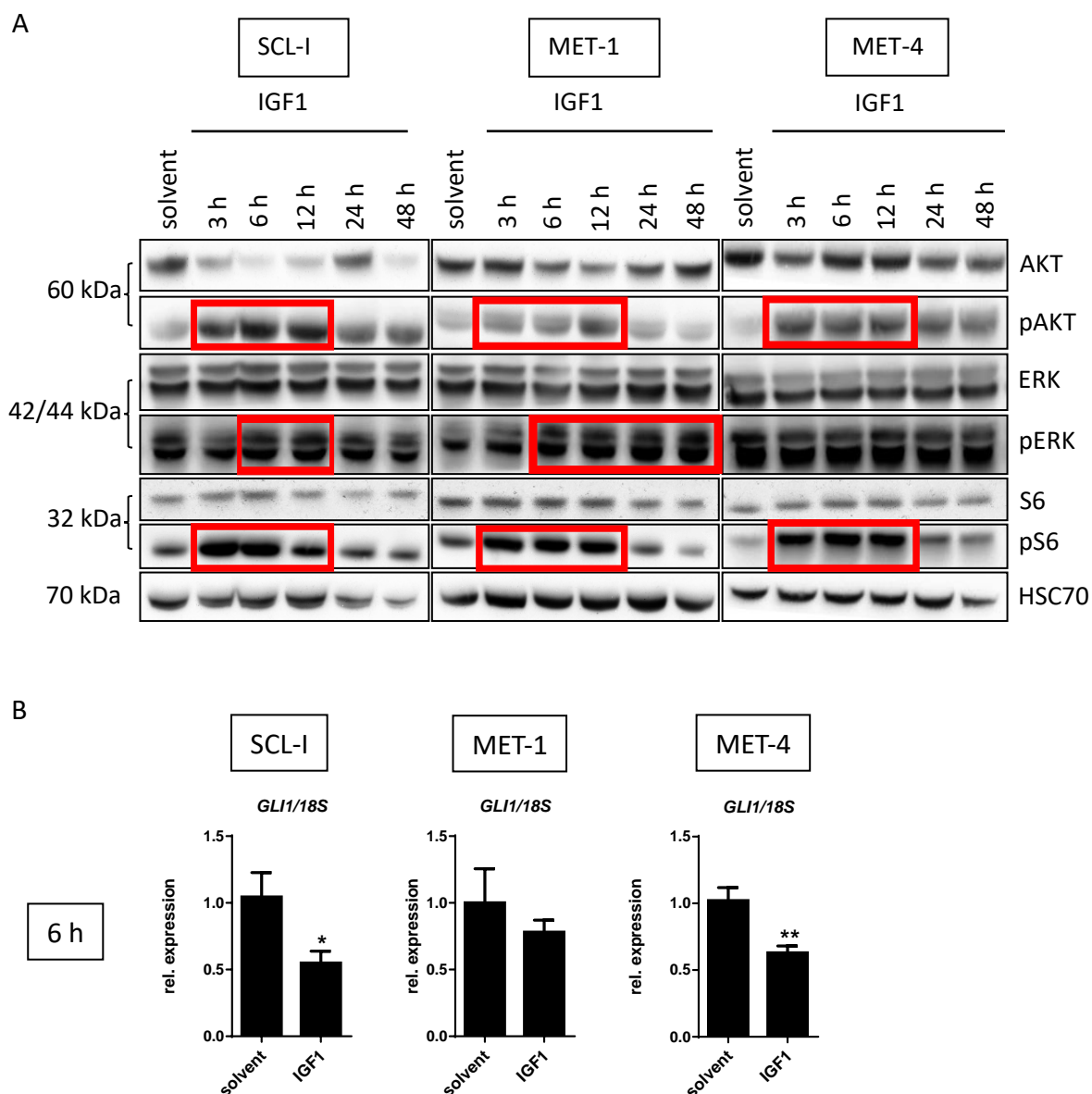
Figure 17: Effects of IGF1 on PI3K/AKT, MEK/ERK and mTOR downstream signaling pathways and on *GLI1* **expression level in cSCC cell lines. A.** Representative Western Blot showing phosphorylation of AKT, ERK and S6 in MET-1, MET-4 and SCL-I cells upon incubation with 50 ng/µl IGF1 for the indicated time points. Red frames highlight the strongest induction of pAKT, pERK and pS6 in each cell line. HSC70 served as reference controls. Protein size is indicated on the left side of the blot. **B.** qPCR showing changes in *GLI1* expression upon incubation with 50 ng/µl of IGF1 for 6 h in SCL-I, MET-1 and MET-4 cells. The *GLI1* data were normalized to the expression of the *18S rRNA* housekeeping gene and the relative expression of control cells was set to 1. Each graph represents a summary of two independent experiments performed in 3 technical replicates. The data are shown as a mean +/- SEM; *, p<0.05; **, p<0.01. Statistical comparisons were done with Mann-Whitney test.

6.4.3. Impact of EGF plus MEK, PI3K, AKT and/or mTOR inhibitors on GLI1 expression level

We next wanted to see, whether the EGF-induced significant *GLI1* inhibition was also mediated by the MEK axis. For this purpose, we combined EGF with UO126, but also with the inhibitors of the PI3K/AKT or mTOR pathway. As already described in the section before, a 3 h incubation with EGF resulted in a decrease in *GLI1* transcription. However, the inhibitors have been used for 24 h (see section 6.4.1.). Therefore, in this experimental design, we preincubated the cells for 21 h and added EGF to the cells for the last 3 h of incubation. Afterwards, the cells were collected for RNA isolation and subjected to gene expression analysis. Indeed, the qPCR data suggest that *GLI1* inhibition is mediated by MEK/ERK rather than by mTOR or PI3K/AKT signaling. This is due to the fact that the combined treatment of EGF plus UO126 (MEK1/2 inhibitor) led to an upregulation of *GLI1* in comparison to EGF treatment alone. This upregulation was observed in all 3 cell lines and resulted in *GLI1* expression that was not significantly modulated with respect to either the solvent- or EGF-mediated values. In MET-1 cells, UO126 even significantly upregulated EGF-mediated *GLI1* expression, when compared to EGF-treatment alone (Fig. 18). On the contrary, treatment with PI3K, AKT or mTOR inhibitors, either alone or in combination with EGF, strengthened the downregulation of *GLI1* expression level, which points to a positive regulatory mechanism between these pathways and HH/GLI signaling (Fig. 18).

In summary, these data foster the assumption that EGF-mediated *GLI1* downregulation is regulated via the MEK/ERK axis.
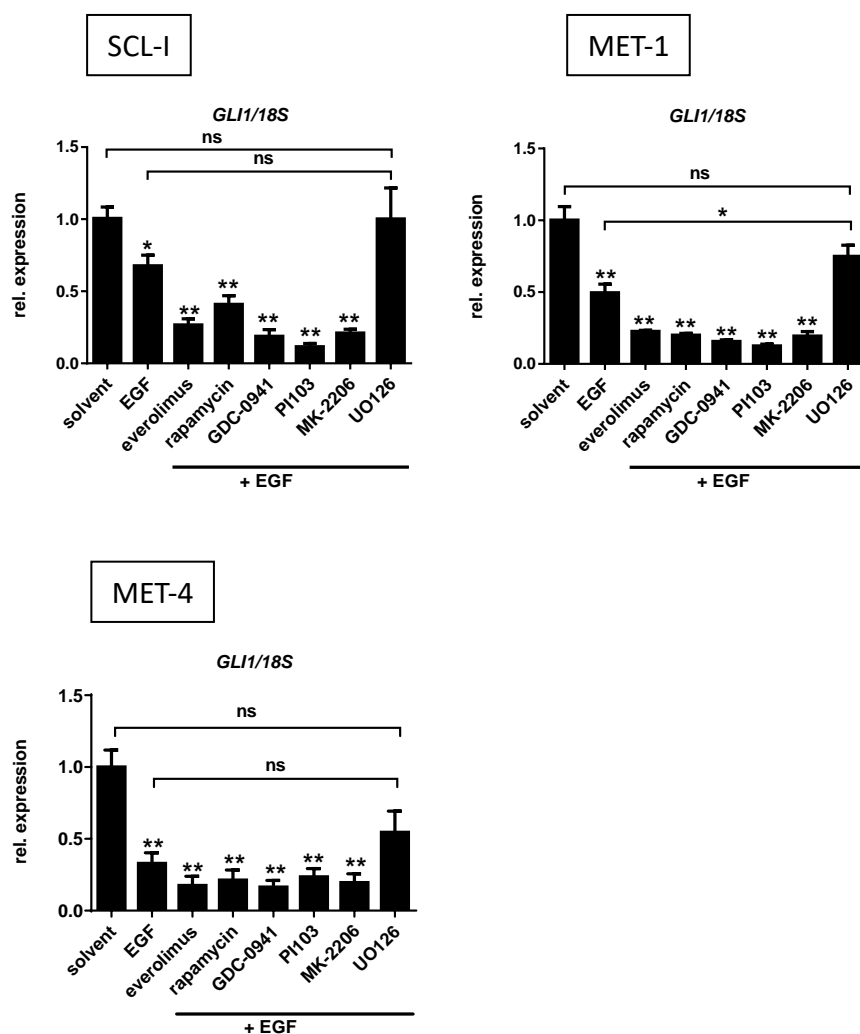
Figure 18: Effects of EGF plus PI3K, AKT, mTOR or MEK1/2 inhibition on *GLI1* expression level in cSCC cell lines. qPCR representing *GLI1* expression upon treatment with EGF or EGF combined with 50 nM everolimus, 100 nM rapamycin, 5 µM MK-2206, 3 µM PI103, 10 µM GDC-0941 or 20µM UO126 in SCL-I, MET-1 and MET-4 cells. The expression level was normalized to *18S rRNA* gene expression and solvent treated controls were set to 1. Data are presented as mean values of three independent experiments measured in triplicates +/- SEM; *, $p<0.05$; **, $p<0.01$. Statistical comparisons were done with Mann-Whitney test.

Besides investigation of the impact of the ligands EGF and IGF1 on *GLI1* expression level we also started to use EGFR and IGF1R blocking antibodies (EGFR ab and IGFR ab, respectively) in order to block the respective receptors. So far, we have used only one condition for EGFR ab (10 ng/µl for 24 h) and have varied the concentration (0.5-10 ng/µl) and the incubation time (1-24 h) for the IGF1R ab. Since the experiments have been done only once so far, the data is preliminary and not reliable at that time and has to be carefully looked at.

In the preliminary setting for EGFR ab treatment, the cells were incubated with 10 ng/µl of EGFR ab for 24 h. This incubation time was chosen because it has been shown that 24 h of treatment with anti-EGFR monoclonal antibodies efficiently decreases levels of pEGFR, pAKT and pERK levels in HNSCC cell lines (Zhang *et al.*, 2008). We noted a strong decrease in pAKT level when compared to the solvent treated control, but we did not detect any obvious changes in phosphorylation of ERK or S6 proteins (Fig. 19). Since the latter effect however is expected, EGFR ab will be used in future experiments at higher or lower concentrations and for shorter or longer incubation times.
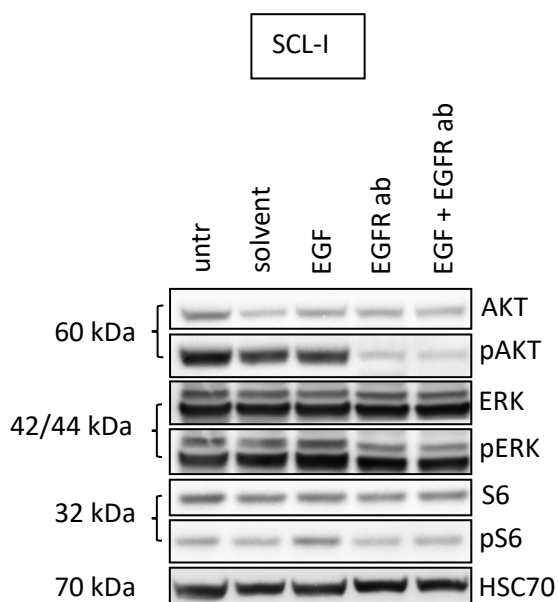
Figure 19: Impact of EGFR neutralizing antibody on PI3K/AKT, MEK/ERK and mTOR signaling in SCC cells. Western Blot showing AKT/pAKT, ERK/pERK and S6/pS6 levels in SCL-I cells that have been treated for 24 h with either 100 ng/µl EGF, 10 ng/µl of the EGFR blocking antibody (EGFR ab) or combination of both (EGF + EGFR ab), HSC70 served as a loading control. Protein sizes in kDA are indicated on the left side of the blot; untr, untreated.

The experiments using the IGF1R ab were first done in MCF-7 control cells, in which 11 ng/µl of the antibody neutralizes IGF1-stimulated proliferation by 50-75% (as specified by R&D Systems, Inc). Moreover, the incubation for 24 h with 11 ng/µl IGF1R ab apparently effectively decreases pAKT level in human astrocytes (Garwood *et al.*, 2015). In our setting, we incubated MCF-7 cells with 0.5-2 ng/µl IGF1R ab for 24 h. Figure 20 A shows that the concentration as low as 0.5 ng/µl of IGF1R ab is sufficient to reduce AKT phosphorylation in MCF-7 cells. This effect is even stronger with increasing concentrations of the antibody. Nevertheless, there was no change in other effector pathways downstream of IGF1R as shown

by unchanged pERK and pS6 level (Fig. 20 A). In parallel, we tried to establish optimal conditions in MET-1, MET-4 and SCL-I cSCC cell lines. For this purpose, we applied the antibody within the same concentration range but unfortunately, we did not observe any effect on AKT, ERK or S6 phosphorylation (data not shown). Thus, in the next step we increased the concentration of the antibody to 10 ng/µl (Fig. 20 B). As shown in Figure 20 B, incubation with IGF1R ab may result in a moderate decrease in pAKT level in MET-4 cells, however, as seen on the same blot, the detection of HSC70 was inadequate (Fig. 20 B). Otherwise we did not observe any changes. Since EGF/IGF1 stimulation showed that phosphorylation of AKT, ERK and S6 in cSCC cell lines is a rapid process (see section 6.4.3., Fig. 16 A and 17 A), we also decreased the incubation time of IGF1R ab and examined AKT/pAKT, ERK/pERK and S6/pS6 upon incubation with 5 ng/µl or 10 ng/µl within the time course ranging from 1 - 6 h in SCL-I cells (Fig. 20 C). The data show a slight decrease in pAKT level after 3 h of incubation with either 5 ng/µl or 10 ng/µl. Furthermore, a decrease in pERK was observed after 1 h and 3 h of incubation with the antibody, whereas pS6 remained unchanged (Fig. 20 C).

Taken together, we showed that IGF1R and EGFR inhibition with blocking antibodies still requires further establishment prior to *GLI1* expression or proliferation analysis.
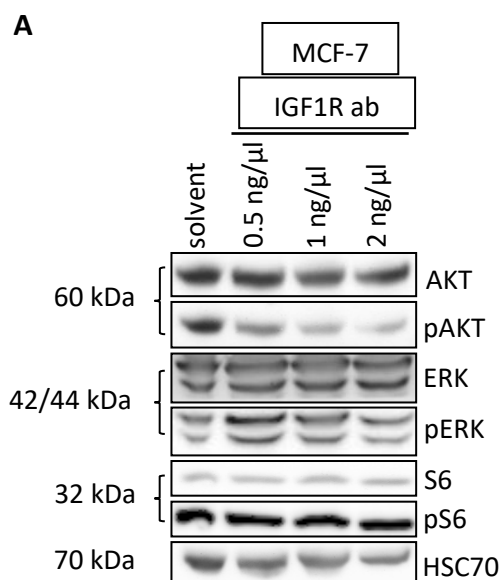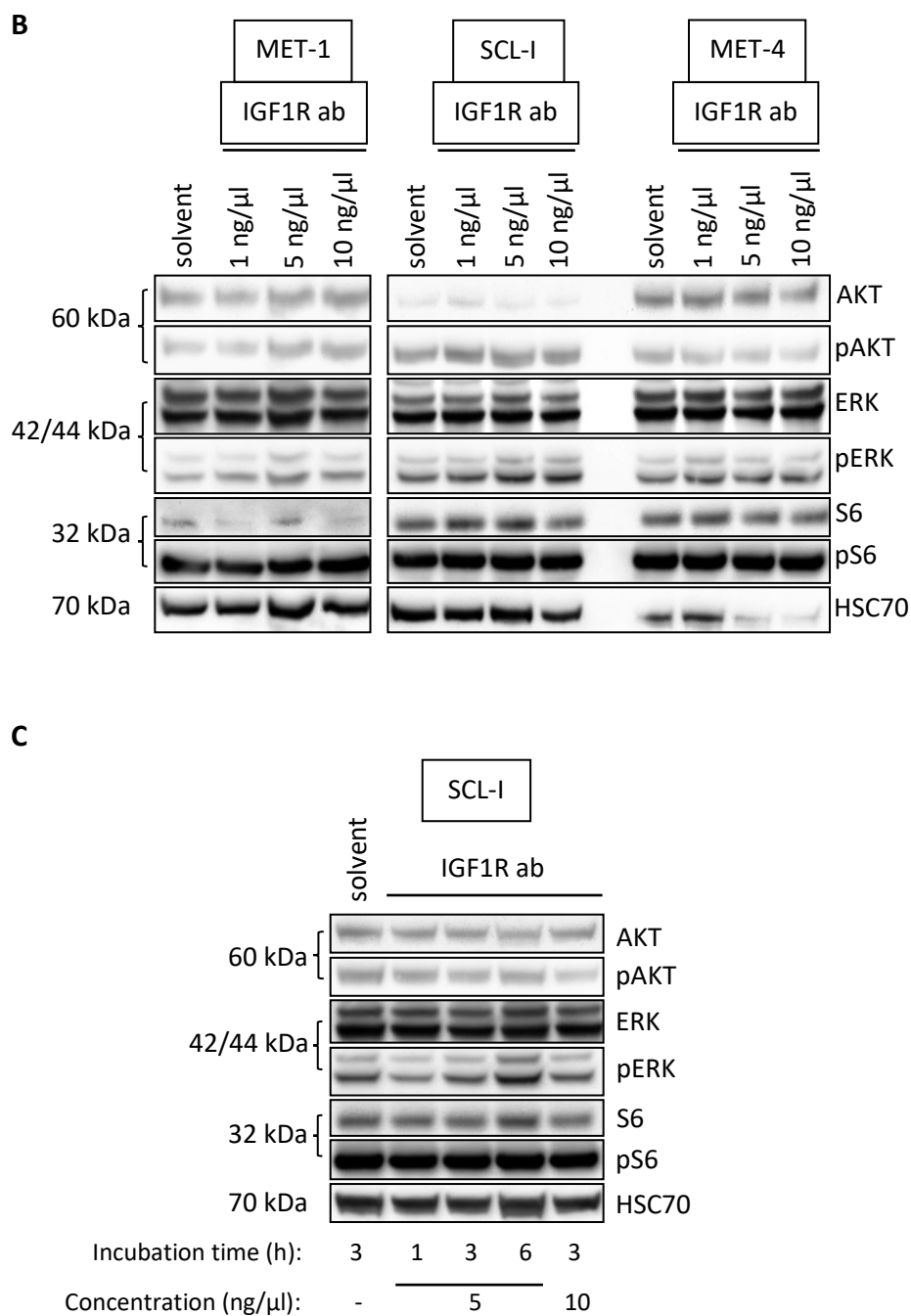
Figure 20: Impact of IGF1R neutralizing antibody on PI3K/AKT, MEK/ERK and mTOR signaling in MCF-7 and cSCC cells. A. Representative Western Blot showing the effects of 24 h incubation with IGF1R neutralizing antibody (IGF1R ab) at the concentration of 0.5, 1, and 2 ng/µl in MCF-7 control cells on the level of AKT/pAKT, ERK/pERK and S6/pS6. **B.** Representative Western Blot showing changes in AKT/pAKT, ERK/pERK and S6/pS6 levels upon treatment with 1, 5 or 10 ng/µl IGF1R ab for 24 h in MET-1, SCL-I and MET-4 cells. **C.** Western Blot showing AKT/pAKT, ERK/pERK and S6/pS6 levels in SCL-I cells that have been treated for 1, 3 or 6 h with either 5 or 10 ng/µl of the IGF1R ab or with the solvent for 3 h. HSC70 served as a loading control. Protein sizes in kDa are indicated on the left side of the blots.

6.5. Impact of canonical and noncanonical HH signaling on metabolic activity, proliferation and apoptosis of cSCC cell lines

6.5.1. Impact of MEK, PI3K/AKT, mTOR and SMO inhibitors

As described in sections, 6.4.1. and 6.4.3. (see Fig. 13 and 18), the incubation of cSCC cells with the mTOR antagonists everolimus or rapamycin and the PI3K and/or AKT inhibitors GDC-0941, PI103 and MK-2206 resulted in a decrease in *GLI1* expression and thus of HH signaling activity. In contrast, the MEK inhibitor UO126 did not change or even increased *GLI1* levels. The SMO inhibitor HhA decreased (in MET-1 and MET-4) or increased (in SCL-I) *GLI1* expression level, whereas vismodegib increased it at the high dose of 60 µM. (see Fig. 10). In order to get an impression if the level of HH signaling activity and EGF-associated decrease in *GLI1* expression alters metabolic activity, proliferation and apoptosis of cSCC cells, we performed WST-1 assay, BrdU incorporation assay and Annexin V/PI staining, respectively, as described in 5.2.13., 5.2.12. and 5.2.14. in the Methods section. To roughly assess the time that cells need to double the population and incorporate BrdU, we counted the cells at the time of seeding and after 24 h of culture. Based on just these two values, the accurate doubling time could not be calculated. However, as shown in Fig. 21, 24 h is more than enough for SCL-I and MET-4 cells lines to double the population (Fig. 21).
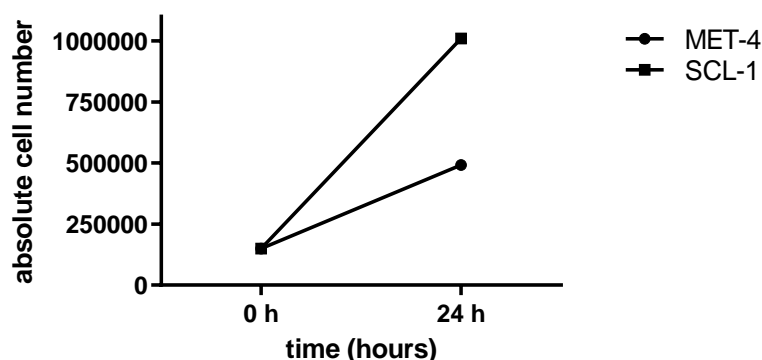
Figure 21: Growth curves showing proliferation of SCL-I and MET-4 cells. The graph shows the absolute number of untreated SCL-I and MET-4 cells at the time of seeding (0 h = 1.5 x 10^5 cells) and after 24 hours of culture (24 h). Dead cells were stained with trypan blue and the living cells were counted using Neubauer counting chamber. The graph represents one exemplary experiment.

Therefore, the inhibitor treatments as well as BrdU labeling were done for 24 h. The same incubation time was used for MET-1 cells, for which the doubling time has not been

determined. As shown in Fig. 22, everolimus, rapamycin and vismodegib were well-tolerated by all three cSCC cell lines because metabolic activity as shown by WST-1 assay was not severely affected (Fig. 22). Additionally, they did not strongly affect proliferation rate of cSCC tumor cells as indicated by the percentage of BrdU positive cells (Fig. 23). MK-2206 was also well-tolerated by SCL-I cells and did not influence the proliferation rate of this cell lines. However, this drug displayed a moderate toxicity on MET-1 and MET-4 cells, which was accompanied by a decrease in BrdU incorporation. GDC-0941 and PI103 strongly reduced both metabolic activity and proliferation rate showing their cytotoxic effects in all three cell lines. In contrast, the MEK1/2 inhibitor UO126 exerted only minor effect on metabolic activity of MET-1 cells and slightly decreased the proliferation of all three cell lines. HhA showed moderate toxicity but at the same time reduced the proliferation rate. The reduction was around 50 – 60% for all cells at a concentration of 30 µM (Fig. 22 and 23). Concerning Annexin V staining, the results show that UO126 increased the number of early apoptotic SCL-I cells (Fig. 24). This stays in contrast to the observation that UO126 only slightly decreased the proliferation of SCL-I cells. However, we did not observe an increase in late apoptotic cells which might indicate that after 24 h of the treatment the cells only start undergoing apoptosis and that this time is too short to observe changes in proliferation. Otherwise, none of the inhibitors induced apoptosis in any of the cell lines examined. Having in mind that UO126 treatment of SCL-I cells resulted in inhibition of MEK1/2 and ERK and concomitantly upregulated *GLI1* expression (see Fig. 12, 13) the data might indicate that *GLI1* in this cell line may promote apoptosis. Finally, the moderate inhibition of proliferation of all UO126-treated cell lines together with *GLI1* upregulation or lack of *GLI1* modulation suggests that *GLI1* and thus HH signaling is not necessary for proliferation of cSCCs.
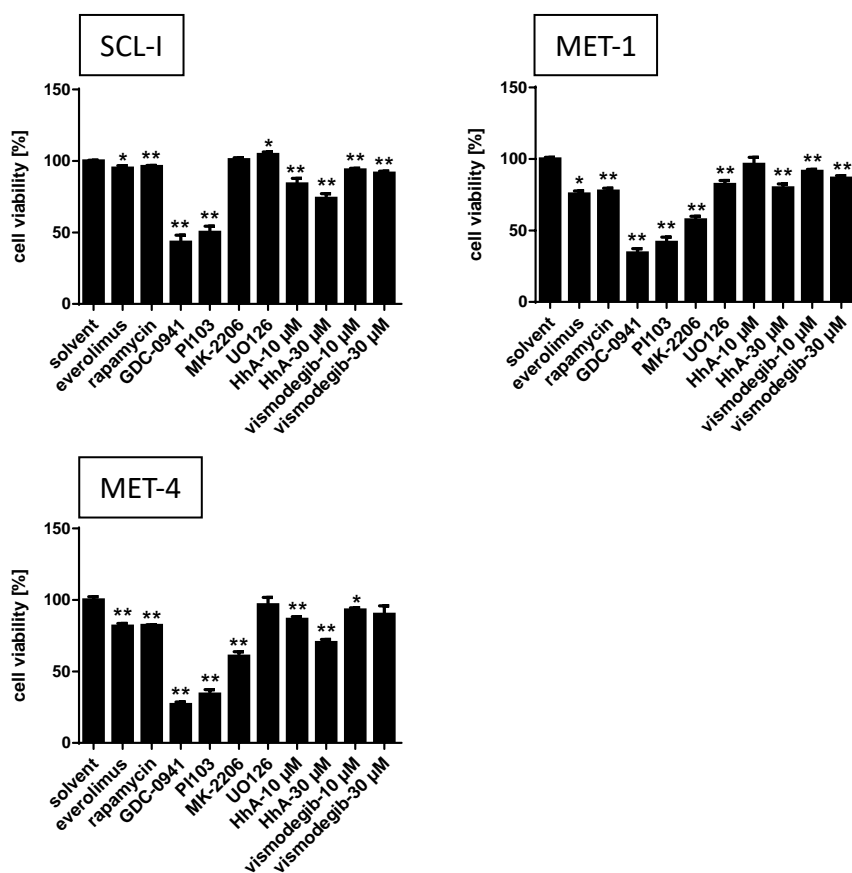
Figure 22: Influence of PI3K/AKT, MEK/ERK, mTOR and HH/GLI inhibitors on metabolic activity of cSCC cells. WST-1 metabolic activity assay showing the influence of 50 nM everolimus, 100 nM rapamycin, 5 µM MK-2206, 3 µM PI103, 10 µM GDC-094, 20µM UO126 as well as HhA and vismodegib at the concentration of 10 µM and 30 µM on the viability of SCL-I, MET-1 and MET-4 cells 24 h after incubation. The number of viable cells from the solvent treated group was set to 100 %. Each graph represents the mean value +/- SEM of three independent experiments; *, p<0.05; **, p<0.01. Statistical analysis was performed using Mann-Whitney test.
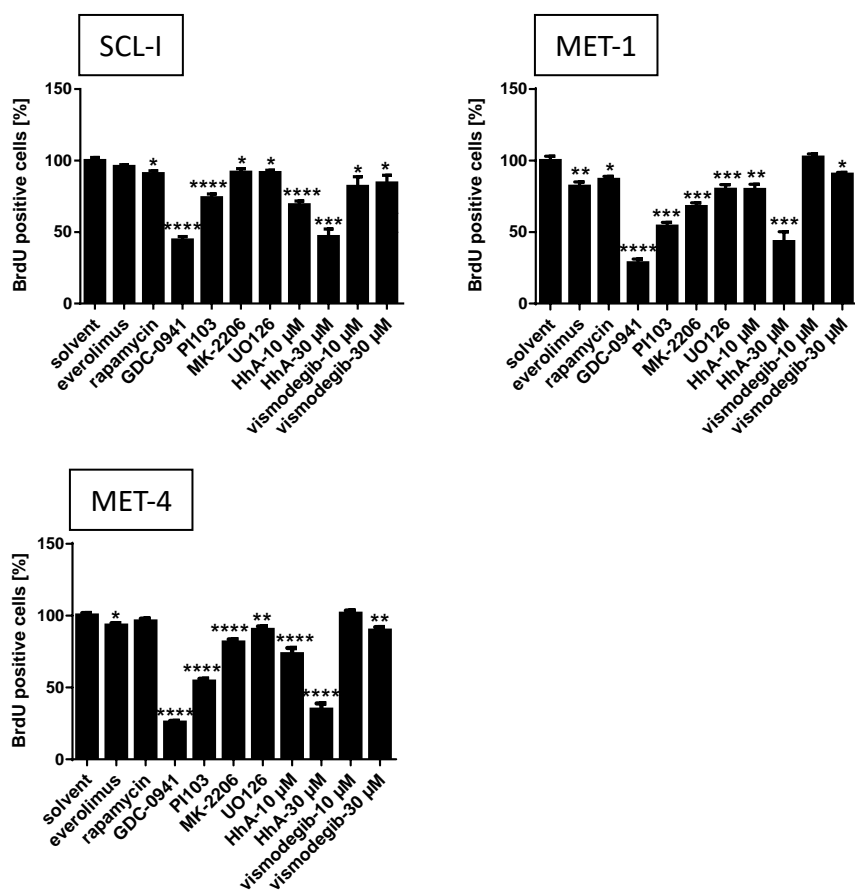
Figure 23: Influence of PI3K/AKT, MEK/ERK, mTOR and HH/GLI pathways inhibitors on proliferation of cSCC cells. BrdU incorporation assay showing the influence of 50 nM everolimus, 100 nM rapamycin, 5 µM MK-2206, 3 µM PI103, 10 µM GDC-094, 20µM UO126 as well as HhA and vismodegib at the concentration of 10 µM and 30 µM on proliferation of SCL-I, MET-1 and MET-4 cells 24 h after incubation. The data are presented as the percentage of BrdU positive with the value of solvent treated cells set to 100 %. Each graph represents the mean value +/- SEM of three independent experiment; *, $p<0.05$; **, $p<0.01$; ***, $p<0.001$; ****, $p<0.0001$. Statistical analysis was performed using Mann-Whitney test.
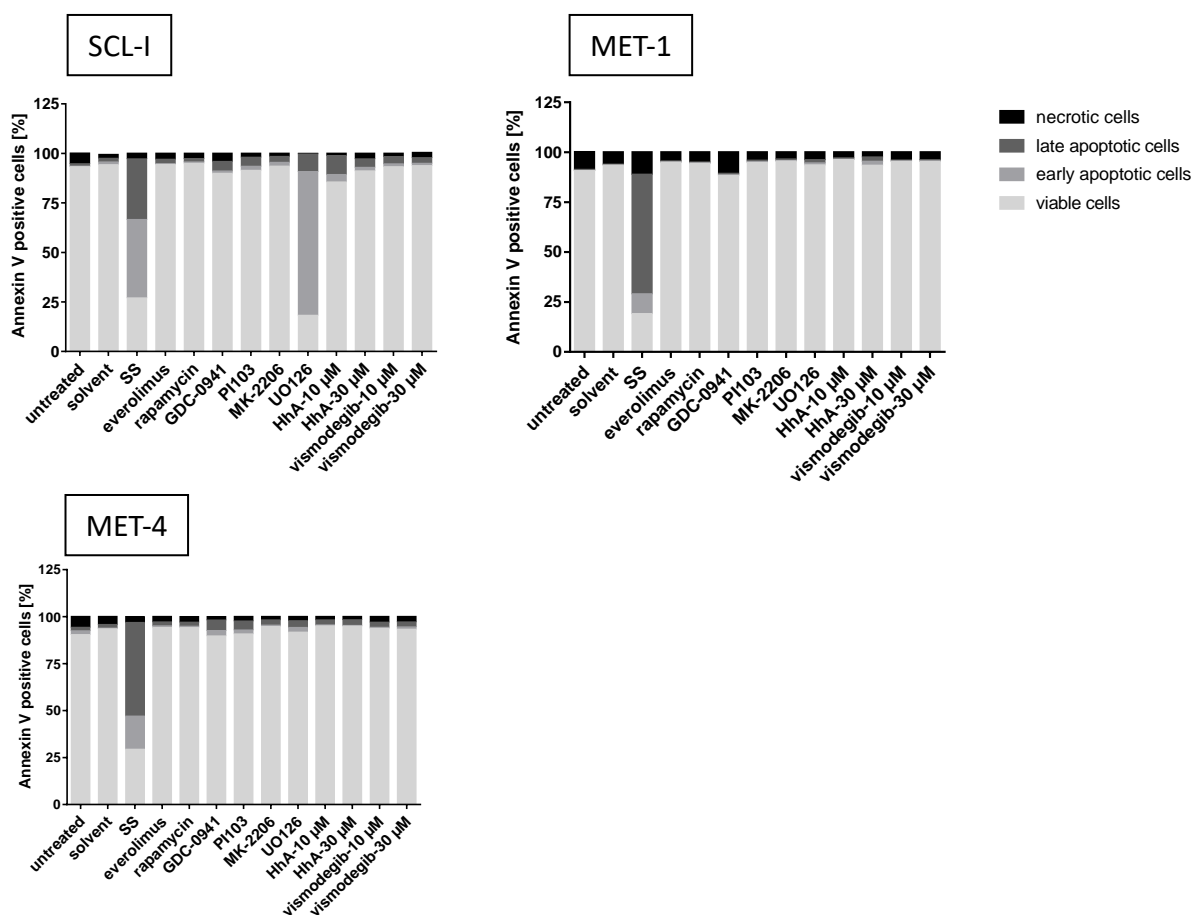
Figure 24: Influence of PI3K/AKT, MEK/ERK, mTOR and HH/GLI pathways inhibitors on apoptosis of cSCC cells. FACS analysis of Annexin V/PI positive cells showing the influence of 50 nM everolimus, 100 nM rapamycin, 5 µM MK-2206, 3 µM PI103, 10 µM GDC-094, 20µM UO126 as well as HhA and vismodegib at the concentration of 10 µM and 30 µM on apoptosis of SCL-I, MET-1 and MET-4 cells. The data show the percentage of viable cells, early- and late- apoptotic as well as necrotic cells in each sample. 5 µM staurosporin (SS) was used as a positive control. Representative graphs from one out of three experiments are shown.

6.5.2. Impact of EGF and IGF1

Since also EGF and IGF1 led to a significant downregulation of *GLI1* mRNA (see Fig. 16 B and 17 B), we also incubated the cells with either EGF or corresponding solvent control along with BrdU for 24 h.

We first incubated MCF-7 cells with EGF, which are known to express EGFR (Comsa *et al.*, 2015) and measured BrdU incorporation after 24 h. Piling up the results from three independent experiments measured in triplicates, MCF-7 cells showed a significant and 30% higher proliferation rate after stimulation with EGF (Fig. 25).

However, when cSCC cell lines were incubated with EGF, we did not observe any changes in BrdU incorporation in MET-1 and MET-4 cells when compared to the solvent control. This suggested that EGF has no impact on proliferation of these cSCC cell lines. Paradoxical, for SCL-I cells, we even noted a statistically significant decrease in proliferation upon incubation with EGF (Fig. 25). Together, because EGF strongly inhibits *GLI1* expression and thus HH signaling in cSCC, these data once again suggest that HH/GLI1 signaling activity is unrelated to cellular proliferation of cSCC cells. It is rather unlikely that the concentration of EGF was too low or that incubation time was too short because in one experimental setting we doubled the EGF concentration (200 ng/µl) and incubation time (48 h) and we did not observe any increase in proliferation (data not shown). However, since this assay was performed under serum starvation conditions (0.5 % FCS), it is possible that cSCC cells in addition to EGF require other factors that are normally included in the serum to boost proliferation. Thus, it would be worth to perform this assay also under full-serum conditions in the future.
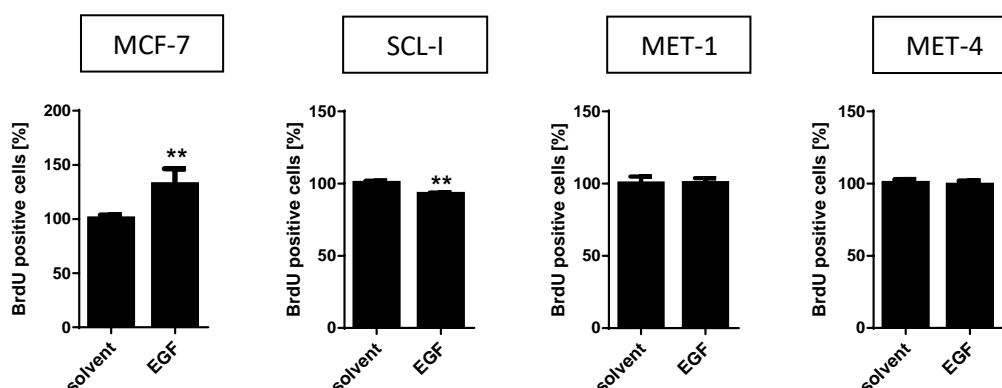
Figure 25: Influence of EGF on proliferation of MCF-7 and cSCC cell lines. BrdU incorporation in solvent treated (set to 100 %) and EGF stimulated MCF-7, SCL-I, MET-1 and MET-4 cells. The cells were incubated with EGF or the solvent along with BrdU for 24 h in the medium containing 0.5 % FCS. Each graph summarizes three independent experiments performed in triplicates. **, $p<0.01$. Statistical analysis was performed using Mann-Whitney test.

6.5.3. Impact of *GLI1* knockdown or *GLI1* overexpression

Finally, in order to prove that *GLI1* is not involved in proliferation of cSCC cells a *GLI1* specific siRNA was transfected into SCL-I and MET-4 cells. In a control experiment and to check for transfection efficiency, *MAPK1* was first knocked down using a siRNA from the Qiagen kit. Indeed, *MAPK1* transcription level was remarkably downregulated in both SCL-I and MET-4 cells (Fig. 26 A, SCL-I data not shown). When MET-4 cells were transfected with

GLI1 specific siRNA, *GLI1* transcripts were significantly downregulated 24 h after transfection in comparison to the scrambled siRNA control (Fig. 26 A) and the effect was sustained at least for 48 h (data not shown). Unfortunately, the transfection and *GLI1* downregulation did not work well in SCL-I cells, which were thus excluded from the analysis.

We next assessed BrdU incorporation in MET-4 cells upon *GLI1* knockdown. BrdU was added to the cells 24 h after transfection for another 24 h. As shown in Figure 26 B, the proliferation rate of the cells was not affected (Fig. 26 B).
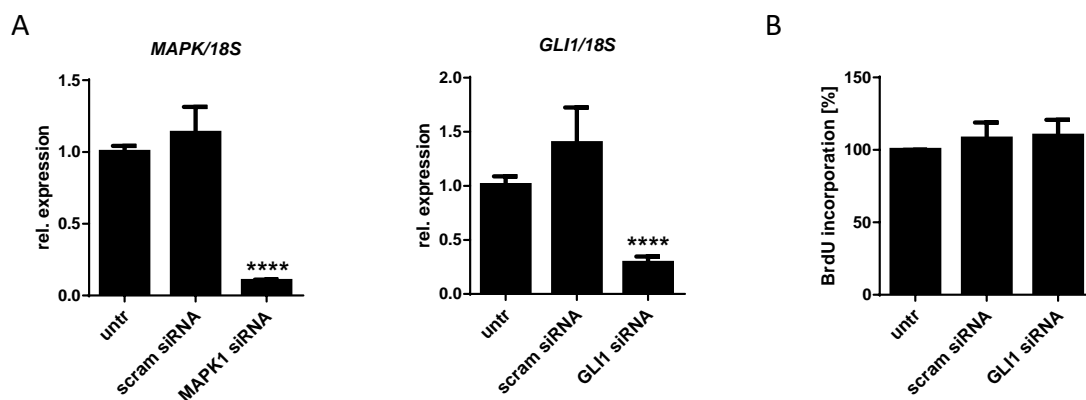
Figure 26: Influence of GLI1 levels on proliferation of MET-4 cells. A. qPCR of *MAPK1* and *GLI1* expression level upon *MAPK1* (used as a positive control) and *GLI1* specific knockdown in MET-4 cells. **B.** Influence of siRNA mediated *GLI1* knockdown on proliferation shown by BrdU incorporation assay. Each graph summarizes three independent experiments. ****, $p < 0.0001$. Statistical analysis was performed using Mann-Whitney test; untr, untransfected; scram, scrambled.

On the other way around, we overexpressed *GLI1* in SCL-I and MET-4 cells by transfection with plasmids encoding murine *Gli1* or human *GLI1*. To first verify the efficiency of overexpression, we analyzed the *GLI1* as well as *GLI2* mRNA levels 24 h after transfection. Since the *GLI1* specific primers detect both endogenous and exogenous *GLI1* we used *GLI2* expression as readout for *GLI1* overexpression. Thus, it is known that *GLI2* expression can be regulated via GLI1 (Regl *et al.*, 2002). qPCR showed that overexpression of either *Gli1* (data not shown) or *GLI1* led to the increase in *GLI1* and *GLI2* transcription level (Fig. 27 A), that however was not significant because the experiment so far has been done only once in triplicates. The data were normalized to the two housekeeping genes *18S rRNA* (Fig. 27 A) and *HPRT* (data not shown) and raised similar results.

To investigate the role of *Gli1* or *GLI1* on proliferation of cSCC cells *Gli1* or *GLI1* were overexpressed for 48 h in SCL-I and MET-4 cells. BrdU was added to the cells after 24 h and its incorporation was measured after 24 h. The data show that there was no significant change in the cellular proliferation rate after *Gli1* (data not shown) or *GLI1* overexpression when compared to the empty vector control in either of cell lines (Fig. 27 B). Taken together, these data suggest that *GLI1* is dispensable for proliferation of cSCC cell lines as neither *GLI1* knockdown nor *Gli1/GLI1* overexpression influenced the cellular proliferation of cSCC cells. Nevertheless, these data are only preliminary because they summarize only one single experiment and need further validation.

A
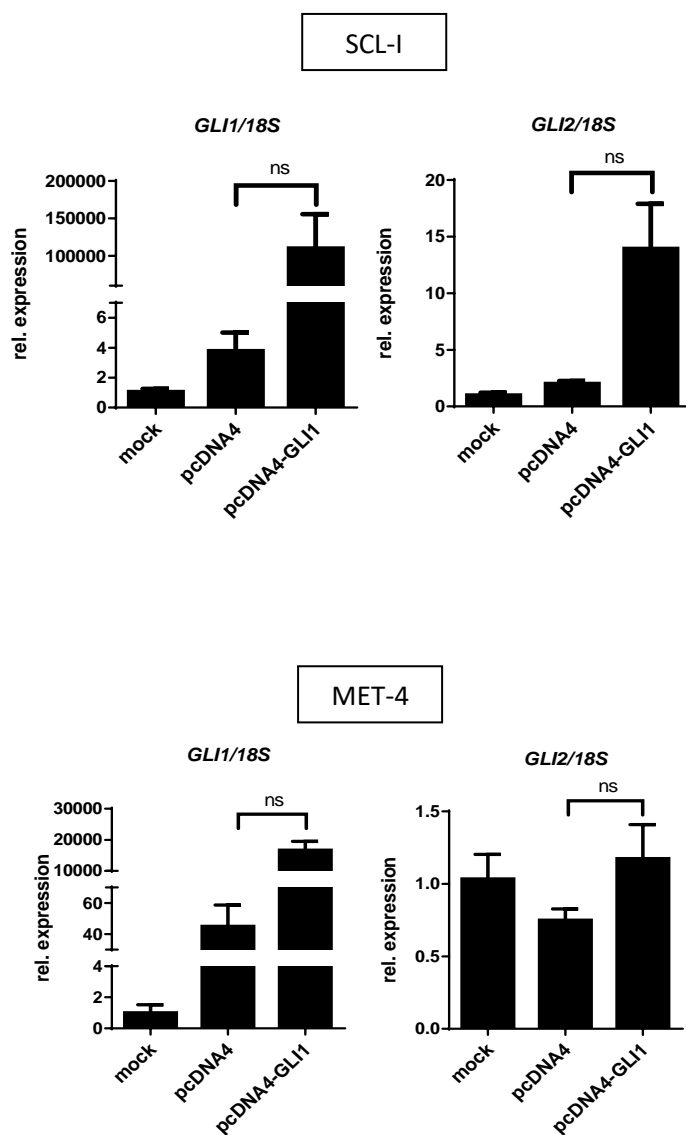
B
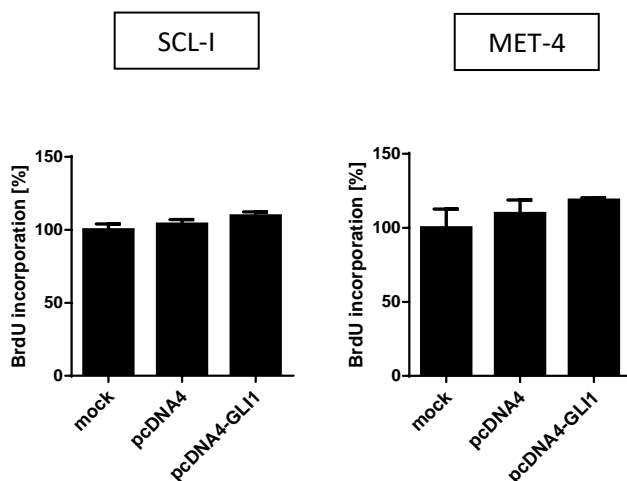
Figure 27: Influence of GLI1 overexpression on proliferation of SCL-I and MET-4 cells. A. qPCR showing changes in *GLI1* and *GLI2* expression level after transfection with a plasmid expressing human *GLI1* or pcDNA4 empty vector in comparison to mock transfected cells. The data show relative expression levels normalized to *18S rRNA* housekeeping gene with the value of mock-transfected cells set to 1. Each graph represents a summary of three independent experiments displayed as mean +/- SEM. **B.** BrdU incorporation assay showing changes in proliferation of SCL-I and MET-4 cells upon overexpression of *GLI1* in comparison to mock-transfected and the empty vector controls. The proliferation of mock-transfected cells was set to 100 %. Each graph represents a summary of three independent experiments displayed as mean +/- SEM. Statistical analysis was performed using Mann-Whitney test; ns, not significant.

7. Discussion

HH signaling pathway plays an important role in embryonic development and is deregulated in many various cancer entities including non-melanoma skin cancer. The link between canonical HH signaling and cancer formation has been well established in BCC and the majority of BCCs are driven by inactivating mutations in PTCH (reviewed in (Epstein, 2008)).

PTCH mutations were also described in a minority of cSCCs (Ping et al., 2001), however there are not many studies showing relevance of canonical HH signaling pathway as a driving force of this tumor. For example, one study claims that canonical HH/GLI signaling plays an important role in proliferation, migration and invasiveness of cSCC. This was due to the fact that the A431 cSCC cell line apparently highly expresses *Gli1,* which seems to be important for tumor biology since cyclopamine treatment resulted in inhibition of proliferation, migration and invasiveness of this cell line. In addition, the authors showed that GLI1 and SHH are correlated with poor overall survival of cSCC patients. Furthermore, the authors claim that the mice treated with cyclopamine or those with a Gli1 knockdown show a lower cSCC incidence in a DMBA/TPA induced model (Sun et al., 2016). However, there are many inconsistencies in this paper so that the data is hard to believe. One example is the animal experiment: Although the authors show data from mice, the animals are described as rats in the material and methods section. Furthermore, the mice are not specified and only described as Gli1- or Gli1+. In addition, the authors talk about "Tumor xenografts in nude mice" when describing the DMBA/TPA treatment of the animals. In contrast to this report, numerous clinical data show that treatment of BCC with vismodegib and thus inhibition of HH signaling and concomitant downregulation of *GLI1* results in development of cSCC. Nevertheless, the mechanism behind it is not yet known and might be quite complex (Aasi et al., 2013; Iarrobino *et al.*, 2013; Orouji et al., 2014) (G. A. Zhu *et al.*, 2014).

Whereas data about the role of HH signaling in cSCC is still conflicting, several other signaling pathways are better described in cSCC. Clinical data show that EGFR receptors are frequently overexpressed in patients suffering from cSCC and thus are a main target for the therapy with however no approved drugs so far (G. B. Fogarty et al., 2007a). Additionally, the fact that OTRs receiving Sirolimus, an immunosuppressive medication that blocks mTOR, show dramatic reduction of cSCC incidence proportion, points to the important role of mTOR

in cSCC pathogenesis (Leblanc *et al.*, 2011; Salgo et al., 2010; Tessmer et al., 2006). Moreover, clinical examination revealed that mutations in p53 carrying hallmarks of UV-induced mutagenesis are detectable in a majority of patients (Brash et al., 1991). Wnt/ß-catenin-, calcium- and integrin- signaling were also shown to be upregulated in cSCC when compared to the normal skin (Ra et al., 2011) (see 2.1. in Introduction section). Also RAS and AKT are frequently activated in cSCC (Barrette *et al.*, 2014; Uribe and Gonzalez, 2011) and thus might be involved in cSCC pathogenesis (for detailed description see 2.1. and 2.3.4. in Introduction section).

However, experimental data unraveling putative crosstalks between different pathways and their influence on expression of genes involved in crucial processes i.e. proliferation in cSCC are scarce.

Here, we investigated the role of canonical and potential noncanonical HH signaling in human tissue samples as well as human cSCC cancer cell lines. Our data reveal that the major downstream target of HH signaling *GLI1* is highly expressed in the tumor center of cSCC, but not in cSCC cells invading the dermis. Furthermore, we suggest that its expression is not regulated via the canonical SHH/PTCH/SMO axis but it is rather suppressed via EGF/MEK/ERK signaling. Moreover, our preliminary data show that *GLI1*, although highly expressed in cSCC, is dispensable for proliferation of cSCC.

7.1. Canonical HH signaling in cSCC

7.1.1. *GLI1* is highly expressed and SHH is not detectable in human cSCC tissue samples

In the first part of this study we examined the expression of important components of canonical HH signaling pathway i.e. *GLI1* and SHH in human cSCC samples. The data show that *GLI1* is highly expressed in the tumor center but not in cSCC cells invading the dermis. This suggests that *GLI1* might play a role in cSCC tumorigenesis but its downregulation is required for tumor progression. Indeed, clinical data show that treatment of BCC with vismodegib which inhibits GLI1 expression results in the development of cSCC (Orouji, Goerdt, Utikal, & Leverkus, 2014; Poulalhon, Dalle, Balme, & Thomas, 2015; Saintes et al., 2015). In addition, there was no positive staining for SHH throughout the tumor tissue (Fig. 5 A). Stromal cells constituting tumor microenvironment were also negative for SHH excluding

thereby possibility of paracrine signaling. This suggests that *GLI1* is an important factor in cSCC pathogenesis, which however, unlike in BCC, seems to be regulated via mechanism independently of the canonical HH/PTCH/SMO axis. This is in contrast to the study showing expression of GLI1, GLI2, GLI3, PTCH, SMO, SHH and IHH via IHC in cSCC. Thus, the tissue microarray data presented by Schneider and colleagues suggest that canonical HH/PTCH/SMO/GLI pathway is important in cSCC pathology. However, all examined proteins display mostly only weak positive signal or no signal at all. Moreover, great majority (85%) of the analyzed tumors were completely negative for GLI2, which is important activator of the HH pathway. In contrast to our data, the authors show that SHH is weakly and moderately expressed in 58% and 9% of analyzed tumors, respectively. However, it is neither indicated on pictures nor stated in the description, which antibody staining is presented on which picture and therefore cannot be reassessed. In addition, they showed that GLI1 is only weakly or moderately expressed in 37% or 5% of analyzed tumors, respectively, while the majority of samples (58%) are negative. This again is in contradiction to our study, in which we presented strong *GLI1* expression in all analyzed tumor samples. However, here we examined mRNA *GLI1* expression but not protein level and thus these data cannot be directly compared. Furthermore, the authors claim that all analyzed HH pathway components were expressed in the cytoplasm of cSCC, however the staining pattern can be hardly assessed based on provided pictures. Nevertheless, cytoplasmic localization of GLIs would indicate that they are sequestered in the cytoplasm and thus not active as transcription factors. Altogether, this data are contradictory and do not provide a reliable proof for canonical HH pathway activity in cSCC (Schneider et al., 2011). In addition, another study showed GLI1 expression in 60% of analyzed cSCC cases, however again the subcellular localization revealed cytoplasmic positivity (Bakry *et al.*, 2015). Nevertheless, we cannot exclude the possibility that in our model, PTCH/SMO activity in cSCC samples might be also regulated via IHH or DHH. Indeed, IHH has been shown to be expressed in 11% of human cSCC cases (Schneider et al., 2011). Although our cell culture experiments rather argue against an involvement of HH ligands in the regulation of *GLI1* expression in cSCC (see *GLI1* expression analysis and GLI reporter assay upon stimulation with SHH-CM in Fig. 8 shown in section 6.3.1.), the expression of IHH and DHH in cSCC samples should be studied in the future.

7.1.2. **No impact of HH/SMO pathway activators and diverse effects of SMO inhibitors on *GLI1* expression level in cSCC cell lines**

As already mentioned, the relevance of canonical HH/GLI signaling pathway in cSCC is still poorly understood. In this study, we investigated the expression of HH pathway components in 6 different cSCC cell lines and HaCaT ras II-4 cells that shows a cSCC phenotype. Via qPCR we could show that most, but not all cSCC cell lines expressed the main pathway components i.e. *GLI1*, *GLI2*, *GLI3*, *SMO* and *PTCH* while *SHH* was expressed only by MET-1 and MET-4 cells (Fig. 6). The latter two cell lines and the cell line SCL-I that except *SHH* does express all other components, were chosen for further analysis. When we tried to regulate the activity of canonical HH/GLI signaling via application of SHH-CM or the SMO agonist SAG or direct overexpression of SMO, we were not able to activate the pathway. On the other hand, treatment of the cells with SMO inhibitors revealed that *GLI1* can be regulated in cSCC cell lines, however the effects were cell type-, concentration- and inhibitor-dependent. Whereas none of the cell lines showed a response towards cyclopamine and lower doses of vismodegib, HhA significantly decreased *GLI1* expression level in MET-1 and MET-4 cells and unexpectedly increased it in SCL-I cells. Similar paradox effect was observed when SCL-I and MET-4 cells were treated with high doses of vismodegib. The lack of response towards cyclopamine and vismodegib could be due to specific SMO mutations that are located in binding pockets that are specific for cyclopamine and vismodegib but not for HhA (Atwood *et al.*, 2015; Sharpe *et al.*, 2015). However, no SMO mutations have been described in cSCC so far (Ransohoff *et al.*, 2015) and detailed genomic analyses of available cSCC cell lines have not been performed. Thus, although it is unlikely that the resistance to cyclopamine and vismodegib in cSCC cell lines is due to SMO mutations, we cannot completely exclude it.

The different effects exerted by the inhibitors on cSCC cell lines can also be explained by different modes of action. Thus, the inhibitors bind different domains of SMO receptor. Cyclopamine, the first discovered SMO inhibitor, apparently blocks the receptor's activity via binding to its 7-transmembrane domain (7TM). This mechanism of action was proposed also for vismodegib. Interestingly, the SMO agonist and activator SAG activates SMO by binding to the same pocket as cyclopamine and vismodegib, suggesting that modulation of SMO activity is a much more complex process (J. K. Chen et al., 2002a; J. K. Chen et al., 2002b; C. Wang *et al.*, 2014). Indeed, SMO inhibitors can either stabilize SMO at a defined

conformation or promote a specific subcellular localization. While cyclopamine stabilizes SMO at its inactive state within the cilium, vismodegib or HhA sequester SMO in the cytoplasm and thus prevent its trafficking into the primary cilium, the process required for full activation (Dijkgraaf *et al.*, 2011; Wilson et al., 2009; V. M. Wu *et al.*, 2012). The concentration-dependent paradoxical effects of HhA and vismodegib could be due to overdosing. Such a scenario has been described for the SMO agonist SAG (J. K. Chen et al., 2002b). Chen and colleagues presented that a concentration of SAG, which is higher than 1 µM results in paradoxical pathway inhibition. In addition, they show that SMO inhibitors block the HH pathway activation mediated by low SAG concentrations, but they do not affect the inhibitory effects observed after high doses of SAG. Based on these data the authors suggest that SAG binds not only to SMO but also to other yet unknown factors, which cooperate with SMO in the regulation of the pathway's activity. Thus, an excess of SAG would associate with both, SMO and its putative effectors thereby interfering with their interaction and leading to the pathway inhibition. Therefore, an optimal concentration of SAG is needed to effectively activate SMO function in association with its putative cellular effectors (J. K. Chen et al., 2002b). On the other way around it is possible that this could also be a mechanism resulting in paradoxical activation of the HH pathway when using SMO inhibitors. However, in our setting the increase in *GLI1* expression upon treatment with HhA in SCL-I cells was not dose-dependent and occurred both with low and high doses of the inhibitor (Fig. 10 C).

7.1.3. HhA-mediated changes in *GLI1* expression negatively correlate with pERK levels

Finally, the paradoxical increase in *GLI1* expression in SCL-I cells upon HhA treatment could also be due to modulation of other signaling pathways. Indeed, our data show that an incubation of SCL-I cells with 10 and 30 µM HhA led to a decrease in the level of phosphorylated AKT and ERK proteins and an increase of pS6 (Fig. 11). In contrast, HhA inhibited *GLI1* expression in MET-1 cells, which was also associated with a decrease in pAKT, but an increase of pERK. This suggests that HhA may influence not only SMO activity but also other effector pathways in dependency of the cellular context. Indeed, in RMS cell lines, HhA can decrease pAKT levels additionally to *GLI1*. However, in RMS it is not known whether changes in pAKT level were dependent or independent of SMO (Ridzewski *et al.*, 2015).

7.1.4. Weak and moderate decrease in cellular viability and proliferation upon treatment with vismodegib and HhA

We also investigated the role of vismodegib and HhA in cellular viability, proliferation and apoptosis. In general, vismodegib did not or only moderately affect viability, proliferation or apoptosis of cSCC cells (Fig. 22, 23, 24). It is worth noticing that the same concentrations of the drug did not alter *GLI1* expression level. In contrast, HhA, which decreased *GLI1* expression level in MET-1 and MET-4 cells showed low to moderate toxicity, which was accompanied by inhibition of proliferation by 50-60% and no changes in apoptosis. This is in line with well-known role of the canonical HH signaling in promoting proliferation. Interestingly, in SCL-I cells HhA exerted the same effects on viability, proliferation and apoptosis as in MET-1 and MET-4 cells, which however were accompanied by increase in *GLI1* expression level. The fact that different levels of *GLI1* caused the same effects on cellular biology suggests that growth inhibition of cSCC cells upon treatment with HhA might not be mediated via inhibition of the SMO/GLI axis. Indeed, the lack of correlation between HH pathway induced *GLI1* expression and proliferation or apoptosis has been described in many different cancer cell types (Yauch et al., 2008).

7.2. Noncanonical HH signaling in cSCC

As already mentioned in section 2.2.4., noncanonical HH signaling have been described in various cancers. The pathways shown to be involved in GLI regulation in a SMO independent manner involve i.a. EGF/EGFR and its downstream effector pathways RAS/RAF/MEK/ERK, PI3K/AKT, and mTOR.

Most of the data so far show a positive activation of GLI factors by the latter pathways. Thus, RAS/RAF/MEK/ERK signaling has been shown to regulate GLI transcriptional activity in pancreatic cancer (Eberl et al., 2012; Ji et al., 2007). Moreover, EGFR mediated MEK/ERK activation plays a role in malignant transformation of keratinocytes (Kasper et al., 2006a; Schnidar et al., 2009). PI3K/AKT has been shown to promote nuclear localization and thus activation of GLI transcription factors (Stecca et al., 2007) while mTOR signaling has been proved to phosphorylate and thus activate GLI1 via S6K1 effector kinase in esophageal cancer (Y. Wang et al., 2012). Nevertheless, it is likely that these pathways also can inhibit GLI transcription factors. This is becoming evident in MB, in which FGF-mediated ERK

activation inhibits HH pathway target genes expression including *GLI1* (M. P. Fogarty et al., 2007b).

The role of non-canonical HH signaling in the regulation of GLI transcription factors in cSCC is not known. However, due to i) the lack of SHH expression in human cSCC samples, ii) the inability of SHH or SAG to induce *GLI1* in cSCC cell lines, iii) the inverse staining pattern of human cSCC samples using a *GLI1* riboprobe and pS6 and pERK antibodies, iv) the sometimes inverse staining pattern between *GLI1* and EGF in human cSCC samples, v) the fact that HhA upregulated *GLI1* in SCL-I cells, which went along with a decrease in phosphorylation of ERK and vi) *vice versa* HhA downregulated *GLI1* in MET-1 cells, which went along with an increase in phosphorylation of ERK, we hypothesized that *GLI1* expression and thus potentially the activity of GLI2 or GLI3 could be negatively regulated by EGF, RAS/RAF/MEK/ERK or mTOR signaling.

7.2.1. Inhibition of *GLI1* expression and decreased proliferation of cSCC cells upon inhibition of PI3K/AKT signaling

As already mentioned in section 6.1., we were not able to detect signals in cSCC samples when using an antibody recognizing pSER473 of AKT (Fig. 5 B). However, the antibody also did not stain glioblastoma tissue which is usually used as a positive control (not shown). Therefore, we cannot exclude that lack of pAKT expression in cSCC is a false negative result. Moreover, there are studies showing that cSCC tumors are strongly positive for cytoplasmic and nuclear pAKT while normal skin stains negative (S. J. Chen et al., 2009). It has also been suggested that higher pAKT expression is related to the invasion capability of cSCC (Barrette et al., 2014). Therefore, and despite the lack of pAKT signals in the IHC analysis, we further assessed the role of PI3K/AKT signaling in cSCC cell lines.

We showed that pharmacological inhibition of PI3K/AKT signaling at the level of PI3K or AKT indeed decreased levels of pAKT when using the pure AKT inhibitor MK-2206, the pure PI3K inhibitor GDC-0941 or the dual PI3K/mTOR inhibitor PI103 (Fig. 12). As already mentioned in section 2.3.2., mTORC1 is a downstream target of PI3K/AKT pathway and inhibition of PI3K/AKT pathway often results in concomitant inhibition of mTOR and thus S6 protein phosphorylation (Laplante and Sabatini, 2012). This was observed for MK-2206 in SCL-I, MET-1 and MET-4 cells and for GDC-0941 in the SCL-I and MET-1 cell lines. We also noted an inhibition of ERK phosphorylation in SCL-I cells upon treatment with PI103, in

MET-1 and MET-4 cells upon treatment with MK-2206 and in MET-1 cells upon treatment with GDC-0941. Why the drugs regulated pS6 and/or pERK levels in such a diverse manner is unclear. However, this suggests a crosstalk between PI3K/AKT, the mTOR and MEK/ERK pathways in cSCC. Similar effects of PI3K inhibitors have been described in breast cancer and may rely on PIP3-mediated activation of Raf/MEK/ERK cascade that is independent of RAS (Ebi *et al.*, 2013).

Nevertheless, the *GLI1* expression level was significantly downregulated in all 3 investigated cSCC cell lines upon treatment with PI103, MK-2206 and GDC-0941 (Fig. 13). This suggests that PI3K/AKT signaling positively regulates *GLI1* expression in cSCC. Indeed, a positive regulation of *GLI1* expression by PI3K/AKT signaling has been shown in melanoma cells, where this pathway promotes GLI1 nuclear localization and thus its transcriptional activity (Stecca et al., 2007).

However, no *GLI1* regulation was observed upon transfection of SCL-I cells with a constitutively active or dominant negative variant of AKT (Fig. 14 C). This is surprising since the AKT isoforms, at least the constitutively active form, were expressed by the cells. One possibility is that the proteins expressed from the vectors have lost their function. Another possibility is that the decrease in *GLI1* expression upon inhibitor treatment in an off-target effect. However, this scenario is rather unlikely because in this occasion all 3 inhibitors should have the same off-targets. Finally, it is possible that AKT is not involved in *GLI1* expression. Thus, PI103 and GDC-0941 were toxic to the cells and therefore could simply have abrogated the expression of *GLI1* due to toxicity. However, toxicity was not observed when using MK-2206 that likewise suppressed *GLI1* expression. Nevertheless, the possibility that AKT is indeed not involved in *GLI1* transcription is fostered by the observation that AKT dephosphorylation by HhA was accompanied by an increase in *GLI1* expression in SCL-I cells, but by a decrease in *GLI1* expression in MET-1 cells.

As already mentioned the application of GDC-0941 or PI103, which inhibit PI3K or PI3K/mTOR, respectively, showed high toxicity and thus also markedly decreased BrdU incorporation (Fig. 22, 23). So, it is hard to judge, whether inhibition of proliferation is not just a toxic effect. Indeed, when the cells' morphology was assessed using the microscope, we observed many dead cells upon treatment with those inhibitors. However, it stays in contrast to the lack of apoptotic cells in Annexin V assay under these treatment conditions (Fig.24).

The treatment with the pure AKT inhibitor MK-2206 was not toxic for SCL-I cells and moderately toxic for MET-1 or MET-4 cells and toxicity correlated perfectly with BrdU incorporation, whereas again the cells showed no signs of apoptosis (Fig. 22, 23, 24). Together with the observation that the cells treated with MK-2206 neither changed their morphology nor died due to the treatment, these data argue against just toxic effects of this AKT inhibitor. Nevertheless, in the future experiments, lower concentration of PI3K and AKT inhibitors should be applied to verify their role in the downregulation of *GLI1* expression as well as in the regulation of metabolic activity, proliferation and apoptosis in cSCC cells.

7.2.2. Inhibition of *GLI1* expression and decreased proliferation of cSCC cells upon inhibition of mTOR signaling

As already mentioned mTOR signaling pathway is a main downstream effector pathway of PI3K/AKT signaling. It regulates protein synthesis and thus plays a role in important cellular processes i.e. cell growth, proliferation and survival. Its activity can be modulated by many different factors such like growth factors, nutrients, cellular stress and importantly by both PI3K/AKT and MEK/ERK signaling pathways (reviewed in (Populo *et al.*, 2012)). When the activity of the mTOR signaling pathway was investigated in cSCC human tissue samples, a strong expression of pS6 and thus mTOR activity was observed in all analyzed cSCCs. Interestingly, the staining was stronger in outer parts of the tumor and cells invading the dermis, which is opposed to the staining pattern of *GLI1* (Fig. 5 B, E). This suggests that mTOR activity might be related to the aggressiveness of cSCC. Indeed, there is a study showing that increased pS6 expression is correlated with the tumor progression and thus may serve as a predictive biomarker for the tumor's aggressiveness (Khandelwal *et al.*, 2016). In the light of this data our analysis now supports a model, in which the cSCC cells invading are pS6 positive, but *GLI1* negative. In other words, whereas mTOR signaling is associated with cSCC aggressiveness, HH/GLI signaling apparently is not. In addition, the opposing activity in cSCC samples also suggested that both signaling pathways may regulate each other in an inverse manner. However, this hypothesis was not supported by the *in vitro* data presented here. Thus, mTOR inhibition with either rapamycin or everolimus resulted in a significant decrease in *GLI1* expression level in almost all settings with the exception of rapamycin-treated MET-1 cells (Fig. 13). These effects were similar to that observed upon PI3K/AKT inhibition. This suggests rather positive regulation between *GLI1* and mTOR in our *in vitro*

model. Indeed a positive crosstalk between HH and mTOR signaling has also been demonstrated e.g. for RMS (Kaylani *et al.*, 2013), and esophageal adenocarcinoma (Y. Wang et al., 2012). We also observed that mTOR inhibition with either everolimus or rapamycin resulted not only in inhibition of pS6, but slightly decreased the phosphorylation of ERK in MET-1 cells. The decrease in ERK phosphorylation in the rapamycin treated MET-1 cells did not result in significant suppression of *GLI1* transcription, which fosters our hypothesis that pERK and *GLI1* transcription are negatively correlated.

In contrast, mTOR inhibition in MET-4 cells increased ERK phosphorylation together with that of AKT. Whereas the role of mTORC1 in negative regulation of AKT and ERK is well established (reviewed in (Manning, 2004)) a positive regulation of ERK phosphorylation is not.

We also showed that in most of the cases, mTOR pathway inhibition reduced both viability and proliferation of cSCC cells in all settings. Although in our cell culture experiments these just-mentioned antitumoral effects were moderate, they are in line with clinical data showing that sirolimus (rapamycin) used as an immunosuppressant in OTRs reduces the risk of development of cSCC. As already mentioned in section 2.1., OTRs are at increased risk for nonmelanoma skin cancer development (reviewed in (Leblanc et al., 2011)) and develop cSCC at 65-250 higher incidence when compared to general population (Euvrard et al., 2003). It has been shown that administration of mTOR inhibitors, when used as immunosuppressive drugs, reduce the number of *de novo* developing cSCC, decelerate development of already existing malignancies and can even induce regression of the tumors (Salgo et al., 2010).

7.2.3. Activation of *GLI1* expression and concomitant decreased proliferation of SCL-I cells upon inhibition of MEK/ERK signaling

In human tissue specimens pERK is only expressed in single tumor cells in the tumor mass. However, its expression is strongly elevated in stromal cells surrounding the tumor tissue (Fig. 5 D, E). This suggests a role of tumor microenvironment in cSCC pathology (see also section 7.12.).

The existing immunohistochemical data from other groups are different from ours and are also inconsistent in comparison to each other. Thus, three independent studies showed strong nuclear pERK staining within human cSCC tumor cells (Khandelwal et al., 2016; Sonavane *et*

al., 2012; Zhang *et al.*, 2007). However, while Khandelwal and colleagues showed no differences in pERK intensity between normal skin and local or metastatic cSCC, Zhang and his group noted an increase in pERK positive tumor cells in poorly differentiated cSCC in comparison to well-differentiated counterparts and no positive staining in normal skin (Zhang et al., 2007). However, none of these studies mentioned pERK positive stromal cells. It is hard to explain the differences between our results and the results obtained by other groups. It is unlikely that it is due to the antibody since Sonavane and colleagues used the same antibody as we did (namely the p44/42 MAPK (ERK 1/2) rabbit monoclonal antibody (Thr202/Tyr204) from Cell Signaling) (Sonavane et al., 2012). One of the reasons could be the staining procedure since different permeabilization and blocking conditions may markedly affect antibody binding. Unfortunately, the protocol for IHC is not clearly described by Sonavane and colleagues. However, in contrast to the tissue specimens, our *in vitro* analysis revealed that cSCC cell lines express pERK, although to a variable extent (Fig. 7). This difference between the tissue specimens and cell lines is hard to explain. However, the high pERK levels in the cultured cells might be due to some specific factors in the culture serum.

Our data now show that cSCC cells with low pERK express high *GLI1* and *vice versa* those with high pERK levels express low levels of *GLI1* i.e. SCL-I and SCL-II (Fig. 6, 7). This suggested a negative regulation between MEK/ERK and *GLI1*. Indeed, when the cells were incubated with the specific MEK1/2 inhibitor UO126, *GLI1* levels were significantly upregulated in SCL-I cells or did not change in the other cell lines, while pERK levels were downregulated. To our knowledge, this is the second report, in which *GLI1* expression and thus probably HH signaling can be negatively regulated by the MEK/ERK axis. Thus, a negative regulation of HH/GLI1 by the FGF/ERK axis has been shown in MB (M. P. Fogarty et al., 2007b). However, up to date all other literature data rather show a positive crosstalk between RAS/MEK/ERK and GLI transcription factors (i.e.(Eberl et al., 2012; Seto *et al.*, 2009)).

In addition, we assessed changes in viability, proliferation and apoptosis upon treatment with UO126. WST-1 assay shows that the drug is in general well-tolerated by the cells (Fig. 22). However, despite unchanged or even upregulated *GLI1* levels, this drug was able to moderately but significantly reduce proliferation of the cells (Fig. 23). Paradoxically, in SCL-I cells we measured increased number of early apoptotic cells in 3 independent experiments (Fig. 24). These data do not fit to the moderate inhibition of proliferation and thus are

inconclusive. Nevertheless, the significant increase in *GLI1* expression level upon UO126 treatment (Fig. 13) suggests that *GLI1* may induce apoptosis in this cell line. An experiment with a longer exposure to UO126 will help to verify these data. Together, these data suggest that active MEK/ERK signaling in cSCC counteracts *GLI1* expression, but is necessary for proliferation of the cells. Of whether this inhibitory effect on *GLI1* expression is downstream of MEK at the pERK level, remains to be established in the future using an ERK inhibitor such as SCH772984.

Besides, the data show that there might be a positive crosstalk between MEK/ERK and mTOR and a negative crosstalk between MEK/ERK and pAKT signaling (Fig. 12). Thus, we noted that MEK1/2 inhibition can reduce phosphorylation level of S6 suggesting a positive crosstalk between MEK/ERK and mTOR. Similar effects have been already shown by other researchers who described that activated ERK can also phosphorylate and thus inhibit function of tuberous sclerosis complex 2 (TSC2), which is a negative regulator of mTOR signaling. The TSC complex is also negatively regulated by AKT-mediated phosphorylation but phosphorylation sites for ERK and AKT are different. Thus, pERK can activate mTOR via PI3K/AKT-independent inactivation of TSC complex (Roux *et al.*, 2004). Furthermore, a negative crosstalk between MEK/ERK and PI3K/AKT has been documented in the literature. For example, one group proposed a mechanism in which ERK phosphorylates 4 amino residues on GAB1 and thus abrogates recruitment of PI3K to the EGFR leading to a decrease in AKT phosphorylation (Lehr *et al.*, 2004). This mechanism could be also true for cSCC cell lines used in this study. If so, this also would foster our hypothesis that AKT is barely involved in regulation of *GLI1* expression.

7.2.4. MEK/ERK-mediated inhibition of *GLI1* expression in cSCC cells upon EGF treatment

As already mentioned, EGFR signaling is deregulated in many different cancer entities including cSCC (G. B. Fogarty et al., 2007a; Shimizu et al., 2001; Toll et al., 2010). Indeed, Toll and colleagues showed that 20% of analyzed cSCCs display amplification of *EGFR*, which positively correlates with EGFR overexpression, as shown by fluorescent ISH (FISH) and IHC, respectively. (Toll et al., 2010). Up to date many monoclonal antibodies targeting and blocking EGFR as well as TKI have been developed and are either being tested in clinical trials or are already approved for the targeted therapy. The EGFR monoclonal antibody

Cetuximab is a prior-ranking drug used in the anti-EGFR therapy and shows advantageous anti-cancer effects in colorectal, non-small cell lung and head and neck cancer and is currently being tested in phase 2 in clinical trials for treatment of cSCC (Maubec *et al.*, 2011). In addition, activating mutations in TK or deletions in extracellular domain of EGFR that are related to anti-EGFR therapy resistance are quite rare in cSCC (Dziunycz *et al.*, 2013; Ridd and Bastian, 2010). Altogether, given the high expression of EGFR and low mutation rate, these data suggest that EGFR is a promising target for cSCC therapy (Mauerer et al., 2011).

Nevertheless, besides immunohistochemical and genomic analysis, there are not much data available that provide an insight into molecular mechanisms of EGF/EGFR signaling in cSCC. In this thesis, we focused on EGF stimulated EGFR signaling, its potential crosstalk with *GLI1* and its impact on cell viability and proliferation. Our data revealed that the EGF ligand is strongly expressed throughout the tumor tissue of cSCC patients and that its expression pattern overlaps with that of pS6 and *GLI1*. However, sometimes the tumors had *GLI1* negative areas in the invasion front that were positive for EGF, suggesting a negative regulation of *GLI1* by EGF (see Fig. 5 E). We further investigated the role of EGF in *GLI1* regulation in our cell lines. The MET-1 and MET-4 cells express EGFR as demonstrated by Clayburgh and colleagues (Clayburgh et al., 2013). Western Blot analysis showed that EGF indeed stimulates its downstream signaling pathways i.e. PI3K/AKT, MEK/ERK and mTOR not only in MET-1 and MET-4 cells, but also in SCL-I cells. This was indicated by increased levels of pAKT, pERK and pS6, respectively (see Fig. 16 A). We also showed that the phosphorylation is a rapid process since elevated levels of pAKT, pERK and pS6 were already seen after 30 min of EGF incubation. Interestingly, when we measured the *GLI1* expression level upon EGF stimulation, we noted a significant decrease in *GLI1* transcription after 3 h of incubation with the ligand (Fig. 16 B). To further unravel the mechanism by which EGF blocks *GLI1* expression we combined EGF stimulation with inhibition of MEK/ERK, PI3K/AKT and/or mTOR signaling. All PI3K/AKT and/or mTOR inhibitors in combination with EGF significantly reduced the level of *GLI1* (Fig. 18). This indicated that EGF-mediated *GLI1* downregulation is not due to activation of PI3K/AKT since blockage of this pathway did not restore basal *GLI1* expression level. These data again suggest that PI3K/AKT and mTOR pathways positively can regulate *GLI1* expression in cSCC cells.

On the contrary, combined treatment of EGF and the MEK1/2 inhibitor showed a tendency to increase *GLI1* expression when compared to EGF treatment alone and this change was

significant in MET-1 cells (see Fig. 18). This is another indication that MEK/ERK signaling may negatively regulate *GLI1* in human cSCC. However, in general *GLI1* expression level was lower in EGF-UO126 combined treatment than in UO126 treatment alone when compared to the respective solvent controls (Fig. 13 and 18). This indicates that additional pathways stimulated by EGF probably inhibit *GLI1* expression. In conclusion, we suggest here a mechanism, in which EGF-induced EGFR signaling stimulates MEK/ERK pathway that inhibits *GLI1* expression in cSCC *in vitro* in specific settings.

When the effect of EGF and the concomitant *GLI1* downregulation on proliferation were analyzed, no changes in BrdU incorporation in MET-1 and MET-4 cells were detected upon treatment with EGF. In SCL-I cells we even noted a slight but significant decrease in the proliferation rate (Fig. 25). Together these data suggest a minor role of EGF in cellular proliferation of cSCC cells. This in contrast to breast cancer cells that show an increase in proliferation of about 25% (see Fig. 25).

To our knowledge there are no studies showing similar experiments and we are not aware of studies that investigated the impact of EGF on *GLI1* expression in cSCC cells. In contrast, several studies analyzed the impact of EGFR on cSCC cells. Thus, in one report, a MTT assay was used to study the effects of Cetuximab on cell survival. The authors showed that EGFR inhibition results in decreased metabolic activity of cSCC cells, including MET-1 and MET-4 cell lines (Clayburgh et al., 2013). Another group presented similar results showing a reduction in metabolic activity upon treatment with Cetuximab in different cSCC cell line (Colo16) (Galer et al., 2011). However, since the MTT assay mirrors cellular viability and not the proliferation rate, Cetuximab may be only toxic to the cells. Moreover, Galer and colleagues also suggested that combined treatment with Cetuximab and the A12 monoclonal antibody that inhibits IGF1R signaling, increases apoptosis in cSCC cells but the data for Cetuximab treatment alone were not investigated. Nevertheless, the authors used propidium iodide (PI) staining to assess apoptosis. PI is known to enter the cells with disrupted cell membrane integrity and thus does not allow for the distinction between late apoptotic and necrotic cells. This again suggests that Cetuximab might be just toxic to the cells.

7.3. GLI1 is dispensable for proliferation of cSCC cells

All the so far performed experiments implicated that the expression of the HH downstream target and transcription factor *GLI1*, which is usually described as a strong inducer of cellular

proliferation (H. Zhu and Lo, 2010), apparently is dispensable for proliferation of cultured cSCC cells. Indeed, a *GLI1* knockdown did not influence proliferation of the MET-4 cell line (Fig. 26), thus again suggesting that *GLI1* is dispensable for cSCC proliferation. This is also fostered by overexpression of *GLI1* that did not influence percentage of proliferating MET-4 and SCL-I cells when compared to the controls (Fig. 27 B). However, the overexpression data are only preliminary and require further validation. Nevertheless, these data indicate that *GLI1* inhibition seems to be irrelevant for cSCC proliferation. One possible reason could be that the transfected *GLI1* DNA is not translated into protein. Another scenario could be that GLI1 proteins derived from the plasmid lose their function or are even degraded within the cells. However, both of these explanations seem to be unlikely since in our model, *GLI1* transfection resulted not only in elevated *GLI1* but also *GLI2* expression. Indeed, regulation of *GLI2* by GLI1 transcription factors has been described in the literature (Regl et al., 2002).

7.4. Model of the crosstalk between EGF and HH signaling and/or *GLI1* expression in cSCC

Whereas data indicating a crosstalk between EGF and HH signaling is sparse in tumors, it has been extensively studied in neuronal development. The integration of EGF and HH signaling has been shown to be crucial for proliferation of neocortical cells with stem cell properties (Palma and Ruiz i Altaba, 2004). Thus, it has been shown that optimal concentrations of EGF and SHH synergize to induce cellular proliferation of neurosphere-forming stem cells as shown via BrdU incorporation assay. Furthermore, the authors showed that cyclopamine treatment inhibits not only *Gli1* but also *Egrf* transcription in mice (Palma and Ruiz i Altaba, 2004). This is in contrast to our study, where we showed that EGF strongly inhibited *GLI1* expression level suggesting rather a negative crosstalk. Palma and Ruiz I Altaba also discussed that both SHH/GLI and EGF/ERK signaling integrate at the level of SMAD proteins leading to their inactivation in the neocortex of mice (Palma and Ruiz i Altaba, 2004). On the other hand, GLI1 has been shown to form complexes with SMAD4 to induce transcription of TGFβ target genes in various cancer cell lines (Nye *et al.*, 2014). Moreover, bone morphogenetic protein (BMP)/SMAD signaling activity is cancer type-specific. Thus, it has been described that in a majority of sporadic colorectal cancers, BMP signaling is inactivated (Kodach *et al.*, 2008), whereas BMP overexpression has been linked to the metaplastic transformation of esophageal squamous cells (Milano *et al.*, 2007). Thus, it is possible that in our model EGF-mediated ERK phosphorylation inactivates SMAD proteins,

which can no longer create complexes with GLI1 leading to changes in gene expression. Indeed, there are studies showing that inactivation of TGFß receptor/SMAD signaling promotes development of cSCC (Cammareri *et al.*, 2016). It is also known that *GLI1* promoter contains GLI binding sites meaning that GLI1 can regulate its own expression (Winklmayr *et al.*, 2010). However, whether in our model *GLI1* transcription is regulated via GLI1/SMAD complexes remains to be investigated in the future.

It also has been reported that in keratinocytes EGF and HH synergize at the promoter level to induce the transcription of the selected subset of GLI target genes (Kasper *et al.*, 2006b). Additionally, Schnidar and colleagues provided evidence that HH/GLI and EGFR signaling pathways synergistically induce malignant transformation of keratinocytes and that dual inhibition of both pathways with Gefitinib and GLI inhibitor GANT61 is beneficial to inhibit growth of BCC in mice (Schnidar et al., 2009). Importantly both studies (Kasper et al., 2006b; Schnidar et al., 2009) suggest that EGFR signals via the MEK/ERK pathway to synergize with the activator form GLI1 and GLI2. In contrast, *in vitro* studies in medulloblastoma Daoy cells showed that simultaneous activation of EGFR and HH signaling with EGF and HH ligand, respectively, resulted in inhibition of expression of typical HH target genes i.e. *GLI1*, *PTCH* and *HHIP*, but in a stabilization of GLI proteins. The mechanism behind still requires clarification (Gotschel *et al.*, 2013). However, Gotschel and colleagues also showed that single treatment with EGF did not inhibit *GLI1* expression when compared to the control. This is in contrast to the results presented here. This discrepancy might be due to the differences in incubation time. Whereas we analyzed *GLI1* expression levels after 3 h incubation with EGF, Gotschel and colleagues stimulated the cells for 24 h. Thus, *GLI1* downregulation might not be a stable effect and could have been overlooked by the other group. This might be due to activation of a feedback loop, in which EGF-mediated lower *GLI1* levels may signal back to enhance activation of GLI transcription factors and thus of *GLI1* expression, possibly via other signaling pathway. Another explanation could be instability and degradation of EGF after 24 h. Finally, EGF effects might be highly cell-type specific resulting in a decrease of *GLI1* in cSCC cells, but not in other tumor cell lines such as the medulloblastoma cell line Daoy.

To summarize our data, we here propose a model for cSCC, in which EGF via activation of its receptor activates EGFR signaling. This results in inhibition of *GLI1* expression via the MEK/ERK pathway in cSCC. A similar mode of action has been proposed in HNSCC.

HNSCC is an epithelial tumor of the squamous epithelium of the mucosa of the head and neck (Keysar *et al.*, 2013). As in our setting, cell culture experiments showed that EGF treatment led to a significant inhibition of *GLI1* expression and decrease in GLI1 protein level. On the other way around, the EGFR inhibitor erlotinib treatment showed exactly opposite effects. Thus, erlotinib induced *GLI1* expression and increased GLI1 protein levels. Most interestingly, EGF treatment of the cells induced an EMT-like phenotype. That means it induced epithelial-mesenchymal transition with upregulation of *ZEB1* and *VIM*. This was associated with increased motility of the cells (Keysar et al., 2013). Thus, a similar mechanism could be proposed for cSCC and it would be highly interesting to investigate whether EGF treatment of the cells and concomitant *GLI1* downregulation results in upregulation of the EMT markers *ZEB1* and *VIM* and increased motility of cSCC cells. We also observed GLI1 downregulation upon incubation of cSCC cells with IGF1. Since IGF1R and EGFR signaling can induce the same downstream signaling pathways including MEK/ERK, IGF1-mediated GLI1 regulation probably follows the same mechanism. Indeed, simultaneous administration of cetuximab and A12, which is an IGF1R blocking antibody, results in inhibition of proliferation, tumor growth and angiogenesis as well as increased apoptosis, both in cSCC cell lines and tumor xenografts (Galer et al., 2011). Of whether this also involves upregulation of *GLI1* is presently unknown.

Together, these data suggest that both EGF/EGFR and IGF1/IGF1R are active in cSCC. Besides activating the PI3K/AKT/mTOR axis, the receptors also activate MEK/ERK signaling. Activation of MEK/ERK then leads to downregulation of *GLI1*. Of whether the inhibitory effect is mediated by MEK or by ERK remains to be established in the future. What is more important is the possibility that downregulation of GLI1 may contribute to cSCC pathogenesis. Thus, GLI1-downregulation may be associated with increased EMT and migratory and invasive capacity of cSCC cells (see above). It, however, does not influence the proliferation rate of cSCC. A summary of this model is shown in Figure 28.
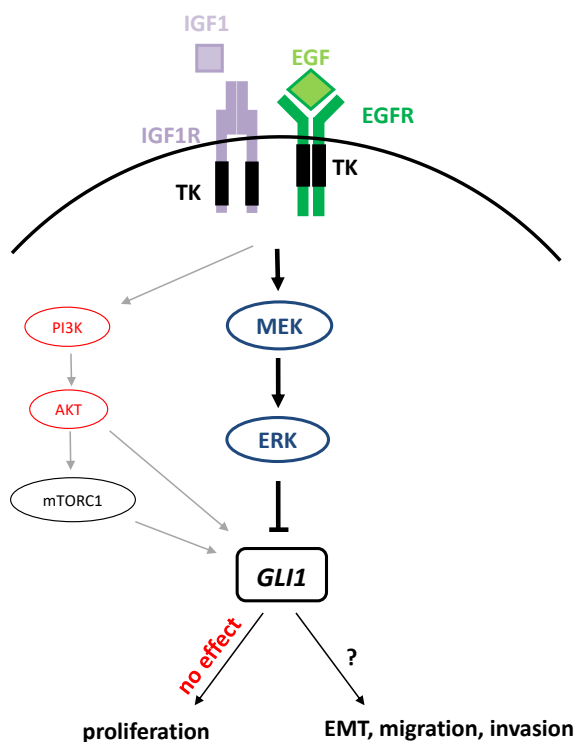
Figure 28: Model of EGF/EGFR and probably also IGF1/IGF1R signaling and associated inhibition of *GLI1* in cSCC. The model also includes the potential function of GLI1 suppression in cSCC. EGF-mediated activation of EGFR initiates both the PI3K/AKT/mTOR and MEK/ERK cascade. Although the exact role of PI3K/AKT and mTOR signaling in regulation of *GLI1* expression is still obscure, it might have a positive effect on *GLI1* expression. In contrast, the MEK/ERK axis rather inhibits *GLI1*. Since MEK/ERK signaling can also stimulate the mTOR and the PI3K/AKT pathway, *GLI1* expression by MEK/ERK is not completely abrogated in cSCC. Moreover, *GLI1* expression level has no influence on cSCC proliferation. However, it is likely that its downregulation is an important step in EMT and in cellular migration and invasion of cSCC cells. Black arrows indicate the most important processes in cSCC, whereas grey arrows apply to the auxiliary mechanisms.

Of whether the MEK/ERK-mediated suppression of *GLI1* expression involves GLI2 or GLI3, which are upstream of *GLI1*, is currently unknown. If so, we would expect that EGF treatment results in i) stabilization of the respective GLI repressor forms, ii) inactivation of the respective GLI activator forms, iii) lack of translocation of the respective GLI activator forms into the nucleus and/or in iv) degradation of GLI protein or mRNA.

However, it is also possible that MEK/ERK signaling inhibits *GLI1* expression without the involvement of the transcription factors GLI2 and GLI3. Thus, ERK also stimulates or activates a plethora of other factors including those that can inhibit gene expression (reviewed in (Whitmarsh, 2007)). One of these factors might be the myc-associated zinc finger protein MAZ. Thus, analysis of the GLI1 promoter sequence shows that besides GLI binding sites, a

consensus sequence for this transcription factor exists (data not shown). MAZ can both induce transcriptional activation and termination (Bossone *et al.*, 1992) and is more and more becoming important as a transcriptional suppressor of several genes including *human teleomerase (Su et al., 2007)*. In addition, MAZ induces EMT by upregulation of *ZEB1* (Luo *et al.*, 2016), which we also consider to occur in cSCC cells, in which *GLI1* is downregulated (see above). However, we did not find any information of whether MAZ itself is regulated by MEK/ERK signaling. Nevertheless, it is possible that MEK/ERK inhibits *GLI1* expression via a mechanism that does not involve the other GLI transcription factors.

7.5. Translation of the cSCC cell culture data into the patient's situation

There are some difficulties, when trying to translate the cell culture data into the patient's situation. We have immunohistochemical data for *GLI1*, pERK, pS6 and EGF. The IHC data shows that pERK is almost exclusively expressed in stromal cells resembling fibroblast. As described in the literature, these are also cells that express EGF (Wayne et al., 2006). The expression of EGF in fibroblast thus could explain the high levels of pERK in the fibroblasts due to an autocrine signaling. Since *GLI1* is negatively regulated by EGF/MEK/pERK, *GLI1* is not expressed in the fibroblasts.

Our data also shows that EGF is expressed by the cSCC tumor cells. Sometimes it overlaps with *GLI1* positive areas and sometimes it overlaps with *GLI1* low/negative areas. Whereas the latter setting fits to our cell culture data, the concomitant EGF staining with *GLI1* positive areas does not. However, due to the more complex setting in the *in vivo* situation, it is possible that there are other more dominant factors than EGF that might positively regulate *GLI1* expression in the tumor cells.

A more important question is however, why *GLI1* is not expressed in tumor cells that are invading the stromal environment. In compliance with the cell culture data one would expect that the invading cells that are *GLI1* low also would express pERK. However, this is not the case. Nevertheless, one possible explanation is again the more complex setting in the *in vivo* situation, in which pERK in stromal cells may regulate the expression of other soluble factors that then signal back to the invasion front of the tumors and block *GLI1* expression. This setting may also explain the fact that the *GLI1* low/neg invading cells highly express pS6. High expression of pS6 is indicative for activation of mTOR signaling and mTOR signaling is associated with cSCC aggressiveness (Khandelwal et al., 2016) and thus may play a very

important role in cSCC invasiveness. With respect to lack of *GLI1* expression in the invading cells (and as already mentioned in section 7.1.) it would thus be highly interesting to analyze whether lack of *GLI1* and concomitant activation of mTOR is necessary for cSCC invasivity and migration. Furthermore, in the style of HNSCC (Keysar et al., 2013), it also would be highly interesting to analyze, whether downregulation of *GLI1* in the invasion front correlates with EMT and upregulation of *VIM* or *ZEB1*.

The fact that the tumor center expresses *GLI1* is also difficult to explain. Apparently, and according to our cell culture data, *GLI1* is not necessary for cSCC proliferation. One possibility is that *GLI1* overexpression in the tumor center is just a bystander effect and has nothing to do with the tumor's biology. However, the fact that cSCC can develop from BCC after treatment with vismodegib strongly argues against such a scenario. BCC is a tumor that shows very high *GLI1* expression throughout the whole tumor mass due to *PTCH* mutations. With respect to vismodegib treatment of advanced stages of BCC, it has been reported that cSCC can either develop in the regions distant from the primary BCC (Aasi et al., 2013; Iarrobino et al., 2013; Orouji et al., 2014), or within the bed of BCC (G. A. Zhu et al., 2014). In the light of these data it is highly interesting that both cSCC and BCC may develop from epidermal stem cells including those within the bulge region of hair follicles or from the interfollicular epidermis (reviewed in (Thieu *et al.*, 2013)). With respect to *GLI1* expression by both tumor entities with cSCC expressing *GLI1* in the tumor center and BCC expressing it all over the tumor, it is possible that the tumors share similar molecular features at very early stages and eventually also the same precursor cell. However, when the tumors further develop, specific molecular changes may specify the fate of the cells, giving rise to either a cSCC or a BCC. Thus, it would be highly interesting to investigate whether the *GLI1* positive cSCC areas share molecular similarities with BCC.

8. References

Aasen, T. and Izpisua Belmonte, J. C. (2010). Isolation and cultivation of human keratinocytes from skin or plucked hair for the generation of induced pluripotent stem cells. *Nat Protoc, 5*(2), 371-382.

Aasi, S., Silkiss, R., Tang, J. Y., Wysong, A., Liu, A., Epstein, E., Oro, A. E. and Chang, A. L. (2013). New onset of keratoacanthomas after vismodegib treatment for locally advanced basal cell carcinomas: a report of 2 cases. *JAMA Dermatol, 149*(2), 242-243.

Abe, Y., Oda-Sato, E., Tobiume, K., Kawauchi, K., Taya, Y., Okamoto, K., Oren, M. and Tanaka, N. (2008). Hedgehog signaling overrides p53-mediated tumor suppression by activating Mdm2. *Proc Natl Acad Sci U S A, 105*(12), 4838-4843.

Aberger, F. and Ruiz, I. A. A. (2014). Context-dependent signal integration by the GLI code: the oncogenic load, pathways, modifiers and implications for cancer therapy. *Semin Cell Dev Biol, 33*, 93-104.

Al-Kuraya, K., Schraml, P., Torhorst, J., Tapia, C., Zaharieva, B., Novotny, H., Spichtin, H., Maurer, R., Mirlacher, M., Kochli, O., Zuber, M., Dieterich, H., Mross, F., Wilber, K., Simon, R. and Sauter, G. (2004). Prognostic relevance of gene amplifications and coamplifications in breast cancer. *Cancer Res, 64*(23), 8534-8540.

Alam, M. and Ratner, D. (2001). Cutaneous squamous-cell carcinoma. *N Engl J Med, 344*(13), 975-983.

Alessi, D. R., Deak, M., Casamayor, A., Caudwell, F. B., Morrice, N., Norman, D. G., Gaffney, P., Reese, C. B., MacDougall, C. N., Harbison, D., Ashworth, A. and Bownes, M. (1997). 3-Phosphoinositide-dependent protein kinase-1 (PDK1): structural and functional homology with the Drosophila DSTPK61 kinase. *Curr Biol, 7*(10), 776-789.

Amakye, D., Jagani, Z. and Dorsch, M. (2013). Unraveling the therapeutic potential of the Hedgehog pathway in cancer. *Nat Med, 19*(11), 1410-1422.

Amari, W., Zeringue, A. L., McDonald, J. R., Caplan, L., Eisen, S. A. and Ranganathan, P. (2011). Risk of non-melanoma skin cancer in a national cohort of veterans with rheumatoid arthritis. *Rheumatology (Oxford), 50*(8), 1431-1439.

Asmis, L. M., Gerber, H., Kaempf, J. and Studer, H. (1995). Epidermal growth factor stimulates cell proliferation and inhibits iodide uptake of FRTL-5 cells in vitro. *J Endocrinol, 145*(3), 513-520.

Atwood, S. X., Sarin, K. Y., Whitson, R. J., Li, J. R., Kim, G., Rezaee, M., Ally, M. S., Kim, J., Yao, C., Chang, A. L., Oro, A. E. and Tang, J. Y. (2015). Smoothened variants explain the majority of drug resistance in basal cell carcinoma. *Cancer Cell, 27*(3), 342-353.

Bakry, O. A., Samaka, R. M., Shoeib, M. A. and Megahed, D. M. (2015). Immunolocalization of glioma-associated oncogene homolog 1 in non melanoma skin cancer. *Ultrastruct Pathol, 39*(2), 135-146.

Barbacci, E. G., Guarino, B. C., Stroh, J. G., Singleton, D. H., Rosnack, K. J., Moyer, J. D. and Andrews, G. C. (1995). The structural basis for the specificity of epidermal growth factor and heregulin binding. *J Biol Chem, 270*(16), 9585-9589.

Barnes, E. A., Kong, M., Ollendorff, V. and Donoghue, D. J. (2001). Patched1 interacts with cyclin B1 to regulate cell cycle progression. *EMBO J, 20*(9), 2214-2223.

Barrette, K., Van Kelst, S., Wouters, J., Marasigan, V., Fieuws, S., Agostinis, P., van den Oord, J. and Garmyn, M. (2014). Epithelial-mesenchymal transition during invasion of cutaneous squamous cell carcinoma is paralleled by AKT activation. *Br J Dermatol, 171*(5), 1014-1021.

Beauchamp, E., Bulut, G., Abaan, O., Chen, K., Merchant, A., Matsui, W., Endo, Y., Rubin, J. S., Toretsky, J. and Uren, A. (2009). GLI1 is a direct transcriptional target of EWS-FLI1 oncoprotein. *J Biol Chem, 284*(14), 9074-9082.

Beauchamp, E., Ringer, L., Bulut, G., Sajwan, K. P., Hall, M. D., Lee, Y. C., Peaceman, D., Ozdemirli, M., Rodriguez, O., Macdonald, T. J., Albanese, C., Toretsky, J. A. and Uren, A. (2011). Arsenic

trioxide inhibits human cancer cell growth and tumor development in mice by blocking Hedgehog/GLI pathway. *J Clin Invest, 121*(1), 148-160.

Beer, C., Buhr, P., Hahn, H., Laubner, D. and Wirth, M. (2003). Gene expression analysis of murine cells producing amphotropic mouse leukaemia virus at a cultivation temperature of 32 and 37 degrees C. *J Gen Virol, 84*(Pt 7), 1677-1686.

Berlin, J., Bendell, J. C., Hart, L. L., Firdaus, I., Gore, I., Hermann, R. C., Mulcahy, M. F., Zalupski, M. M., Mackey, H. M., Yauch, R. L., Graham, R. A., Bray, G. L. and Low, J. A. (2013). A randomized phase II trial of vismodegib versus placebo with FOLFOX or FOLFIRI and bevacizumab in patients with previously untreated metastatic colorectal cancer. *Clin Cancer Res, 19*(1), 258-267.

Bikle, D. D., Oda, Y. and Xie, Z. (2004). Calcium and 1,25(OH)2D: interacting drivers of epidermal differentiation. *J Steroid Biochem Mol Biol, 89-90*(1-5), 355-360.

Binns, W., James, L. F., Keeler, R. F. and Balls, L. D. (1968). Effects of teratogenic agents in range plants. *Cancer Res, 28*(11), 2323-2326.

Bossone, S. A., Asselin, C., Patel, A. J. and Marcu, K. B. (1992). MAZ, a zinc finger protein, binds to c-MYC and C2 gene sequences regulating transcriptional initiation and termination. *Proc Natl Acad Sci U S A, 89*(16), 7452-7456.

Boukamp, P., Petrussevska, R. T., Breitkreutz, D., Hornung, J., Markham, A. and Fusenig, N. E. (1988). Normal keratinization in a spontaneously immortalized aneuploid human keratinocyte cell line. *J Cell Biol, 106*(3), 761-771.

Boukamp, P., Stanbridge, E. J., Foo, D. Y., Cerutti, P. A. and Fusenig, N. E. (1990). c-Ha-ras oncogene expression in immortalized human keratinocytes (HaCaT) alters growth potential in vivo but lacks correlation with malignancy. *Cancer Res, 50*(9), 2840-2847.

Boukamp, P., Tilgen, W., Dzarlieva, R. T., Breitkreutz, D., Haag, D., Riehl, R. K., Bohnert, A. and Fusenig, N. E. (1982). Phenotypic and genotypic characteristics of a cell line from a squamous cell carcinoma of human skin. *J Natl Cancer Inst, 68*(3), 415-427.

Brand, T. M., Iida, M. and Wheeler, D. L. (2011). Molecular mechanisms of resistance to the EGFR monoclonal antibody cetuximab. *Cancer Biol Ther, 11*(9), 777-792.

Brash, D. E., Rudolph, J. A., Simon, J. A., Lin, A., McKenna, G. J., Baden, H. P., Halperin, A. J. and Ponten, J. (1991). A role for sunlight in skin cancer: UV-induced p53 mutations in squamous cell carcinoma. *Proc Natl Acad Sci U S A, 88*(22), 10124-10128.

Briscoe, J. and Therond, P. P. (2013). The mechanisms of Hedgehog signalling and its roles in development and disease. *Nat Rev Mol Cell Biol, 14*(7), 416-429.

Burness, C. B. (2015). Sonidegib: First Global Approval. *Drugs, 75*(13), 1559-1566.

Busse, D., Yakes, F. M., Lenferink, A. E. and Arteaga, C. L. (2001). Tyrosine kinase inhibitors: rationale, mechanisms of action, and implications for drug resistance. *Semin Oncol, 28*(5 Suppl 16), 47-55.

Cammareri, P., Rose, A. M., Vincent, D. F., Wang, J., Nagano, A., Libertini, S., Ridgway, R. A., Athineos, D., Coates, P. J., McHugh, A., Pourreyron, C., Dayal, J. H., Larsson, J., Weidlich, S., Spender, L. C., Sapkota, G. P., Purdie, K. J., Proby, C. M., Harwood, C. A., Leigh, I. M., Clevers, H., Barker, N., Karlsson, S., Pritchard, C., Marais, R., Chelala, C., South, A. P., Sansom, O. J. and Inman, G. J. (2016). Inactivation of TGFbeta receptors in stem cells drives cutaneous squamous cell carcinoma. *Nat Commun, 7*, 12493.

Capiod, T., Shuba, Y., Skryma, R. and Prevarskaya, N. (2007). Calcium signalling and cancer cell growth. *Subcell Biochem, 45*, 405-427.

Celebi, A. R., Kiratli, H. and Soylemezoglu, F. (2016). Evaluation of the 'Hedgehog' signaling pathways in squamous and basal cell carcinomas of the eyelids and conjunctiva. *Oncol Lett, 12*(1), 467-472.

Chalhoub, N. and Baker, S. J. (2009). PTEN and the PI3-kinase pathway in cancer. *Annu Rev Pathol, 4*, 127-150.

Chen, J. K., Taipale, J., Cooper, M. K. and Beachy, P. A. (2002a). Inhibition of Hedgehog signaling by direct binding of cyclopamine to Smoothened. *Genes Dev, 16*(21), 2743-2748.

Chen, J. K., Taipale, J., Young, K. E., Maiti, T. and Beachy, P. A. (2002b). Small molecule modulation of Smoothened activity. *Proc Natl Acad Sci U S A, 99*(22), 14071-14076.

Chen, S. J., Nakahara, T., Takahara, M., Kido, M., Dugu, L., Uchi, H., Takeuchi, S., Tu, Y. T., Moroi, Y. and Furue, M. (2009). Activation of the mammalian target of rapamycin signalling pathway in epidermal tumours and its correlation with cyclin-dependent kinase 2. *Br J Dermatol, 160*(2), 442-445.

Chuang, P. T. and McMahon, A. P. (1999). Vertebrate Hedgehog signalling modulated by induction of a Hedgehog-binding protein. *Nature, 397*(6720), 617-621.

Chung, J. H. and Bunz, F. (2013). A loss-of-function mutation in PTCH1 suggests a role for autocrine hedgehog signaling in colorectal tumorigenesis. *Oncotarget, 4*(12), 2208-2211.

Chung, U. I., Schipani, E., McMahon, A. P. and Kronenberg, H. M. (2001). Indian hedgehog couples chondrogenesis to osteogenesis in endochondral bone development. *J Clin Invest, 107*(3), 295-304.

Clark, A. M., Garland, K. K. and Russell, L. D. (2000). Desert hedgehog (Dhh) gene is required in the mouse testis for formation of adult-type Leydig cells and normal development of peritubular cells and seminiferous tubules. *Biol Reprod, 63*(6), 1825-1838.

Clayburgh, D. R., Gross, N. D., Proby, C., Koide, J. and Wong, M. H. (2013). Effects of epidermal growth factor receptor and insulin-like growth factor 1 receptor inhibition on proliferation and intracellular signaling in cutaneous SCCHN: potential for dual inhibition as a therapeutic modality. *Head Neck, 35*(1), 86-93.

Cohen, S. (1962). Isolation of a mouse submaxillary gland protein accelerating incisor eruption and eyelid opening in the new-born animal. *J Biol Chem, 237*, 1555-1562.

Cohen, S. and Carpenter, G. (1975). Human epidermal growth factor: isolation and chemical and biological properties. *Proc Natl Acad Sci U S A, 72*(4), 1317-1321.

Comsa, S., Cimpean, A. M. and Raica, M. (2015). The Story of MCF-7 Breast Cancer Cell Line: 40 years of Experience in Research. *Anticancer Res, 35*(6), 3147-3154.

Danaee, H., Karagas, M. R., Kelsey, K. T., Perry, A. E. and Nelson, H. H. (2006). Allelic loss at Drosophila patched gene is highly prevalent in Basal and squamous cell carcinomas of the skin. *J Invest Dermatol, 126*(5), 1152-1158.

Dennler, S., Andre, J., Alexaki, I., Li, A., Magnaldo, T., ten Dijke, P., Wang, X. J., Verrecchia, F. and Mauviel, A. (2007). Induction of sonic hedgehog mediators by transforming growth factor-beta: Smad3-dependent activation of Gli2 and Gli1 expression in vitro and in vivo. *Cancer Res, 67*(14), 6981-6986.

Dennler, S., Andre, J., Verrecchia, F. and Mauviel, A. (2009). Cloning of the human GLI2 Promoter: transcriptional activation by transforming growth factor-beta via SMAD3/beta-catenin cooperation. *J Biol Chem, 284*(46), 31523-31531.

Di Marcotullio, L., Ferretti, E., Greco, A., De Smaele, E., Screpanti, I. and Gulino, A. (2007). Multiple ubiquitin-dependent processing pathways regulate hedgehog/gli signaling: implications for cell development and tumorigenesis. *Cell Cycle, 6*(4), 390-393.

Dijkgraaf, G. J., Alicke, B., Weinmann, L., Januario, T., West, K., Modrusan, Z., Burdick, D., Goldsmith, R., Robarge, K., Sutherlin, D., Scales, S. J., Gould, S. E., Yauch, R. L. and de Sauvage, F. J. (2011). Small molecule inhibition of GDC-0449 refractory smoothened mutants and downstream mechanisms of drug resistance. *Cancer Res, 71*(2), 435-444.

Doglioni, C., Piccinin, S., Demontis, S., Cangi, M. G., Pecciarini, L., Chiarelli, C., Armellin, M., Vukosavljevic, T., Boiocchi, M. and Maestro, R. (2003). Alterations of beta-catenin pathway in non-melanoma skin tumors: loss of alpha-ABC nuclear reactivity correlates with the presence of beta-catenin gene mutation. *Am J Pathol, 163*(6), 2277-2287.

Dubey, A. K., Dubey, S., Handu, S. S. and Qazi, M. A. (2013). Vismodegib: the first drug approved for advanced and metastatic basal cell carcinoma. *J Postgrad Med, 59*(1), 48-50.

Dziunycz, P. J., Lazarova, Z., Duncan, N., Wong, S., Neuburg, M., Hofbauer, G. F. and Olasz, E. B. (2013). EGFRvIII expression in squamous cell carcinoma of the skin. *JAMA Dermatol, 149*(10), 1240-1242.

Eberl, M., Klingler, S., Mangelberger, D., Loipetzberger, A., Damhofer, H., Zoidl, K., Schnidar, H., Hache, H., Bauer, H. C., Solca, F., Hauser-Kronberger, C., Ermilov, A. N., Verhaegen, M. E., Bichakjian, C. K., Dlugosz, A. A., Nietfeld, W., Sibilia, M., Lehrach, H., Wierling, C. and Aberger, F. (2012). Hedgehog-EGFR cooperation response genes determine the oncogenic phenotype of basal cell carcinoma and tumour-initiating pancreatic cancer cells. *EMBO Mol Med, 4*(3), 218-233.

Ebi, H., Costa, C., Faber, A. C., Nishtala, M., Kotani, H., Juric, D., Della Pelle, P., Song, Y., Yano, S., Mino-Kenudson, M., Benes, C. H. and Engelman, J. A. (2013). PI3K regulates MEK/ERK signaling in breast cancer via the Rac-GEF, P-Rex1. *Proc Natl Acad Sci U S A, 110*(52), 21124-21129.

Ehtesham, M., Sarangi, A., Valadez, J. G., Chanthaphaychith, S., Becher, M. W., Abel, T. W., Thompson, R. C. and Cooper, M. K. (2007). Ligand-dependent activation of the hedgehog pathway in glioma progenitor cells. *Oncogene, 26*(39), 5752-5761.

El-Bahrawy, M., El-Masry, N., Alison, M., Poulsom, R. and Fallowfield, M. (2003). Expression of beta-catenin in basal cell carcinoma. *Br J Dermatol, 148*(5), 964-970.

Epstein, E. H. (2008). Basal cell carcinomas: attack of the hedgehog. *Nature Reviews Cancer, 8*(10), 743-754.

Euvrard, S., Kanitakis, J. and Claudy, A. (2003). Skin cancers after organ transplantation. *N Engl J Med, 348*(17), 1681-1691.

Filbin, M. G., Dabral, S. K., Pazyra-Murphy, M. F., Ramkissoon, S., Kung, A. L., Pak, E., Chung, J., Theisen, M. A., Sun, Y., Franchetti, Y., Shulman, D. S., Redjal, N., Tabak, B., Beroukhim, R., Wang, Q., Zhao, J., Dorsch, M., Buonamici, S., Ligon, K. L., Kelleher, J. F. and Segal, R. A. (2013). Coordinate activation of Shh and PI3K signaling in PTEN-deficient glioblastoma: new therapeutic opportunities. *Nat Med, 19*(11), 1518-1523.

Fogarty, G. B., Conus, N. M., Chu, J. and McArthur, G. (2007a). Characterization of the expression and activation of the epidermal growth factor receptor in squamous cell carcinoma of the skin. *Br J Dermatol, 156*(1), 92-98.

Fogarty, M. P., Emmenegger, B. A., Grasfeder, L. L., Oliver, T. G. and Wechsler-Reya, R. J. (2007b). Fibroblast growth factor blocks Sonic hedgehog signaling in neuronal precursors and tumor cells. *Proc Natl Acad Sci U S A, 104*(8), 2973-2978.

Fritsch, A. (2014). *Analysen zu Interaktionen zwischen dem Vitamin-D-Rezeptor Signalweg und der Hedgehog-Signalkaskade.* Georg-August Universität Göttingen.

Galer, C. E., Corey, C. L., Wang, Z., Younes, M. N., Gomez-Rivera, F., Jasser, S. A., Ludwig, D. L., El-Naggar, A. K., Weber, R. S. and Myers, J. N. (2011). Dual inhibition of epidermal growth factor receptor and insulin-like growth factor receptor I: reduction of angiogenesis and tumor growth in cutaneous squamous cell carcinoma. *Head Neck, 33*(2), 189-198.

Garwood, C. J., Ratcliffe, L. E., Morgan, S. V., Simpson, J. E., Owens, H., Vazquez-Villasenor, I., Heath, P. R., Romero, I. A., Ince, P. G. and Wharton, S. B. (2015). Insulin and IGF1 signalling pathways in human astrocytes in vitro and in vivo; characterisation, subcellular localisation and modulation of the receptors. *Mol Brain, 8*, 51.

Gordon, A. T., Brinkschmidt, C., Anderson, J., Coleman, N., Dockhorn-Dworniczak, B., Pritchard-Jones, K. and Shipley, J. (2000). A novel and consistent amplicon at 13q31 associated with alveolar rhabdomyosarcoma. *Genes Chromosomes Cancer, 28*(2), 220-226.

Gotschel, F., Berg, D., Gruber, W., Bender, C., Eberl, M., Friedel, M., Sonntag, J., Rungeler, E., Hache, H., Wierling, C., Nietfeld, W., Lehrach, H., Frischauf, A., Schwartz-Albiez, R., Aberger, F. and

Korf, U. (2013). Synergism between Hedgehog-GLI and EGFR signaling in Hedgehog-responsive human medulloblastoma cells induces downregulation of canonical Hedgehog-target genes and stabilized expression of GLI1. *PLoS One, 8*(6), e65403.

Green, A. C. and Olsen, C. M. (2017). Cutaneous squamous cell carcinoma: an epidemiological review. *Br J Dermatol*

Hahn, H., Wicking, C., Zaphiropoulous, P. G., Gailani, M. R., Shanley, S., Chidambaram, A., Vorechovsky, I., Holmberg, E., Unden, A. B., Gillies, S., Negus, K., Smyth, I., Pressman, C., Leffell, D. J., Gerrard, B., Goldstein, A. M., Dean, M., Toftgard, R., Chenevix-Trench, G., Wainwright, B. and Bale, A. E. (1996). Mutations of the human homolog of Drosophila patched in the nevoid basal cell carcinoma syndrome. *Cell, 85*(6), 841-851.

Hahn, H., Wojnowski, L., Specht, K., Kappler, R., Calzada-Wack, J., Potter, D., Zimmer, A., Muller, U., Samson, E. and Quintanilla-Martinez, L. (2000). Patched target Igf2 is indispensable for the formation of medulloblastoma and rhabdomyosarcoma. *J Biol Chem, 275*(37), 28341-28344.

Hallahan, A. R., Pritchard, J. I., Hansen, S., Benson, M., Stoeck, J., Hatton, B. A., Russell, T. L., Ellenbogen, R. G., Bernstein, I. D., Beachy, P. A. and Olson, J. M. (2004). The SmoA1 mouse model reveals that notch signaling is critical for the growth and survival of sonic hedgehog-induced medulloblastomas. *Cancer Res, 64*(21), 7794-7800.

Harris, R. B., Griffith, K. and Moon, T. E. (2001). Trends in the incidence of nonmelanoma skin cancers in southeastern Arizona, 1985-1996. *J Am Acad Dermatol, 45*(4), 528-536.

Hartmann, W., Koch, A., Brune, H., Waha, A., Schuller, U., Dani, I., Denkhaus, D., Langmann, W., Bode, U., Wiestler, O. D., Schilling, K. and Pietsch, T. (2005). Insulin-like growth factor II is involved in the proliferation control of medulloblastoma and its cerebellar precursor cells. *Am J Pathol, 166*(4), 1153-1162.

Hollestein, L. M., de Vries, E., Aarts, M. J., Schroten, C. and Nijsten, T. E. (2014). Burden of disease caused by keratinocyte cancer has increased in The Netherlands since 1989. *J Am Acad Dermatol, 71*(5), 896-903.

Iarrobino, A., Messina, J. L., Kudchadkar, R. and Sondak, V. K. (2013). Emergence of a squamous cell carcinoma phenotype following treatment of metastatic basal cell carcinoma with vismodegib. *J Am Acad Dermatol, 69*(1), e33-34.

Ingham, P. W., Nakano, Y. and Seger, C. (2011). Mechanisms and functions of Hedgehog signalling across the metazoa. *Nat Rev Genet, 12*(6), 393-406.

Iqbal, S. and Lenz, H. J. (2004). Integration of novel agents in the treatment of colorectal cancer. *Cancer Chemother Pharmacol, 54 Suppl 1*, S32-39.

Janes, S. M. and Watt, F. M. (2006). New roles for integrins in squamous-cell carcinoma. *Nat Rev Cancer, 6*(3), 175-183.

Jensen, A. O., Thomsen, H. F., Engebjerg, M. C., Olesen, A. B., Friis, S., Karagas, M. R. and Sorensen, H. T. (2009). Use of oral glucocorticoids and risk of skin cancer and non-Hodgkin's lymphoma: a population-based case-control study. *Br J Cancer, 100*(1), 200-205.

Ji, Z., Mei, F. C., Xie, J. and Cheng, X. (2007). Oncogenic KRAS activates hedgehog signaling pathway in pancreatic cancer cells. *J Biol Chem, 282*(19), 14048-14055.

Johnson, R. L., Rothman, A. L., Xie, J., Goodrich, L. V., Bare, J. W., Bonifas, J. M., Quinn, A. G., Myers, R. M., Cox, D. R., Epstein, E. H., Jr. and Scott, M. P. (1996). Human homolog of patched, a candidate gene for the basal cell nevus syndrome. *Science, 272*(5268), 1668-1671.

Jung, G. W., Metelitsa, A. I., Dover, D. C. and Salopek, T. G. (2010). Trends in incidence of nonmelanoma skin cancers in Alberta, Canada, 1988-2007. *Br J Dermatol, 163*(1), 146-154.

Karagas, M. R., Cushing, G. L., Jr., Greenberg, E. R., Mott, L. A., Spencer, S. K. and Nierenberg, D. W. (2001). Non-melanoma skin cancers and glucocorticoid therapy. *Br J Cancer, 85*(5), 683-686.

Kasper, M., Regl, G., Frischauf, A. M. and Aberger, F. (2006a). GLI transcription factors: mediators of oncogenic Hedgehog signalling. *Eur J Cancer, 42*(4), 437-445.

Kasper, M., Schnidar, H., Neill, G. W., Hanneder, M., Klingler, S., Blaas, L., Schmid, C., Hauser-Kronberger, C., Regl, G., Philpott, M. P. and Aberger, F. (2006b). Selective modulation of Hedgehog/GLI target gene expression by epidermal growth factor signaling in human keratinocytes. *Mol Cell Biol, 26*(16), 6283-6298.

Kaye, S. B., Fehrenbacher, L., Holloway, R., Amit, A., Karlan, B., Slomovitz, B., Sabbatini, P., Fu, L., Yauch, R. L., Chang, I. and Reddy, J. C. (2012). A phase II, randomized, placebo-controlled study of vismodegib as maintenance therapy in patients with ovarian cancer in second or third complete remission. *Clin Cancer Res, 18*(23), 6509-6518.

Kaylani, S. Z., Xu, J., Srivastava, R. K., Kopelovich, L., Pressey, J. G. and Athar, M. (2013). Rapamycin targeting mTOR and hedgehog signaling pathways blocks human rhabdomyosarcoma growth in xenograft murine model. *Biochem Biophys Res Commun, 435*(4), 557-561.

Keysar, S. B., Le, P. N., Anderson, R. T., Morton, J. J., Bowles, D. W., Paylor, J. J., Vogler, B. W., Thorburn, J., Fernandez, P., Glogowska, M. J., Takimoto, S. M., Sehrt, D. B., Gan, G. N., Eagles-Soukup, J. R., Serracino, H., Hirsch, F. R., Lucia, M. S., Thorburn, A., Song, J. I., Wang, X. J. and Jimeno, A. (2013). Hedgehog signaling alters reliance on EGF receptor signaling and mediates anti-EGFR therapeutic resistance in head and neck cancer. *Cancer Res, 73*(11), 3381-3392.

Khandelwal, A. R., Ma, X., Egan, P., Kaskas, N. M., Moore-Medlin, T., Caldito, G., Abreo, F., Gu, X., Aubrey, L., Milligan, E. and Nathan, C. A. (2016). Biomarker and Pathologic Predictors of Cutaneous Squamous Cell Carcinoma Aggressiveness. *Otolaryngol Head Neck Surg, 155*(2), 281-288.

Kim, E. J., Sahai, V., Abel, E. V., Griffith, K. A., Greenson, J. K., Takebe, N., Khan, G. N., Blau, J. L., Craig, R., Balis, U. G., Zalupski, M. M. and Simeone, D. M. (2014). Pilot clinical trial of hedgehog pathway inhibitor GDC-0449 (vismodegib) in combination with gemcitabine in patients with metastatic pancreatic adenocarcinoma. *Clin Cancer Res, 20*(23), 5937-5945.

Kinzler, K. W., Bigner, S. H., Bigner, D. D., Trent, J. M., Law, M. L., O'Brien, S. J., Wong, A. J. and Vogelstein, B. (1987). Identification of an amplified, highly expressed gene in a human glioma. *Science, 236*(4797), 70-73.

Kodach, L. L., Wiercinska, E., de Miranda, N. F., Bleuming, S. A., Musler, A. R., Peppelenbosch, M. P., Dekker, E., van den Brink, G. R., van Noesel, C. J., Morreau, H., Hommes, D. W., Ten Dijke, P., Offerhaus, G. J. and Hardwick, J. C. (2008). The bone morphogenetic protein pathway is inactivated in the majority of sporadic colorectal cancers. *Gastroenterology, 134*(5), 1332-1341.

Kohn, A. D., Takeuchi, F. and Roth, R. A. (1996). Akt, a pleckstrin homology domain containing kinase, is activated primarily by phosphorylation. *J Biol Chem, 271*(36), 21920-21926.

Korc, M., Chandrasekar, B., Yamanaka, Y., Friess, H., Buchier, M. and Beger, H. G. (1992). Overexpression of the epidermal growth factor receptor in human pancreatic cancer is associated with concomitant increases in the levels of epidermal growth factor and transforming growth factor alpha. *J Clin Invest, 90*(4), 1352-1360.

Lam, C. W., Xie, J., To, K. F., Ng, H. K., Lee, K. C., Yuen, N. W., Lim, P. L., Chan, L. Y., Tong, S. F. and McCormick, F. (1999). A frequent activated smoothened mutation in sporadic basal cell carcinomas. *Oncogene, 18*(3), 833-836.

Laplante, M. and Sabatini, D. M. (2012). mTOR signaling in growth control and disease. *Cell, 149*(2), 274-293.

Lauth, M., Bergstrom, A. and Toftgard, R. (2007). Phorbol esters inhibit the Hedgehog signalling pathway downstream of Suppressor of Fused, but upstream of Gli. *Oncogene, 26*(35), 5163-5168.

Leblanc, K. G., Jr., Hughes, M. P. and Sheehan, D. J. (2011). The role of sirolimus in the prevention of cutaneous squamous cell carcinoma in organ transplant recipients. *Dermatol Surg, 37*(6), 744-749.

Lee, M. Y., Chou, C. Y., Tang, M. J. and Shen, M. R. (2008). Epithelial-mesenchymal transition in cervical cancer: correlation with tumor progression, epidermal growth factor receptor overexpression, and snail up-regulation. *Clin Cancer Res, 14*(15), 4743-4750.

Lehr, S., Kotzka, J., Avci, H., Sickmann, A., Meyer, H. E., Herkner, A. and Muller-Wieland, D. (2004). Identification of major ERK-related phosphorylation sites in Gab1. *Biochemistry, 43*(38), 12133-12140.

Levi, F., Randimbison, L., Te, V. C. and La Vecchia, C. (1996). Non-Hodgkin's lymphomas, chronic lymphocytic leukaemias and skin cancers. *Br J Cancer, 74*(11), 1847-1850.

Liao, H. W., Hsu, J. M., Xia, W., Wang, H. L., Wang, Y. N., Chang, W. C., Arold, S. T., Chou, C. K., Tsou, P. H., Yamaguchi, H., Fang, Y. F., Lee, H. J., Lee, H. H., Tai, S. K., Yang, M. H., Morelli, M. P., Sen, M., Ladbury, J. E., Chen, C. H., Grandis, J. R., Kopetz, S. and Hung, M. C. (2015). PRMT1-mediated methylation of the EGF receptor regulates signaling and cetuximab response. *J Clin Invest, 125*(12), 4529-4543.

Libermann, T. A., Nusbaum, H. R., Razon, N., Kris, R., Lax, I., Soreq, H., Whittle, N., Waterfield, M. D., Ullrich, A. and Schlessinger, J. (1985). Amplification and overexpression of the EGF receptor gene in primary human glioblastomas. *J Cell Sci Suppl, 3*, 161-172.

Lin, S. Y., Makino, K., Xia, W., Matin, A., Wen, Y., Kwong, K. Y., Bourguignon, L. and Hung, M. C. (2001). Nuclear localization of EGF receptor and its potential new role as a transcription factor. *Nat Cell Biol, 3*(9), 802-808.

Lipinski, R. J., Hutson, P. R., Hannam, P. W., Nydza, R. J., Washington, I. M., Moore, R. W., Girdaukas, G. G., Peterson, R. E. and Bushman, W. (2008). Dose- and route-dependent teratogenicity, toxicity, and pharmacokinetic profiles of the hedgehog signaling antagonist cyclopamine in the mouse. *Toxicol Sci, 104*(1), 189-197.

Lomas, A., Leonardi-Bee, J. and Bath-Hextall, F. (2012). A systematic review of worldwide incidence of nonmelanoma skin cancer. *Br J Dermatol, 166*(5), 1069-1080.

Lu, Z., Jiang, G., Blume-Jensen, P. and Hunter, T. (2001). Epidermal growth factor-induced tumor cell invasion and metastasis initiated by dephosphorylation and downregulation of focal adhesion kinase. *Mol Cell Biol, 21*(12), 4016-4031.

Luo, W., Zhu, X., Liu, W., Ren, Y., Bei, C., Qin, L., Miao, X., Tang, F., Tang, G. and Tan, S. (2016). MYC associated zinc finger protein promotes the invasion and metastasis of hepatocellular carcinoma by inducing epithelial mesenchymal transition. *Oncotarget, 7*(52), 86420-86432.

Maeda, O., Kondo, M., Fujita, T., Usami, N., Fukui, T., Shimokata, K., Ando, T., Goto, H. and Sekido, Y. (2006). Enhancement of GLI1-transcriptional activity by beta-catenin in human cancer cells. *Oncol Rep, 16*(1), 91-96.

Maesawa, C., Tamura, G., Iwaya, T., Ogasawara, S., Ishida, K., Sato, N., Nishizuka, S., Suzuki, Y., Ikeda, K., Aoki, K., Saito, K. and Satodate, R. (1998). Mutations in the human homologue of the Drosophila patched gene in esophageal squamous cell carcinoma. *Genes Chromosomes Cancer, 21*(3), 276-279.

Manning, B. D. (2004). Balancing Akt with S6K: implications for both metabolic diseases and tumorigenesis. *J Cell Biol, 167*(3), 399-403.

Mao, J., Maye, P., Kogerman, P., Tejedor, F. J., Toftgard, R., Xie, W., Wu, G. and Wu, D. (2002). Regulation of Gli1 transcriptional activity in the nucleus by Dyrk1. *J Biol Chem, 277*(38), 35156-35161.

Martinelli, E., De Palma, R., Orditura, M., De Vita, F. and Ciardiello, F. (2009). Anti-epidermal growth factor receptor monoclonal antibodies in cancer therapy. *Clin Exp Immunol, 158*(1), 1-9.

Martinez-Cruz, A. B., Santos, M., Lara, M. F., Segrelles, C., Ruiz, S., Moral, M., Lorz, C., Garcia-Escudero, R. and Paramio, J. M. (2008). Spontaneous squamous cell carcinoma induced by the somatic inactivation of retinoblastoma and Trp53 tumor suppressors. *Cancer Res, 68*(3), 683-692.

Masuda, H., Zhang, D., Bartholomeusz, C., Doihara, H., Hortobagyi, G. N. and Ueno, N. T. (2012). Role of epidermal growth factor receptor in breast cancer. *Breast Cancer Res Treat, 136*(2), 331-345.

Maubec, E., Petrow, P., Scheer-Senyarich, I., Duvillard, P., Lacroix, L., Gelly, J., Certain, A., Duval, X., Crickx, B., Buffard, V., Basset-Seguin, N., Saez, P., Duval-Modeste, A. B., Adamski, H., Mansard, S., Grange, F., Dompmartin, A., Faivre, S., Mentre, F. and Avril, M. F. (2011). Phase II study of cetuximab as first-line single-drug therapy in patients with unresectable squamous cell carcinoma of the skin. *J Clin Oncol, 29*(25), 3419-3426.

Mauerer, A., Herschberger, E., Dietmaier, W., Landthaler, M. and Hafner, C. (2011). Low incidence of EGFR and HRAS mutations in cutaneous squamous cell carcinomas of a German cohort. *Exp Dermatol, 20*(10), 848-850.

McGillis, S. T. and Fein, H. (2004). Topical treatment strategies for non-melanoma skin cancer and precursor lesions. *Semin Cutan Med Surg, 23*(3), 174-183.

Mendoza, M. C., Er, E. E. and Blenis, J. (2011). The Ras-ERK and PI3K-mTOR pathways: cross-talk and compensation. *Trends Biochem Sci, 36*(6), 320-328.

Milano, F., van Baal, J. W., Buttar, N. S., Rygiel, A. M., de Kort, F., DeMars, C. J., Rosmolen, W. D., Bergman, J. J., J, V. A. M., Wang, K. K., Peppelenbosch, M. P. and Krishnadath, K. K. (2007). Bone morphogenetic protein 4 expressed in esophagitis induces a columnar phenotype in esophageal squamous cells. *Gastroenterology, 132*(7), 2412-2421.

Myers, M. G., Jr., Grammer, T. C., Wang, L. M., Sun, X. J., Pierce, J. H., Blenis, J. and White, M. F. (1994). Insulin receptor substrate-1 mediates phosphatidylinositol 3'-kinase and p70S6k signaling during insulin, insulin-like growth factor-1, and interleukin-4 stimulation. *J Biol Chem, 269*(46), 28783-28789.

Nedelcu, D., Liu, J., Xu, Y., Jao, C. and Salic, A. (2013). Oxysterol binding to the extracellular domain of Smoothened in Hedgehog signaling. *Nat Chem Biol, 9*(9), 557-564.

Nicolas, M., Wolfer, A., Raj, K., Kummer, J. A., Mill, P., van Noort, M., Hui, C. C., Clevers, H., Dotto, G. P. and Radtke, F. (2003). Notch1 functions as a tumor suppressor in mouse skin. *Nat Genet, 33*(3), 416-421.

Niewiadomski, P., Kong, J. H., Ahrends, R., Ma, Y., Humke, E. W., Khan, S., Teruel, M. N., Novitch, B. G. and Rohatgi, R. (2014). Gli protein activity is controlled by multisite phosphorylation in vertebrate Hedgehog signaling. *Cell Rep, 6*(1), 168-181.

Nikolaou, V., Stratigos, A. J. and Tsao, H. (2012). Hereditary nonmelanoma skin cancer. *Semin Cutan Med Surg, 31*(4), 204-210.

Nitzki, F. (2008). *Patched associated tumors: Modifier genes and pathogenesis.* Dissertation.

Nolan-Stevaux, O., Lau, J., Truitt, M. L., Chu, G. C., Hebrok, M., Fernandez-Zapico, M. E. and Hanahan, D. (2009). GLI1 is regulated through Smoothened-independent mechanisms in neoplastic pancreatic ducts and mediates PDAC cell survival and transformation. *Genes Dev, 23*(1), 24-36.

Northcott, P. A., Hielscher, T., Dubuc, A., Mack, S., Shih, D., Remke, M., Al-Halabi, H., Albrecht, S., Jabado, N., Eberhart, C. G., Grajkowska, W., Weiss, W. A., Clifford, S. C., Bouffet, E., Rutka, J. T., Korshunov, A., Pfister, S. and Taylor, M. D. (2011). Pediatric and adult sonic hedgehog medulloblastomas are clinically and molecularly distinct. *Acta Neuropathol, 122*(2), 231-240.

Northcott, P. A., Nakahara, Y., Wu, X., Feuk, L., Ellison, D. W., Croul, S., Mack, S., Kongkham, P. N., Peacock, J., Dubuc, A., Ra, Y. S., Zilberberg, K., McLeod, J., Scherer, S. W., Sunil Rao, J., Eberhart, C. G., Grajkowska, W., Gillespie, Y., Lach, B., Grundy, R., Pollack, I. F., Hamilton, R. L., Van Meter, T., Carlotti, C. G., Boop, F., Bigner, D., Gilbertson, R. J., Rutka, J. T. and Taylor, M. D. (2009). Multiple recurrent genetic events converge on control of histone lysine methylation in medulloblastoma. *Nat Genet, 41*(4), 465-472.

Noubissi, F. K., Goswami, S., Sanek, N. A., Kawakami, K., Minamoto, T., Moser, A., Grinblat, Y. and Spiegelman, V. S. (2009). Wnt signaling stimulates transcriptional outcome of the Hedgehog pathway by stabilizing GLI1 mRNA. *Cancer Res, 69*(22), 8572-8578.

Nusslein-Volhard, C. and Wieschaus, E. (1980). Mutations affecting segment number and polarity in Drosophila. *Nature, 287*(5785), 795-801.

Nye, M. D., Almada, L. L., Fernandez-Barrena, M. G., Marks, D. L., Elsawa, S. F., Vrabel, A., Tolosa, E. J., Ellenrieder, V. and Fernandez-Zapico, M. E. (2014). The transcription factor GLI1 interacts with SMAD proteins to modulate transforming growth factor beta-induced gene expression in a p300/CREB-binding protein-associated factor (PCAF)-dependent manner. *J Biol Chem, 289*(22), 15495-15506.

Oh, S. T., Eun, Y. S., Yoo, D. S., Park, H. J., Kim, T. Y., Cho, B. K., Stark, A. and Reichrath, J. (2014). Expression of insulin-like growth factor-1 receptor in conventional cutaneous squamous cell carcinoma with different histological grades of differentiation. *Am J Dermatopathol, 36*(10), 807-811.

Oro, A. E., Higgins, K. M., Hu, Z., Bonifas, J. M., Epstein, E. H., Jr. and Scott, M. P. (1997). Basal cell carcinomas in mice overexpressing sonic hedgehog. *Science, 276*(5313), 817-821.

Orouji, A., Goerdt, S., Utikal, J. and Leverkus, M. (2014). Multiple highly and moderately differentiated squamous cell carcinomas of the skin during vismodegib treatment of inoperable basal cell carcinoma. *Br J Dermatol, 171*(2), 431-433.

Osborne, C. K., Hamilton, B., Titus, G. and Livingston, R. B. (1980). Epidermal growth factor stimulation of human breast cancer cells in culture. *Cancer Res, 40*(7), 2361-2366.

Padilla, R. S., Sebastian, S., Jiang, Z., Nindl, I. and Larson, R. (2010). Gene expression patterns of normal human skin, actinic keratosis, and squamous cell carcinoma: a spectrum of disease progression. *Arch Dermatol, 146*(3), 288-293.

Palma, V. and Ruiz i Altaba, A. (2004). Hedgehog-GLI signaling regulates the behavior of cells with stem cell properties in the developing neocortex. *Development, 131*(2), 337-345.

Parmantier, E., Lynn, B., Lawson, D., Turmaine, M., Namini, S. S., Chakrabarti, L., McMahon, A. P., Jessen, K. R. and Mirsky, R. (1999). Schwann cell-derived Desert hedgehog controls the development of peripheral nerve sheaths. *Neuron, 23*(4), 713-724.

Petrova, R. and Joyner, A. L. (2014). Roles for Hedgehog signaling in adult organ homeostasis and repair. *Development, 141*(18), 3445-3457.

Pierceall, W. E., Goldberg, L. H., Tainsky, M. A., Mukhopadhyay, T. and Ananthaswamy, H. N. (1991). Ras gene mutation and amplification in human nonmelanoma skin cancers. *Mol Carcinog, 4*(3), 196-202.

Ping, X. L., Ratner, D., Zhang, H., Wu, X. L., Zhang, M. J., Chen, F. F., Silvers, D. N., Peacocke, M. and Tsou, H. C. (2001). PTCH mutations in squamous cell carcinoma of the skin. *J Invest Dermatol, 116*(4), 614-616.

Polizio, A. H., Chinchilla, P., Chen, X., Manning, D. R. and Riobo, N. A. (2011). Sonic Hedgehog activates the GTPases Rac1 and RhoA in a Gli-independent manner through coupling of smoothened to Gi proteins. *Sci Signal, 4*(200), pt7.

Popp, S., Waltering, S., Holtgreve-Grez, H., Jauch, A., Proby, C., Leigh, I. M. and Boukamp, P. (2000). Genetic characterization of a human skin carcinoma progression model: from primary tumor to metastasis. *J Invest Dermatol, 115*(6), 1095-1103.

Populo, H., Lopes, J. M. and Soares, P. (2012). The mTOR signalling pathway in human cancer. *Int J Mol Sci, 13*(2), 1886-1918.

Poulalhon, N., Dalle, S., Balme, B. and Thomas, L. (2015). Fast-growing cutaneous squamous cell carcinoma in a patient treated with vismodegib. *Dermatology, 230*(2), 101-104.

Ra, S. H., Li, X. and Binder, S. (2011). Molecular discrimination of cutaneous squamous cell carcinoma from actinic keratosis and normal skin. *Mod Pathol, 24*(7), 963-973.

Ransohoff, K. J., Tang, J. Y. and Sarin, K. Y. (2015). Squamous Change in Basal-Cell Carcinoma with Drug Resistance. *N Engl J Med, 373*(11), 1079-1082.

Regl, G., Neill, G. W., Eichberger, T., Kasper, M., Ikram, M. S., Koller, J., Hintner, H., Quinn, A. G., Frischauf, A. M. and Aberger, F. (2002). Human GLI2 and GLI1 are part of a positive feedback mechanism in Basal Cell Carcinoma. *Oncogene, 21*(36), 5529-5539.

Reifenberger, J., Wolter, M., Weber, R. G., Megahed, M., Ruzicka, T., Lichter, P. and Reifenberger, G. (1998). Missense mutations in SMOH in sporadic basal cell carcinomas of the skin and primitive neuroectodermal tumors of the central nervous system. *Cancer Res, 58*(9), 1798-1803.

Rheinwald, J. G. and Beckett, M. A. (1981). Tumorigenic keratinocyte lines requiring anchorage and fibroblast support cultured from human squamous cell carcinomas. *Cancer Res, 41*(5), 1657-1663.

Ridd, K. and Bastian, B. C. (2010). Somatic mutation of epidermal growth factor receptor in a small subset of cutaneous squamous cell carcinoma. *J Invest Dermatol, 130*(3), 901-903.

Ridzewski, R., Rettberg, D., Dittmann, K., Cuvelier, N., Fulda, S. and Hahn, H. (2015). Hedgehog Inhibitors in Rhabdomyosarcoma: A Comparison of Four Compounds and Responsiveness of Four Cell Lines. *Front Oncol, 5*, 130.

Rimkus, T. K., Carpenter, R. L., Qasem, S., Chan, M. and Lo, H. W. (2016). Targeting the Sonic Hedgehog Signaling Pathway: Review of Smoothened and GLI Inhibitors. *Cancers (Basel), 8*(2)

Riobo, N. A., Haines, G. M. and Emerson, C. P., Jr. (2006). Protein kinase C-delta and mitogen-activated protein/extracellular signal-regulated kinase-1 control GLI activation in hedgehog signaling. *Cancer Res, 66*(2), 839-845.

Rittie, L., Kansra, S., Stoll, S. W., Li, Y., Gudjonsson, J. E., Shao, Y., Michael, L. E., Fisher, G. J., Johnson, T. M. and Elder, J. T. (2007). Differential ErbB1 signaling in squamous cell versus basal cell carcinoma of the skin. *Am J Pathol, 170*(6), 2089-2099.

Robsahm, T. E., Helsing, P. and Veierod, M. B. (2015). Cutaneous squamous cell carcinoma in Norway 1963-2011: increasing incidence and stable mortality. *Cancer Med, 4*(3), 472-480.

Roux, P. P., Ballif, B. A., Anjum, R., Gygi, S. P. and Blenis, J. (2004). Tumor-promoting phorbol esters and activated Ras inactivate the tuberous sclerosis tumor suppressor complex via p90 ribosomal S6 kinase. *Proc Natl Acad Sci U S A, 101*(37), 13489-13494.

Sainsbury, J. R., Farndon, J. R., Needham, G. K., Malcolm, A. J. and Harris, A. L. (1987). Epidermal-growth-factor receptor status as predictor of early recurrence of and death from breast cancer. *Lancet, 1*(8547), 1398-1402.

Saintes, C., Saint-Jean, M., Brocard, A., Peuvrel, L., Renaut, J. J., Khammari, A., Quereux, G. and Dreno, B. (2015). Development of squamous cell carcinoma into basal cell carcinoma under treatment with Vismodegib. *J Eur Acad Dermatol Venereol, 29*(5), 1006-1009.

Salgo, R., Gossmann, J., Schofer, H., Kachel, H. G., Kuck, J., Geiger, H., Kaufmann, R. and Scheuermann, E. H. (2010). Switch to a sirolimus-based immunosuppression in long-term renal transplant recipients: reduced rate of (pre-)malignancies and nonmelanoma skin cancer in a prospective, randomized, assessor-blinded, controlled clinical trial. *Am J Transplant, 10*(6), 1385-1393.

Sarbassov, D. D., Guertin, D. A., Ali, S. M. and Sabatini, D. M. (2005). Phosphorylation and regulation of Akt/PKB by the rictor-mTOR complex. *Science, 307*(5712), 1098-1101.

Sato, T., Nakashima, A., Guo, L., Coffman, K. and Tamanoi, F. (2010). Single amino-acid changes that confer constitutive activation of mTOR are discovered in human cancer. *Oncogene, 29*(18), 2746-2752.

Savage, C. R., Jr., Hash, J. H. and Cohen, S. (1973). Epidermal growth factor. Location of disulfide bonds. *J Biol Chem, 248*(22), 7669-7672.

Schiff, B. A., McMurphy, A. B., Jasser, S. A., Younes, M. N., Doan, D., Yigitbasi, O. G., Kim, S., Zhou, G., Mandal, M., Bekele, B. N., Holsinger, F. C., Sherman, S. I., Yeung, S. C., El-Naggar, A. K. and

Myers, J. N. (2004). Epidermal growth factor receptor (EGFR) is overexpressed in anaplastic thyroid cancer, and the EGFR inhibitor gefitinib inhibits the growth of anaplastic thyroid cancer. *Clin Cancer Res, 10*(24), 8594-8602.

Schmults, C. D., Karia, P. S., Carter, J. B., Han, J. and Qureshi, A. A. (2013). Factors predictive of recurrence and death from cutaneous squamous cell carcinoma: a 10-year, single-institution cohort study. *JAMA Dermatol, 149*(5), 541-547.

Schneider, S., Thurnher, D., Kloimstein, P., Leitner, V., Petzelbauer, P., Pammer, J., Brunner, M. and Erovic, B. M. (2011). Expression of the Sonic hedgehog pathway in squamous cell carcinoma of the skin and the mucosa of the head and neck. *Head Neck, 33*(2), 244-250.

Schnidar, H., Eberl, M., Klingler, S., Mangelberger, D., Kasper, M., Hauser-Kronberger, C., Regl, G., Kroismayr, R., Moriggl, R., Sibilia, M. and Aberger, F. (2009). Epidermal growth factor receptor signaling synergizes with Hedgehog/GLI in oncogenic transformation via activation of the MEK/ERK/JUN pathway. *Cancer Res, 69*(4), 1284-1292.

Seto, M., Ohta, M., Asaoka, Y., Ikenoue, T., Tada, M., Miyabayashi, K., Mohri, D., Tanaka, Y., Ijichi, H., Tateishi, K., Kanai, F., Kawabe, T. and Omata, M. (2009). Regulation of the hedgehog signaling by the mitogen-activated protein kinase cascade in gastric cancer. *Mol Carcinog, 48*(8), 703-712.

Sharpe, H. J., Pau, G., Dijkgraaf, G. J., Basset-Seguin, N., Modrusan, Z., Januario, T., Tsui, V., Durham, A. B., Dlugosz, A. A., Haverty, P. M., Bourgon, R., Tang, J. Y., Sarin, K. Y., Dirix, L., Fisher, D. C., Rudin, C. M., Sofen, H., Migden, M. R., Yauch, R. L. and de Sauvage, F. J. (2015). Genomic analysis of smoothened inhibitor resistance in basal cell carcinoma. *Cancer Cell, 27*(3), 327-341.

Shaul, Y. D. and Seger, R. (2007). The MEK/ERK cascade: from signaling specificity to diverse functions. *Biochim Biophys Acta, 1773*(8), 1213-1226.

Shaw, A., Gipp, J. and Bushman, W. (2009). The Sonic Hedgehog pathway stimulates prostate tumor growth by paracrine signaling and recapitulates embryonic gene expression in tumor myofibroblasts. *Oncogene, 28*(50), 4480-4490.

Sheng, T., Li, C., Zhang, X., Chi, S., He, N., Chen, K., McCormick, F., Gatalica, Z. and Xie, J. (2004). Activation of the hedgehog pathway in advanced prostate cancer. *Mol Cancer, 3*, 29.

Shimizu, T., Izumi, H., Oga, A., Furumoto, H., Murakami, T., Ofuji, R., Muto, M. and Sasaki, K. (2001). Epidermal growth factor receptor overexpression and genetic aberrations in metastatic squamous-cell carcinoma of the skin. *Dermatology, 202*(3), 203-206.

Sizeland, A. M. and Burgess, A. W. (1992). Anti-sense transforming growth factor alpha oligonucleotides inhibit autocrine stimulated proliferation of a colon carcinoma cell line. *Mol Biol Cell, 3*(11), 1235-1243.

Soeda, H., Shimodaira, H., Watanabe, M., Suzuki, T., Gamoh, M., Mori, T., Komine, K., Iwama, N., Kato, S. and Ishioka, C. (2013). Clinical usefulness of KRAS, BRAF, and PIK3CA mutations as predictive markers of cetuximab efficacy in irinotecan- and oxaliplatin-refractory Japanese patients with metastatic colorectal cancer. *Int J Clin Oncol, 18*(4), 670-677.

Sonavane, K., Phillips, J., Ekshyyan, O., Moore-Medlin, T., Roberts Gill, J., Rong, X., Lakshmaiah, R. R., Abreo, F., Boudreaux, D., Clifford, J. L. and Nathan, C. A. (2012). Topical curcumin-based cream is equivalent to dietary curcumin in a skin cancer model. *J Skin Cancer, 2012*, 147863.

Soule, H. D., Vazguez, J., Long, A., Albert, S. and Brennan, M. (1973). A human cell line from a pleural effusion derived from a breast carcinoma. *J Natl Cancer Inst, 51*(5), 1409-1416.

Staples, M. P., Elwood, M., Burton, R. C., Williams, J. L., Marks, R. and Giles, G. G. (2006). Non-melanoma skin cancer in Australia: the 2002 national survey and trends since 1985. *Med J Aust, 184*(1), 6-10.

Stecca, B., Mas, C., Clement, V., Zbinden, M., Correa, R., Piguet, V., Beermann, F. and Ruiz, I. A. A. (2007). Melanomas require HEDGEHOG-GLI signaling regulated by interactions between GLI1 and the RAS-MEK/AKT pathways. *Proc Natl Acad Sci U S A, 104*(14), 5895-5900.

Stecca, B. and Ruiz i Altaba, A. (2009). A GLI1-p53 inhibitory loop controls neural stem cell and tumour cell numbers. *EMBO J, 28*(6), 663-676.

Stortelers, C., van De Poll, M. L., Lenferink, A. E., Gadellaa, M. M., van Zoelen, C. and van Zoelen, E. J. (2002). Epidermal growth factor contains both positive and negative determinants for interaction with ErbB-2/ErbB-3 heterodimers. *Biochemistry, 41*(13), 4292-4301.

Su, J. M., Lai, X. M., Lan, K. H., Li, C. P., Chao, Y., Yen, S. H., Chang, F. Y., Lee, S. D. and Lee, W. P. (2007). X protein of hepatitis B virus functions as a transcriptional corepressor on the human telomerase promoter. *Hepatology, 46*(2), 402-413.

Sun, Q., Bai, J. and Lv, R. (2016). Hedgehog/Gli1 signal pathway facilitates proliferation, invasion, and migration of cutaneous SCC through regulating VEGF. *Tumour Biol*

Takezaki, T., Hide, T., Takanaga, H., Nakamura, H., Kuratsu, J. and Kondo, T. (2011). Essential role of the Hedgehog signaling pathway in human glioma-initiating cells. *Cancer Sci, 102*(7), 1306-1312.

Taylor, M. D., Liu, L., Raffel, C., Hui, C. C., Mainprize, T. G., Zhang, X., Agatep, R., Chiappa, S., Gao, L., Lowrance, A., Hao, A., Goldstein, A. M., Stavrou, T., Scherer, S. W., Dura, W. T., Wainwright, B., Squire, J. A., Rutka, J. T. and Hogg, D. (2002). Mutations in SUFU predispose to medulloblastoma. *Nat Genet, 31*(3), 306-310.

Taylor, M. D., Northcott, P. A., Korshunov, A., Remke, M., Cho, Y. J., Clifford, S. C., Eberhart, C. G., Parsons, D. W., Rutkowski, S., Gajjar, A., Ellison, D. W., Lichter, P., Gilbertson, R. J., Pomeroy, S. L., Kool, M. and Pfister, S. M. (2012). Molecular subgroups of medulloblastoma: the current consensus. *Acta Neuropathol, 123*(4), 465-472.

Tessmer, C. S., Magalhaes, L. V., Keitel, E., Valar, C., Gnatta, D., Pra, R. L., Silveira, F. R., Dos Santos, A. F., Goldani, J. C., Garcia, V. D. and Garcia, C. D. (2006). Conversion to sirolimus in renal transplant recipients with skin cancer. *Transplantation, 82*(12), 1792-1793.

Thayer, S. P., di Magliano, M. P., Heiser, P. W., Nielsen, C. M., Roberts, D. J., Lauwers, G. Y., Qi, Y. P., Gysin, S., Fernandez-del Castillo, C., Yajnik, V., Antoniu, B., McMahon, M., Warshaw, A. L. and Hebrok, M. (2003). Hedgehog is an early and late mediator of pancreatic cancer tumorigenesis. *Nature, 425*(6960), 851-856.

Thibert, C., Teillet, M. A., Lapointe, F., Mazelin, L., Le Douarin, N. M. and Mehlen, P. (2003). Inhibition of neuroepithelial patched-induced apoptosis by sonic hedgehog. *Science, 301*(5634), 843-846.

Thieu, K., Ruiz, M. E. and Owens, D. M. (2013). Cells of origin and tumor-initiating cells for nonmelanoma skin cancers. *Cancer Lett, 338*(1), 82-88.

Tilgen, W., Boukamp, P., Breitkreutz, D., Dzarlieva, R. T., Engstner, M., Haag, D. and Fusenig, N. E. (1983). Preservation of morphological, functional, and karyotypic traits during long-term culture and in vivo passage of two human skin squamous cell carcinomas. *Cancer Res, 43*(12 Pt 1), 5995-6011.

Tillotson, J. K. and Rose, D. P. (1991). Endogenous secretion of epidermal growth factor peptides stimulates growth of DU145 prostate cancer cells. *Cancer Lett, 60*(2), 109-112.

Toll, A., Salgado, R., Yebenes, M., Martin-Ezquerra, G., Gilaberte, M., Baro, T., Sole, F., Alameda, F., Espinet, B. and Pujol, R. M. (2010). Epidermal growth factor receptor gene numerical aberrations are frequent events in actinic keratoses and invasive cutaneous squamous cell carcinomas. *Exp Dermatol, 19*(2), 151-153.

Uribe, P. and Gonzalez, S. (2011). Epidermal growth factor receptor (EGFR) and squamous cell carcinoma of the skin: molecular bases for EGFR-targeted therapy. *Pathol Res Pract, 207*(6), 337-342.

Varjosalo, M., Bjorklund, M., Cheng, F., Syvanen, H., Kivioja, T., Kilpinen, S., Sun, Z., Kallioniemi, O., Stunnenberg, H. G., He, W. W., Ojala, P. and Taipale, J. (2008). Application of active and kinase-deficient kinome collection for identification of kinases regulating hedgehog signaling. *Cell, 133*(3), 537-548.

Veale, D., Ashcroft, T., Marsh, C., Gibson, G. J. and Harris, A. L. (1987). Epidermal growth factor receptors in non-small cell lung cancer. *Br J Cancer, 55*(5), 513-516.

Vilella-Bach, M., Nuzzi, P., Fang, Y. and Chen, J. (1999). The FKBP12-rapamycin-binding domain is required for FKBP12-rapamycin-associated protein kinase activity and G1 progression. *J Biol Chem, 274*(7), 4266-4272.

Wang, C., Wu, H., Evron, T., Vardy, E., Han, G. W., Huang, X. P., Hufeisen, S. J., Mangano, T. J., Urban, D. J., Katritch, V., Cherezov, V., Caron, M. G., Roth, B. L. and Stevens, R. C. (2014). Structural basis for Smoothened receptor modulation and chemoresistance to anticancer drugs. *Nat Commun, 5*, 4355.

Wang, Y., Ding, Q., Yen, C. J., Xia, W., Izzo, J. G., Lang, J. Y., Li, C. W., Hsu, J. L., Miller, S. A., Wang, X., Lee, D. F., Hsu, J. M., Huo, L., Labaff, A. M., Liu, D., Huang, T. H., Lai, C. C., Tsai, F. J., Chang, W. C., Chen, C. H., Wu, T. T., Buttar, N. S., Wang, K. K., Wu, Y., Wang, H., Ajani, J. and Hung, M. C. (2012). The crosstalk of mTOR/S6K1 and Hedgehog pathways. *Cancer Cell, 21*(3), 374-387.

Wang, Z. C., Gao, J., Zi, S. M., Yang, M., Du, P. and Cui, L. (2013). Aberrant expression of sonic hedgehog pathway in colon cancer and melanosis coli. *J Dig Dis, 14*(8), 417-424.

Wayne, J., Sielski, J., Rizvi, A., Georges, K. and Hutter, D. (2006). ERK regulation upon contact inhibition in fibroblasts. *Mol Cell Biochem, 286*(1-2), 181-189.

Weichselbaum, R. R., Dunphy, E. J., Beckett, M. A., Tybor, A. G., Moran, W. J., Goldman, M. E., Vokes, E. E. and Panje, W. R. (1989). Epidermal growth factor receptor gene amplification and expression in head and neck cancer cell lines. *Head Neck, 11*(5), 437-442.

Whisenant, T. C., Ho, D. T., Benz, R. W., Rogers, J. S., Kaake, R. M., Gordon, E. A., Huang, L., Baldi, P. and Bardwell, L. (2010). Computational prediction and experimental verification of new MAP kinase docking sites and substrates including Gli transcription factors. *PLoS Comput Biol, 6*(8)

Whitmarsh, A. J. (2007). Regulation of gene transcription by mitogen-activated protein kinase signaling pathways. *Biochim Biophys Acta, 1773*(8), 1285-1298.

Wilson, C. W., Chen, M. H. and Chuang, P. T. (2009). Smoothened adopts multiple active and inactive conformations capable of trafficking to the primary cilium. *PLoS One, 4*(4), e5182.

Winklmayr, M., Schmid, C., Laner-Plamberger, S., Kaser, A., Aberger, F., Eichberger, T. and Frischauf, A. M. (2010). Non-consensus GLI binding sites in Hedgehog target gene regulation. *BMC Mol Biol, 11*, 2.

Wong, A. J., Bigner, S. H., Bigner, D. D., Kinzler, K. W., Hamilton, S. R. and Vogelstein, B. (1987). Increased expression of the epidermal growth factor receptor gene in malignant gliomas is invariably associated with gene amplification. *Proc Natl Acad Sci U S A, 84*(19), 6899-6903.

Wu, V. M., Chen, S. C., Arkin, M. R. and Reiter, J. F. (2012). Small molecule inhibitors of Smoothened ciliary localization and ciliogenesis. *Proc Natl Acad Sci U S A, 109*(34), 13644-13649.

Wu, W., O'Reilly, M. S., Langley, R. R., Tsan, R. Z., Baker, C. H., Bekele, N., Tang, X. M., Onn, A., Fidler, I. J. and Herbst, R. S. (2007). Expression of epidermal growth factor (EGF)/transforming growth factor-alpha by human lung cancer cells determines their response to EGF receptor tyrosine kinase inhibition in the lungs of mice. *Mol Cancer Ther, 6*(10), 2652-2663.

Xie, J. (2005). Hedgehog signaling in prostate cancer. *Future Oncol, 1*(3), 331-338.

Xie, J., Murone, M., Luoh, S. M., Ryan, A., Gu, Q., Zhang, C., Bonifas, J. M., Lam, C. W., Hynes, M., Goddard, A., Rosenthal, A., Epstein, E. H., Jr. and de Sauvage, F. J. (1998). Activating Smoothened mutations in sporadic basal-cell carcinoma. *Nature, 391*(6662), 90-92.

Yauch, R. L., Gould, S. E., Scales, S. J., Tang, T., Tian, H., Ahn, C. P., Marshall, D., Fu, L., Januario, T., Kallop, D., Nannini-Pepe, M., Kotkow, K., Marsters, J. C., Rubin, L. L. and de Sauvage, F. J. (2008). A paracrine requirement for hedgehog signalling in cancer. *Nature, 455*(7211), 406-410.

Yoon, J. W., Lamm, M., Iannaccone, S., Higashiyama, N., Leong, K. F., Iannaccone, P. and Walterhouse, D. (2015). p53 modulates the activity of the GLI1 oncogene through interactions with the shared coactivator TAF9. *DNA Repair (Amst), 34*, 9-17.

Zeng, F. and Harris, R. C. (2014). Epidermal growth factor, from gene organization to bedside. *Semin Cell Dev Biol, 28*, 2-11.

Zhang, X., Makino, T., Muchemwa, F. C., Lin, T., Wakasugi, S., Egawa, K. and Ihn, H. (2007). Activation of the extracellular signal-regulated kinases signaling pathway in squamous cell carcinoma of the skin. *Biosci Trends, 1*(3), 156-160.

Zhang, X., Zhang, H., Tighiouart, M., Lee, J. E., Shin, H. J., Khuri, F. R., Yang, C. S., Chen, Z. and Shin, D. M. (2008). Synergistic inhibition of head and neck tumor growth by green tea (-)-epigallocatechin-3-gallate and EGFR tyrosine kinase inhibitor. *Int J Cancer, 123*(5), 1005-1014.

Zhao, H., Shu, G. and Wang, S. (2016). The risk of non-melanoma skin cancer in HIV-infected patients: new data and meta-analysis. *Int J STD AIDS, 27*(7), 568-575.

Zhou, B. P., Hu, M. C., Miller, S. A., Yu, Z., Xia, W., Lin, S. Y. and Hung, M. C. (2000a). HER-2/neu blocks tumor necrosis factor-induced apoptosis via the Akt/NF-kappaB pathway. *J Biol Chem, 275*(11), 8027-8031.

Zhou, H., Li, X. M., Meinkoth, J. and Pittman, R. N. (2000b). Akt regulates cell survival and apoptosis at a postmitochondrial level. *J Cell Biol, 151*(3), 483-494.

Zhu, G. A., Sundram, U. and Chang, A. L. (2014). Two different scenarios of squamous cell carcinoma within advanced Basal cell carcinomas: cases illustrating the importance of serial biopsy during vismodegib usage. *JAMA Dermatol, 150*(9), 970-973.

Zhu, H. and Lo, H. W. (2010). The Human Glioma-Associated Oncogene Homolog 1 (GLI1) Family of Transcription Factors in Gene Regulation and Diseases. *Curr Genomics, 11*(4), 238-245.

9. Abbreviations

4E-BP1	eIF4E-binding protein 1
5-FU	5-fluoruracil
7TM	7-pass transmembrane
AEC	3-amino-9-ethylcarbazole
AIDS	acquired immune deficiency syndrome
AK	actinic keratosis
AKT	v-akt murine thymoma viral oncogene homolog
ATO	arsenic trioxide
ATP	adenosine triphosphate
BCA	bicinchoninic acid
BCC	basal cell carcinoma
Bcl2	B-cell lymphoma 2
BMP	bone morphogenetic protein
bp	base pairs
BrdU	5-bromo-2-deoxyuridine
BSA	bovine serum albumin
C	cysteine
C-terminal	carboxyterminal
cDNA	complementary deoxyribonucleic acid
Ci	cubitus interruptus
CK1	casein kinase 1
CM	conditioned medium
CMV	cytomegalovirus
CRD-BP	coding region determinant-binding protein
cSCC	cutaneous squamous cell carcinoma
DAPI	4',6-diamidin-2-phenylindol
ddH$_2$O	double distilled water
DEPC	diethyl pyrocarbonate
DHH	desert hedgehog
DMEM	Dulbecco's Modified Eagle Medium
DMSO	dimethyl sulfoxide

DNA	deoxyribonucleic acid
dNTP	deoxyribonucleotide triphosphate
DTT	dithiothreitol
DYRK	dual specificity tyrosine-phosphorylation-regulated kinase
E. coli	*Escherichia coli*
EDTA	ethylenediaminetetraacetic acid
EGF	epidermal growth factor
EGFR/HER/ErbB	epidermal growth factor receptor
EMT	epithelial to mesenchymal transition
EtOH	ethanol
ERK	extracellular signal-regulated kinases
FCS	fetal calf serum
FDA	Food and Drug Administration
FGFR	fibroblast growth factor receptor
FITC	fluorescein isothiocyanate
GLI/Gli	glioma-associated oncogene
GLI act	GLI activator form
GLI rep	GLI repressor form
Grb2	growth factor receptor-bound protein 2
GSK3	glycogen synthase kinase 3
GTP	guanosine triphosphate
GTPase	guanosine triphosphate hydrolase
HE	haematoxylin eosin
HH	hedgehog
HhA	HH antagonist
HHIP	hedgehog interacting protein
HNSCC	head and neck squamous cell carcinoma
HPRT	hypoxanthine-guanine phosphoribosyl transferase
HRP	horseradish peroxidase
HSC70	heat shock protein 70
HSV	herpes simplex virus
IGF1/2	insulin-like growth factor 1/2
IGF1R	insulin-like growth factor 1 receptor

IHC	immunohistochemistry
IHH	indian hedgehog
IRS-1	insulin receptor substrate 1
ISH	*in situ* hybridization
kDa	kilodalton
LEF	lymphoid enhancer factor
LOH	loss of heterozygosity
MB	medulloblastoma
MEK/MAPK	mitogen-activated protein kinase kinase
mRNA	messenger ribonucleic acid
mTOR	mammalian target of rapamycin
Myc	myelocytomatosis oncogene
N-terminal	amino terminal
NEAA	non-essential amino acids
NSCLC	non-small cell lung cancer
OTRs	organ transplant recipients
P	phosphorylation
PBS	phosphate buffered saline
PBST	phosphate buffered saline - tween 20
PCR	polymerase chain reaction
PDGFR	platelet derived growth factor receptor
PDK1	phosphoinositide-dependent kinase 1
PFA	paraformaldehyde
PH	plextrin homology domain
PI	propidium iodide
PI3K	phosphatidylinositol-4,5-biphosphate-3-kinase
PIP2	phosphatidylinositol 4,5-bisphosphate
PIP3	phosphatidylinositol 3,4,5-trisphosphate
PKA	protein kinase A
PKC	protein kinase C
PLC	phospholipase C
PRMT1	protein arginine methyltransferase 1
P/S	penicillin streptomycin

PTCH /Ptch	Patched
PTEN	phosphatase and tensin homolog deleted on chromosome 10
PP2	protein phosphatase 2
py	person-years
p53	transformation related protein 53
qPCR	quantitative polymerase chain reaction
Rac1	ras-related C3 botulinum toxin substrate 1
Raf	rapidly accelerated fibrosarcoma
RAS	rat sarcoma
Rb	retinoblastoma
RHEB	ras homolog enriched in brain
RhoA	ras homolog family member A
RMS	rhabdomyosarcoma
RT	room temperature
RTK	receptor tyrosine kinases
S6	ribosomal S6 protein
S6K1	S6 kinase beta-1
SAG	smoothened agonist
SDS	sodiumdodecylsulfate
SEM	standard error of the mean
Ser	serine
SH2/3	Src homology 2/3
SHH/Shh	sonic hedgehog
SMO/Smo	smoothened
SOS	son of sevenless
SUFU/SuFu	suppressor of fused
T	thymidine
TBE	tris-boric acid-EDTA
TBS	tris-buffered saline
TBST	tris-buffered saline-Triton X-100
TCF	T-cell factor
TEA	triethanolamine
TGFα/ß	transforming growth factor α/ß

Thr	threonine
TK	thymidine kinase
TKI	tyrosine kinase inhibitors
TPA	12-O-tetradecanoylphorbol 13-acetate
TSC2	tuberous sclerosis complex 2
Tyr	tyrosine
UO126	1,4-diamino-2,3-dicyano-1,4-*bis*[2-aminophenylthio]butadiene
UV	ultraviolet
VEGF	vascular endothelial growth factor receptor
WST	water soluble tetrazolium salt 1

10. Acknowledgement

11. Curriculum Vitae

09/2013 – 07/2017	**Ph.D., Tumor Genetics, Georg-August-University of Göttingen** University Medical Center Göttingen; Institute of Human Genetics, Tumor Genetics group Within the doctoral program Molecular Medicine that is part of GAUSS (Georg-August-University School of Science) Thesis title: Hedgehog signaling in cutaneous squamous cell carcinoma
10/2010 – 10/2013	**M.Sc., Biology, Genetics, Jagiellonian University in Krakow, Genetics Department** Master thesis: Identification and characterization of proteins interacting with ZFP819, a novel pluripotency-specific protein
03/2011 – 03/2012	Two semesters abroad at Georg-August University in Göttingen, Germany, Institute of Human Genetics, Stem Cell group
10/2007 – 10/2010	**B.Sc., Biology, Jagiellonian University in Krakow, Genetics Department** Bachelor thesis: Strategies of curing cancer
09/2009 – 10/2009	Practical assistant at Independent Laboratory of Molecular Biology and Research, The John Paul II Hospital in Krakow
06/2007	Abitur, Sports High School in Krakow Intensive courses: Biology and Chemistry

Publications:

Almazán-Moga A, Zarzosa P, Molist C, Velasco P, **Pyczek J**, Simon-Keller K, Giralt I, Vidal I, Navarro N, Segura MF, Soriano A, Navarro S, Tirado OM, Ferreres JC, Santamaria A, Rota R, Hahn H, Sánchez de Toledo J, Roma J, Gallego S (2017). Ligand-dependent Hedgehog pathway activation in Rhabdomyosarcoma: the oncogenic role of the ligands. *Br J Cancer 117*(9), 1314-1325.

Curriculum Vitae

Pyczek, J., Buslei, R., Schult, D., Holsken, A., Buchfelder, M., Hess, I., Hahn, H. and Uhmann, A. (2016). Hedgehog signaling activation induces stem cell proliferation and hormone release in the adult pituitary gland. *Sci Rep, 6*, 24928.

Zheng, Y., Tan, X., **Pyczek, J**., Nolte, J., Pantakani, D. V. and Engel, W. (2013). Generation and characterization of yeast two-hybrid cDNA libraries derived from two distinct mouse pluripotent cell types. *Mol Biotechnol, 54*(2), 228-237.